# RADIOLOGICAL AND ENVIRONMENTAL RESEARCH DIVISION ANNUAL REPORT

## Atmospheric Physics

## January—December 1977

U of C-AUA-USDOE

ARGONNE NATIONAL LABORATORY, ARGONNE, ILLINOIS

Prepared for the U. S. DEPARTMENT OF ENERGY
under Contract W-31-109-Eng-38

ANL-77-65
Part IV

ARGONNE NATIONAL LABORATORY
9700 South Cass Avenue
Argonne, Illinois 60439

# RADIOLOGICAL AND ENVIRONMENTAL
# RESEARCH DIVISION
# ANNUAL REPORT

Atmospheric Physics

January through December 1977

R. E. Rowland, Division Director
B. B. Hicks, Section Head

Preceding Report: ANL-76-88 Part IV, January-December 1976

This report consists of a collection of intentionally brief articles selected to illustrate the breadth of activities of this Section. The programs which are addressed are much the same as in previous years, although changes in approach might be apparent to the reader. Work on the planetary boundary layer, regional-scale numerical modeling, remote probing, and surface deposition of pollutants falls under the MAP3S program of DOE (MAP3S is the Multistate Atmospheric Power Production Pollution Study). Work on air-water heat transfer and on fog formation is part of a study of the atmospheric effects of cooling ponds, which is undertaken in cooperation with the DOE Meteorological Effects of Thermal Energy Release program. Studies of dispersion characteristics in the wakes of buildings and in coastal regimes and measurements of pollutant fluxes to water surfaces are part of an investigation of potential problems associated with the siting of electricity generating stations in coastal and offshore regions.

The extent of cooperation with the Ecological Sciences Section (ESS) of this Division has expanded dramatically. Many of the field investigations of gaseous dry deposition have been conducted at the site used in ESS experiments concerning the effects of atmospheric sulfur dioxide on field crops. Clearly, the determinations of gas fluxes to the surface made in this Section's studies help determine the pollutant input rates necessary for developing dose-response relationships. Studies of dispersion and deposition over water surfaces continue to be in cooperation with the Great Lakes Program of ESS. In this particular case, the active sharing of facilities and interaction of programs results from an awareness that fluxes from the air constitute a major input of many pollutants into the Great Lakes. A third area of collaboration with ESS concerns the parameterization of wet removal processes for inclusion in the numerical simulations of the MAP3S program. Some of the relatively simple formulations developed from prior Argonne investigations of radioactive fallout are being examined for applicability to the case of airborne sulfur. The experimental part of this work is being undertaken largely within ESS, where the major interest is in the pH of rainfall and the ecological effects of its chemical contaminants.

i

This report concludes with some abstracts of recent papers. Abstracts have been selected to represent lines of work which are not otherwise represented here.

# A DIAGNOSTIC ATMOSPHERIC CROSS-SECTION EXPERIMENT FOR MAP3S

D. L. Sisterson and J. D. Shannon

## Introduction

The diurnal cycle of atmospheric stability in the lowest several kilometers of the atmosphere is of great importance to the long-range transport of pollutants. Although models of pollutant transport in the lower atmosphere may be adequate, available data are insufficient for model verification and thus field studies are necessary. In August 1977, an opportunity arose for the first MAP3S Diagnostic Atmospheric Cross-Section Experiment (DACSE-I), carried out in conjunction with the first intensive period of observation of the Sulfate Regional Experiment of the Electric Power Research Institute (Environmental Research and Technology, Inc., 1976). Coordinated by ANL, DACSE-I combined upper-air soundings from selected National Weather Service rawinsonde stations with air quality profiles collected by a research aircraft from Battelle Pacific Northwest Laboratories. Additional information on the evolving vertical structure of the atmosphere was supplied by an ANL acoustic sounder. Analysis and archiving of the data are being performed by ANL.

## Data Collection

Special arrangements with the National Weather Service provided five soundings daily (special soundings at 0800Z, 1500Z, and 2000Z, in addition to the regular schedule of 1200Z and 0000Z) for the period 1-10 August 1977 at each of three stations: Salem, Ill., Dayton, O., and Pittsburgh, Pa. These stations are located on the WSW-ENE ($\approx 252°$) line, lying approximately 100-150 km north of the Ohio River (Figure 1). The vertical structure of the atmosphere, including temperature, humidity, wind, and pressure, was thus sampled fifty times along this line to a height of at least three kilometers. In addition, at 1200Z and 0000Z, the times of regular soundings, the cross-sections could be extended eastward to New York City and westward to Monett. Mo.

The acoustic sounder was located at the site near Manilla, Ind., where the AMBIENS field experiment was subsequently centered. Although the
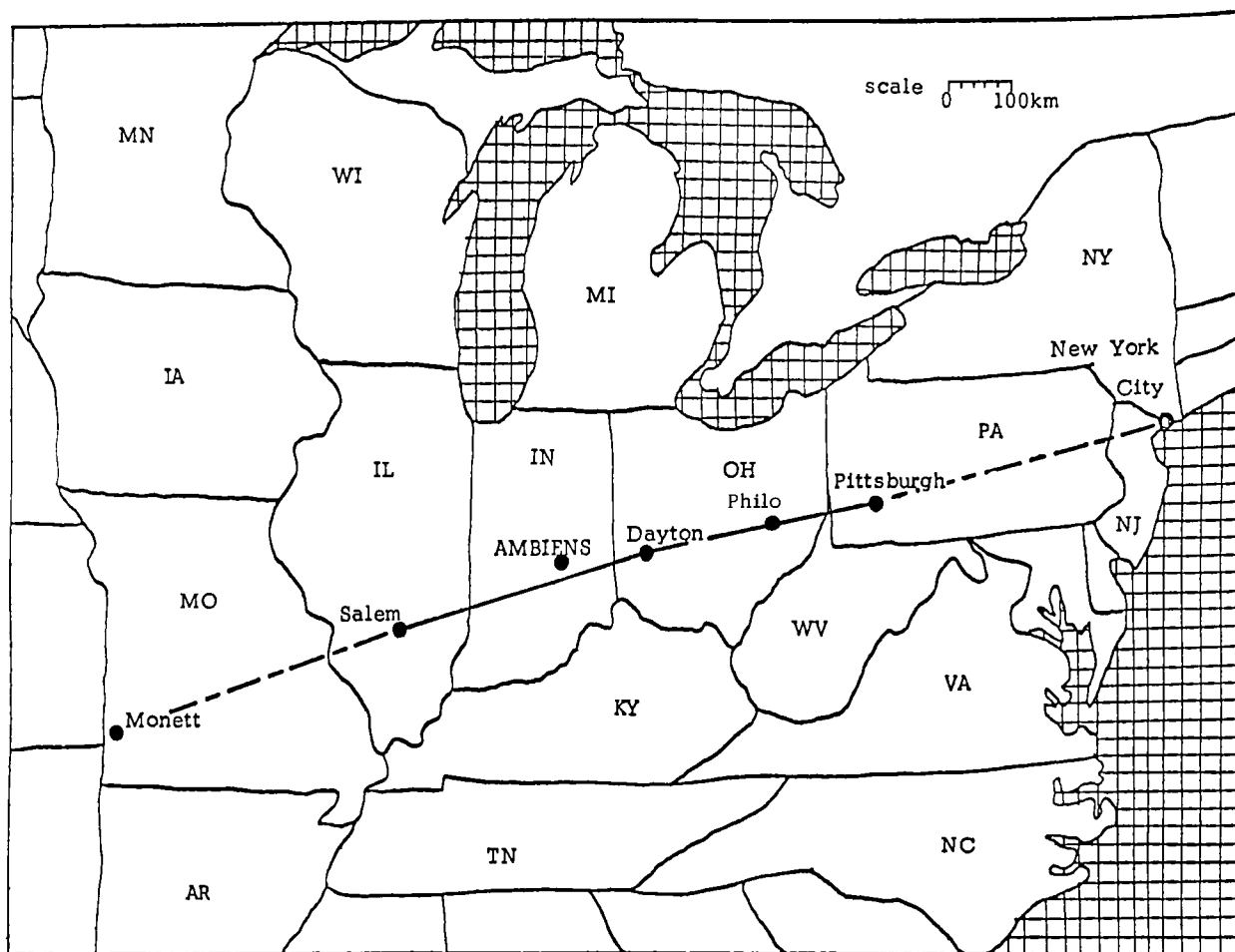
FIG. 1.--Surface projection of the vertical cross section defined by the special sounding (solid line) at Salem, Dayton, and Pittsburgh, and regular soundings (dashed lines) at Monett and New York City.

acoustic sounder could not determine temperatures directly, it could detect stable layers in the lowest kilometer, and thus could be used to help determine the heights of concentrated isentropic surfaces.

Plans for the experiment called for the PNL DC-3 aircraft to be available for this study for a three-day sampling period. By 3 August it appeared that a favorable synoptic situation was developing (essentially, a westward extension of the Bermuda high), so the PNL aircraft and crew moved on 4 August to a temporary base at Columbus, O., where they were joined on 5 August by an ANL observer. Early morning and late afternoon flights, which included frequent vertical profiles, were made on both 5 and 6 August along a route

between Greensburg, Ind., 25 km southeast of the acoustic sounder site, and Steubenville, O., 50 km west of Pittsburgh. Similar flights scheduled for 7 August had to be cancelled because of thunderstorms along the route. Measurements recorded during the successful flights included wind, temperature, humidity, ultraviolet radiation, $b_{scat}$, and concentrations of sulfur dioxide, ozone, nitric oxides, and small aerosols.

Throughout most of the experiment the synoptic situation included an E-W ridge extending from the Bermuda high through much of the Southeast, and a stationary front along the lower Great Lakes. The passage of short waves aloft led to frequent convective activity along and south of the frontal zone. The flow during the aircraft flights was typically moderate to strong from the southwest quadrant.

Data Analysis

Figures 2, 3, and 4 illustrate some features of the atmospheric transport process that can be examined with this method of presentation. Each cross-section has been analyzed for potential temperature $\theta$ (solid lines every 2°K), mixing ratio w (dot-dash lines every 2 g water vapor/kg dry air), and wind speed (m s$^{-1}$). For the latter the longitudinal wind component u (positive from 252°) is shown as a wind arrow with each full barb representing 5 m s$^{-1}$; the transverse wind component v (positive from 162°) is plotted numerically. Nephelometer data ($b_{scat}$ in units of $10^{-4}$ m$^{-1}$) were found to depict the most detail in the vertical distribution of any of the air quality variables measured; therefore, these data are used in these analyses.

The analysis of 0700 EST August 5, shown in Figure 2, suggests the development of the mixed layer progressing from east to west with the rising sun. On the western side the isentropes are compressed in the stably stratified lower atmosphere; to the east they increasingly diverge as the mixed layer becomes re-established. A moist tongue of air, stretching from 800 mb over Monett to 750 mb over Dayton, indicates moisture advection from the southwest, probably associated with flow from the Gulf, around the Bermuda high extension. The rather limited $b_{scat}$ analysis, based upon several aircraft

3
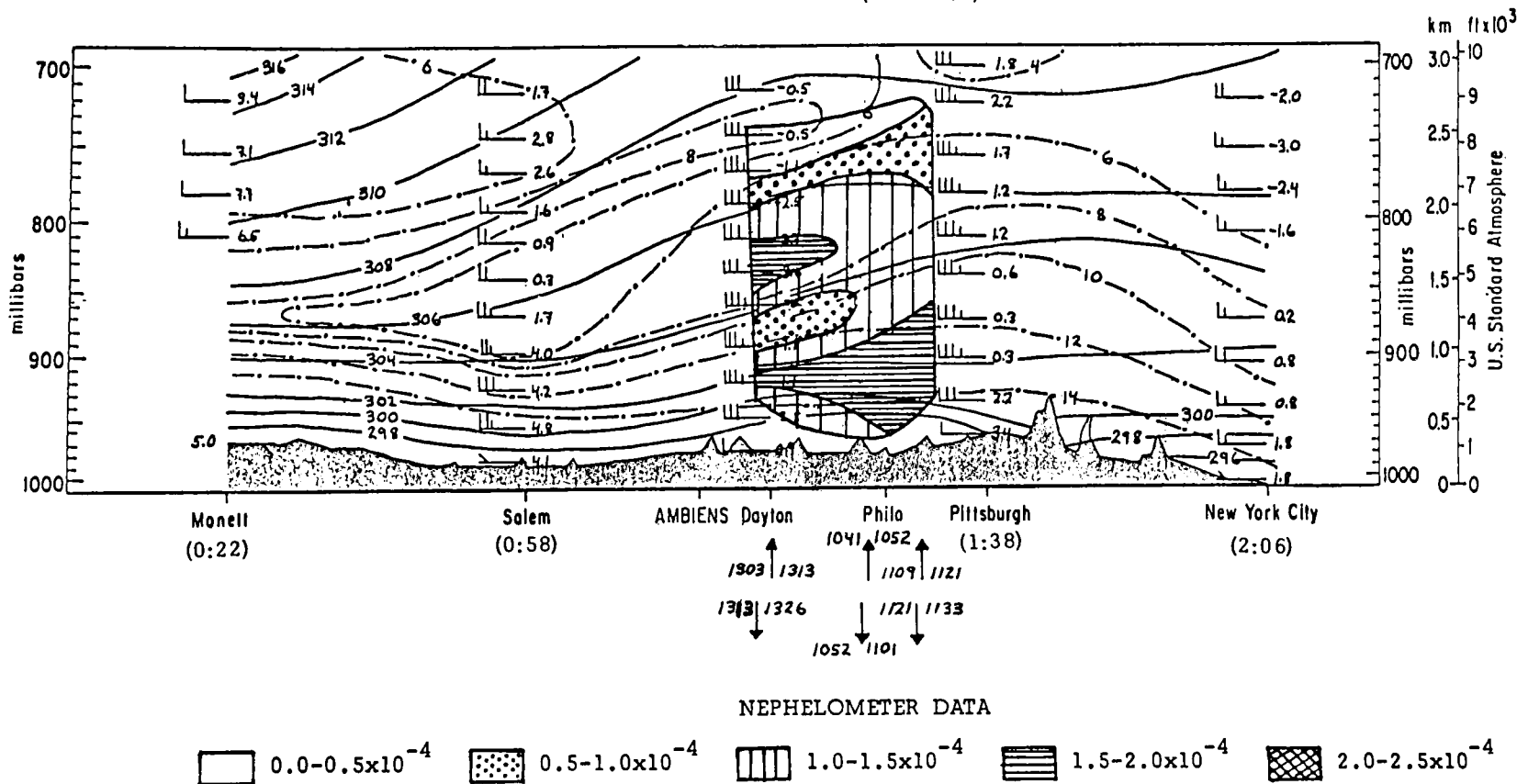
FIG. 2.--Analyses of potential temperature, mixing ratio, and $b_{scat}$ on 5 August 1977 at 1200Z (0700 EST). Potential temperature (°K) and mixing ratio (g kg$^{-1}$) analyses are solid and dot-dash lines, respectively. Layers of $b_{scat}$ are depicted by cross-hatching. Time since sunrise is parenthesized below the respective city. Arrows show location and direction of aircraft soundings. Soundings plotted are within ±1 hour of the time of the cross section.

5 AUGUST 1977     1500 Z (1000 EST)



NEPHELOMETER DATA

| | | | | |
|---|---|---|---|---|
| $0.0-0.5\times10^{-4}$ | $0.5-1.0\times10^{-4}$ | $1.0-1.5\times10^{-4}$ | $1.5-2.0\times10^{-4}$ | $2.0-2.5\times10^{-4}$ |
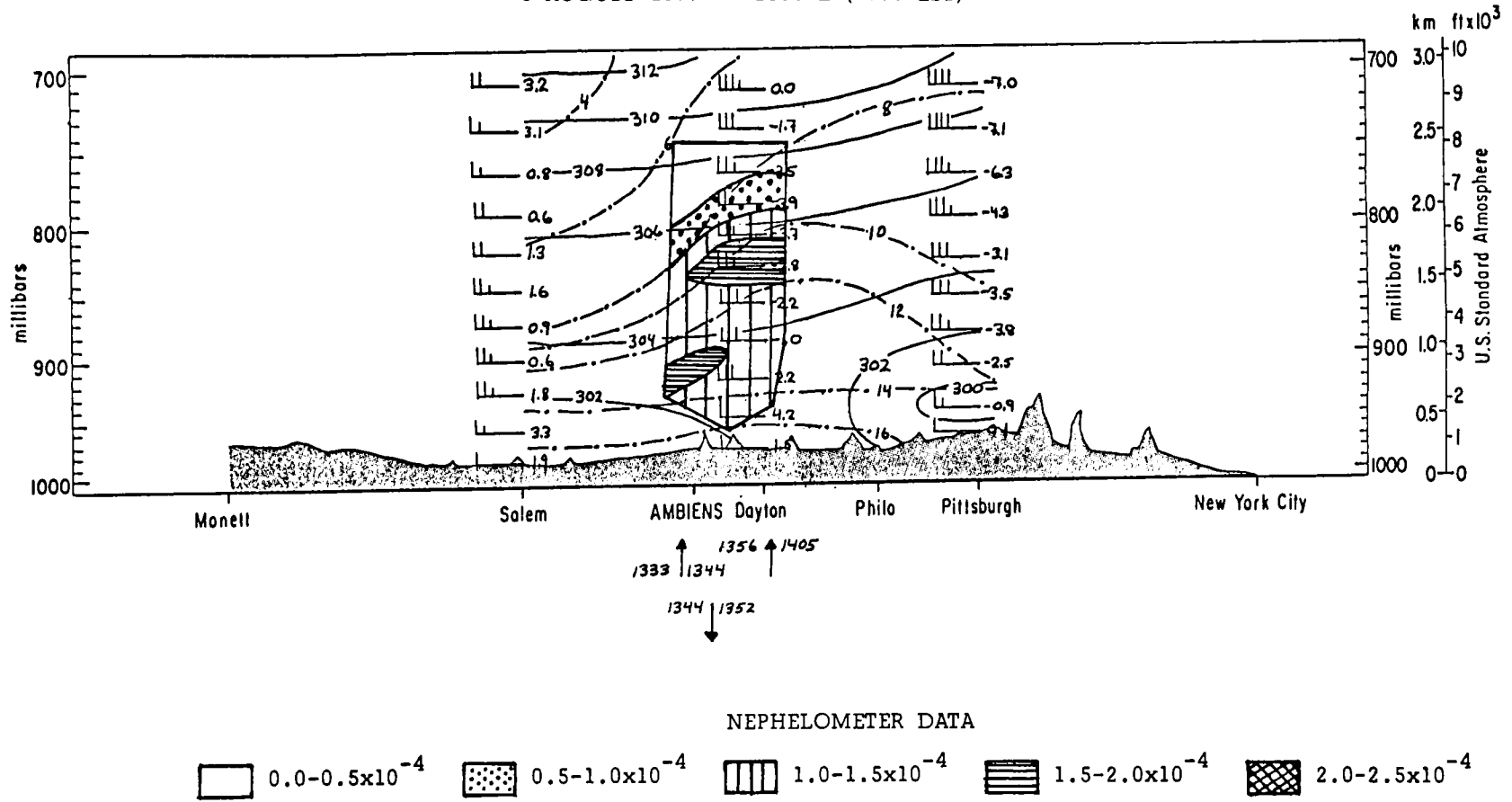
FIG. 3.--Analyses of potential temperature, mixing ratio, and $b_{scat}$ on 5 August 1977 at 1500Z (1000 EST). See Figure 2 for details.

9

NEPHELOMETER DATA

☐ 0.0-0.5x10$^{-4}$   ▦ 0.5-1.0x10$^{-4}$   ⦀ 1.0-1.5x10$^{-4}$   ▤ 1.5-2.0x10$^{-4}$   ▨ 2.0-2.5x10$^{-4}$
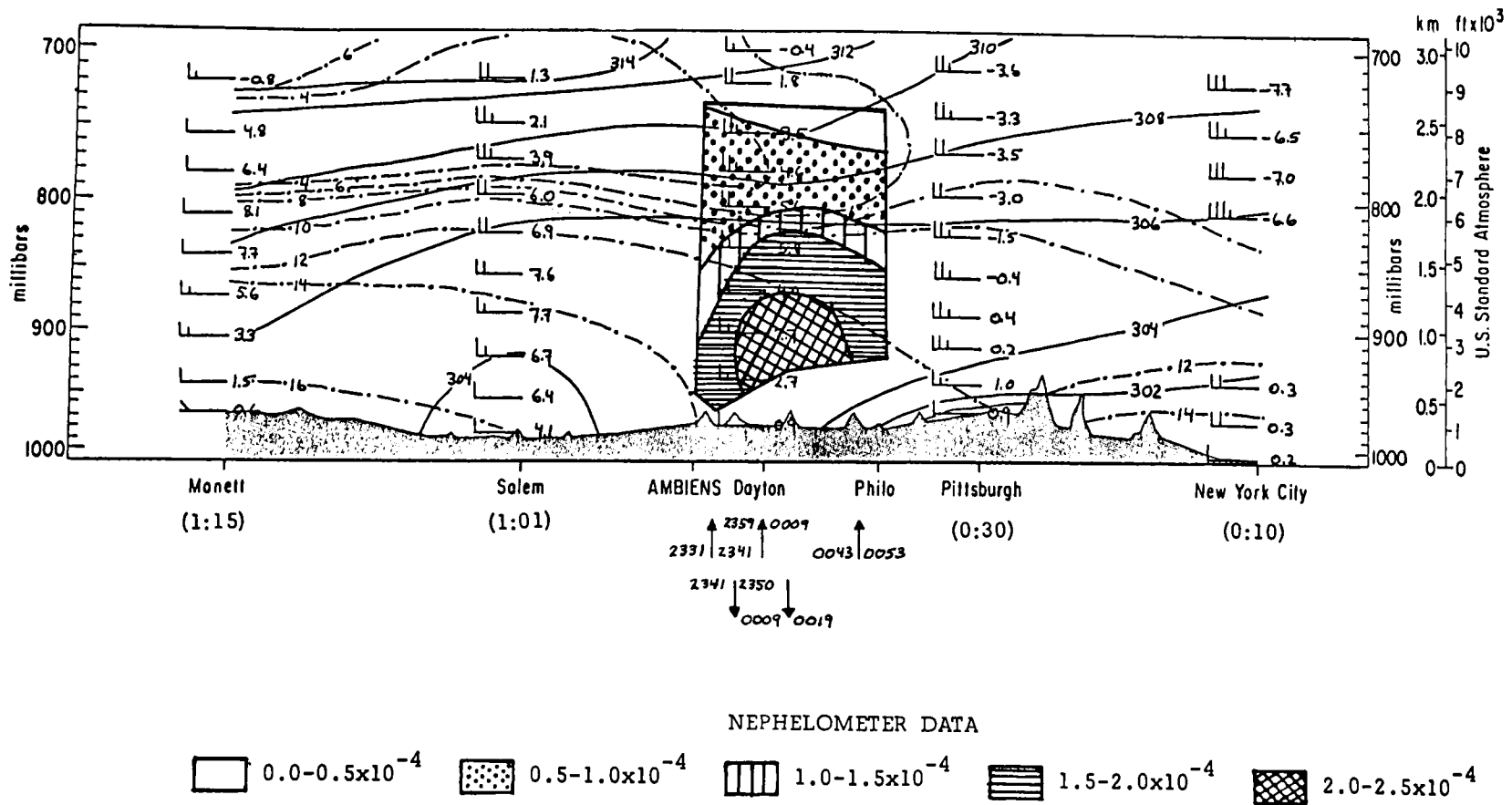
FIG. 4.--Analyses of potential temperature, mixing ratio, and $b_{scat}$ on 6 August 1977 at 0000Z (1900 EST on 5 August).  See Figure 2 for details.  Time before sunset is parenthesized below the respective city.

soundings taken within plus or minus one hour of the time of the cross-section, shows two distinct layers of relatively high $b_{scat}$, centered around 910 and 820 mb and stretching between Dayton and Philo. The lower layer may be explained by the trapping of light-scattering particles beneath the nocturnal inversion. The upper layer is probably the remnant of particles mixed to that level upwind of Dayton on the previous day or days. East of Philo, however, the layered structure has apparently been eliminated by vertical mixing caused by surface heating.

Figure 3 shows the increased depth of the well-mixed boundary layer in this region three hours later. There are still two distinct layers of higher $b_{scat}$, but the lower layer is evident only west of Dayton, while the upper layer can still be found over the city. The lower layer may have been eliminated over Dayton by the onset of mixing in the lower atmosphere. Figure 4, the analysis at 1900 EST, shows the east-to-west onset of increasing stability associated with sunset. The $b_{scat}$ maximum shown here over Dayton probably indicates the presence of an urban pall.

Discussion

Isentropic surfaces have been used in modeling tropospheric and stratospheric transport (David and Wendell, 1976; Danielsen and Deaven, 1974). In theory, pollutants emitted into the mixed layer during the day are dispersed through the depth of the mixed layer, more or less uniformly. As surface heating diminishes, stable layers form. Pollutants within these layers cease to disperse vertically; more importantly, they decouple from surface deposition processes. Pollutants aloft are then transported by the mean flow along the isentropic surfaces. If sufficient heating is available the following day, the boundary layer will again rise to its previous full depth and reincorporate the pollutants into the mixed layer. If surface heating is weaker, the maximum boundary layer height will be below the isentropic layers containing the previous day's pollutants, and the layer established during the night will remain essentially intact.

The $b_{scat}$ analyses in Figures 2 and 3 do suggest transport of pollutants along the isentropic surfaces. The $b_{scat}$ maximum occurs at the 305°K isentrope in both analyses. Because the boundary layer eventually grew to a sufficient height (306 °K isentrope, Figure 4), the denser layer of light-scattering particles was diffused into the mixed layer by late afternoon.

Results obtained in this trial are considered quite promising, and further experiments of this kind are planned.

## References

Danielsen, E. F. and D. G. Deaven, 1974: Northern hemispheric analysis methods for deriving two-dimensional transport model of troposphere and stratosphere from isentropic trjectories and potential vorticity. Proceedings, International Conference on Structure, Composition, and General Circulation of the Upper and Lower Atmosphere, and Possible Anthropogenic Perturbations, Melbourne, Australia, January 14—25, 1974, pp. 835—848.

Davis, W. E. and L. L. Wendell, 1976: Some effects of isentropic vertical motion simulation in a regional scale quasi-Lagrangian air quality model. Preprints, Third Symposium on Atmospheric Turbulence, Diffusion, and Air Quality, Raleigh NC, October 19—22, 1976, pp. 403—406.

Environmental Research and Technology, Inc., 1976: Design of the Sulfate Regional Experiment. EPRI EC-125, I-IV.

# THE AMBIENS EXPERIMENT

B. B. Hicks

## Introduction

The Sangamon experiments of 1975 and 1976 were intensive investigations of the evolution of the Planetary Boundary Layer (PBL), conducted over flat farmland in central Illinois (Hess and Hicks, 1975; Sisterson et al., 1976). Portions of the Sangamon studies addressed questions regarding the depth of the mixed layer in which pollutants emitted near the surface are free to disperse (Yamada and Berman, 1977), the evaluation of geostrophic winds (Lipschutz, 1975; Yamada et al., 1977), the derivation of spatially averaged sensible heat and momentum fluxes (Hicks and Wesely, 1977a,b), and the surface deposition of pollutants (Wesely et al., 1977). Cooperative work with other organizations addressed questions of air chemistry, such as sulfate speciation and trace metal concentrations. In 1976 considerable support from other MAP3S[*] laboratories was received. In particular, a Battelle Pacific Northwest Laboratory aircraft was used to monitor pollutant profiles through the PBL above and site of the Sangamon study.

Several of the laboratories participating in the MAP3S program have been actively pursuing field experimental programs closely related to the Sangamon efforts. In October 1977, the MAP3S community conducted a combined experimental investigation of the Atmospheric Mass Balance of Industrially Emitted and Natural Sulfur (AMBIENS). This experiment was seen as a logical extension of previous single-laboratory experiments, each of which addressed parts of the problem of pollutant transformation, transport, diffusion, and deposition that confront the MAP3S program as a whole. The specific aim of the AMBIENS experiment was to combine previously independent investigations of pollutant behavior in order to test how well contemporary methods for formulating the above processes succeed in explaining observations.

---

[*]The Multistate Atmospheric Power Production Pollution Study of the U.S. Department of Energy.

For AMBIENS, it was proposed to attempt a pollutant box-budget study in an area similar to that defined by the grid mesh of regional-scale numerical models. A "box" of about 100 km × 100 km was selected as a compromise between conflicting chemical and meteorological requirements, and an early decision was made to locate the box in an area with very few local sources (see Figure 1). In this way, regional pollution that results from transport over long distances, greater than in previous studies of plumes from well-identified single point sources, was to be investigated. Southeastern Indiana was chosen as the location of the study. This area is relatively flat, has no large pollution sources, and in southwesterly flow is downwind of large sources in the Ohio River Valley.

## Experiment Description

Figure 2 shows the distribution of equipment and facilities at the AMBIENS central site, which was located midway between Shelbyville and Rushville, near Manilla, Indiana. A photograph of the site is presented elsewhere (Wesely, 1977). Table 1 summarizes the goals of the AMBIENS experiment by listing the key questions which were addressed and the methods (and organizations) identified in response to each item. Table 2 presents a different breakdown of the experiment; the list is of core experimental components, sorted according to participating organization. A number of peripheral experiments are also listed. The extensive investigation of PBL evolution conducted by this Laboratory during the AMBIENS study has been entitled the "Rush Experiment" in order to separate this extension of earlier PBL experiments from the pollutant budget studies performed under AMBIENS. In keeping with the identification procedure used in previous studies of this type, the Rush Experiment is named after the country in which the main field site was located.

At the central site, basic air quality and meteorological measurements were made on all but two days between 3 and 14 October 1977. High resolution profiles of wind and temperature were obtained hourly from 0700 to 1600 by the use of balloon-borne miniature radiosondes tracked by means of automatically-interrogated digital theodolites. The depth of the mixed layer was

10

FIG. 1.--The area of the 1977
AMBIENS experiment, showing the
preferred orientation of the AMBIENS
"box" in southern Indiana. The
main site was located near Manilla,
and aircraft were operated from air-
ports at Columbus (PNL) and
Shelbyville (BNL). Crosses indicate
the sites of the ANL microbarograph
network.
(ANL Neg. 149-78-149)
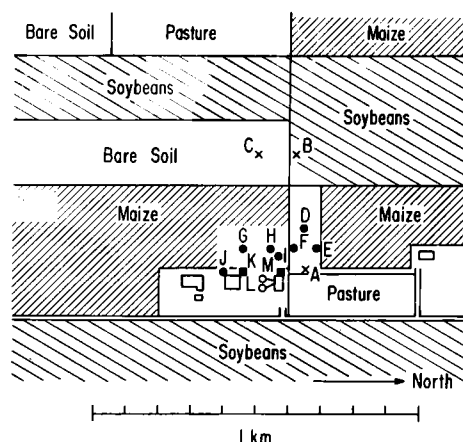
FIG. 2.--The distribution of
equipment at the main AMBIENS
field site near Manilla, Indiana.
WHAT system baselines were
determined by the theodolite
locations A, B, and C. (B and C
were alternative locations for the
remote theodolite). Basic meteor-
ological data were measured by
use of a ten-meter tower at D; E
and F identify alternative sites
for eddy flux measurement (selec-
ted according to the prevailing
wind); G and H are sites for
gradient measurements of particle
concentration (at G) and wind and
temperature (at H). Net radiation
was measured at I. An acoustic
sounder and a set-dry precipitation
collector were operated at J; K and
M are the sites of trailers used as
centers for PBL and micrometeor-
ological activities, respectively;
L marks the location of lidar
operations; N shows the site of
ground-level "filter-pack" mea-
surements made by BNL.
(ANL Neg. 149-78-148)

Table 1. A Breakdown of the AMBIENS Core Experiment (Laboratory Designations are as Identified in Table 2)

Aim: To test our understanding of the behavior of atmospheric sulfur compounds over distances of the order of 100 kilometers

Contributing Key Questions:

| | |
|---|---|
| Chemical transformation | Aircraft (BNL; PNL) |
| Horizontal flux divergence | Aircraft (BNL; PNL); COSPEC (EMI) |
| Surface pollutant fluxes | Eddy correlation for ozone, particles (ANL); gradient method for particulate sulfur (PNL); aerodynamic technique for $SO_2$ (ANL) |
| Planetary boundary layer structure | Lidar (SRI); Sodar (ANL); WHAT system profiles (ANL) |
| Micrometeorology | Normal meteorological observations, plus wind gradients and eddy fluxes of heat and momentum at main site (ANL) |
| Geostrophic winds | Microbarograph network (ANL) |
| Meteorological support | National Weather Service support (ANL); ARAC (LLL) |
| "Box integrity" test | Tracer experiments (BNL; ANL) |
| Precipitation chemistry | Wet/dry collector (ANL; Network (PNL) |
| Surface air chemistry | Sulfur compounds (BNL; PNL; EMI; ANL); trace metals (BNL; PNL); ozone (ANL) |

Table 2. The Breakdown of Tasks Contributing to the AMBIENS Core Experiment, and a Listing of Peripheral Studies

| Laboratory | Core experiment component | Peripheral experiment |
|---|---|---|
| Brookhaven National Laboratory (BNL) | Aircraft monitoring<br>Surface filter packs<br>$SF_6$ tracer experiment | Trace metals |
| Battelle Pacific Northwest Laboratory (PNL) | Aircraft monitoring<br>Particle fluxes | Trace metals |
| Argonne National Laboratory (ANL) | WHAT system profiles<br>Sodar<br>Geostrophic and thermal winds<br>Micrometeorology<br>Particle fluxes<br>Surface sulfur<br>Precip. chemistry | PBL evolution<br>Deuterated ethane<br>Ozone fluxes |
| Lawrence Livermore Laboratory (LLL) | Atmospheric release<br>Advisory capability | Test of ARAC |
| SRI International (SRI) | Lidar<br>Nephelometry | |
| Environmental Measurements, Incorporated (EMI) | COSPEC<br>Surface sulfur | |
| Naval Research Laboratory | | Atmospheric conductivity |

13

monitored by sodar, and the presence of pollutant layers aloft was detected by lidar. Surface fluxes of sensible heat and momentum were measured during most daylight hours, and a number of determinations of pollutant eddy fluxes were also made. The pollutant flux measurements were supported by gradient measurements on some occasions. Some of the resuls obtained in studies at the central site are given elsewhere in this report.

In order to test the accuracy with which trajectories through the AMBIENS box can be computed from wind observations at the Manilla site, three tracer experiments were performed. Two of these experiments used sulfur hexafluoride and were performed by personnel from Brookhaven National Laboratory in conjunction with tests of an airborne real-time $SF_6$ detector. A third tracer experiment tested a new material, deuterated ethane, presently being developed as an atmospheric tracer by this Laboratory.

Aircraft operated by Brookhaven National Laboratory and by Battelle Pacific Northwest Laboratory were based at Shelbyville and Columbus, Indiana, respectively. On meteorologically suitable occasions, these aircraft were used to determine the transport of pollutants out of the Ohio River region and into the previously defined area of southeastern Indiana. Several hours later, the same aircraft measured the transport of material leaving the chosen area, in the same air mass. A mobile, vertically-pointing correlation spectrometer was used to monitor the amounts of sulfur dioxide entering and leaving the AMBIENS box. The experimental plan calls for these measurements to be coupled with chemical transformation and surface deposition data in order to derive pollutant budgets in the area of interest. Analyses of data derived in these studies are still under way; results will be presented in due course by the individual laboratories concerned. It already seems clear that only three occasions were suitable for close scrutiny: 5, 7, and 10 October. On these days, attempts were made to determine the horizontal fluxes of sulfur dioxide on the basis of ventilation winds obtained at the Manilla site and $SO_2$ overburdens measured by correlation spectrometry. The spectrometer data in this demanding application appear to be subject to relatively large errors, which will make interpretation of the flux data exceedingly difficult (q.v., Peache, 1978).

However, on these (and other) days the correlation spectrometer succeeded in monitoring a number of individual plumes as they passed across the AMBIENS box. On every occasion, total mass flux of sulfur dioxide decreased with increasing distance downwind in the plume. It remains, therefore, to relate these observations to aircraft determinations of chemical transformation rates and micrometeorological evaluations of surface removal rates.

## References

Hess, G. D. and B. B. Hicks, 1975; A Study of PBL Structure: The Sangamon Experiment of 1975. Argonne National Laboratory Radiological and Environmental Research Division Annual Report January-December 1975, ANL-75-60, Part IV, pp. 1—4.

Hicks, B. B. and M. L. Wesely, 1977a: Momentum fluxes over adjacent soybeans and maize fields: Sangamon 1975. This report.

_____, and M. L. Wesely, 1977b: Thermal characteristics of adjacent soybean and maize fields: Sangamon 1975. This report.

Lipschutz, R. C., 1975: Sangamon Experiment — Geostrophic Wind Profiles. Argonne National Laboratory Radiological and Environmental Research Division Annual Report, January-December 1975, ANL-75-60, Part IV, pp. 16—21.

Peache, M. A., 1978: Sulfur Dioxide Measurements and Mass Flux Calculations in Support of the AMBIENS Field Experiment. Technical Report— EMI Project 1410, available from Environmental Measurements, Inc., San Francisco.

Sisterson, D. L., B. B. Hicks, and M. L. Wesely, 1976: An Outline of the 1976 Sangamon Experiment. Argonne National Laboratory Radiological and Environmental Research Division Annual Report, January-December 1976, ANL-76-88, Part IV, pp. 1—6.

Wesely, M. L., 1977: Surface characteristics of the 1977 AMBIENS site. This report.

_____, J. A. Eastman, D. R. Cook, and B. B. Hicks, 1977: A comparison of aerodynamic-to-canopy resistances for ozone uptake by maize. This report.

Yamada, T. and S. Berman, 1977: Estimating the growth of the mixing layer height with the model of Tennekes. This report.

_____, R. G. Everett, and S. Berman, 1977: Surface geostrophic winds during the 1975, 1976, and 1977 experiments. This report.

# SURFACE CHARACTERISTICS OF THE 1977 AMBIENS SITE

M. L. Wesely

## Introduction

Studies of the transport and diffusion of pollutants in the Planetary Boundary Layer (PBL) are aided substantially by knowledge of surface characteristics. Information concerning momentum and heat fluxes has been gathered in some previous PBL field studies, such as the 1975 and 1976 Sangamon experiments described in this and previous Annual Reports. In the 1977 AMBIENS[*] experiment (Hicks, 1977), these fluxes were again measured by eddy-correlation techniques at the central site. A further requirement for the AMBIENS effort was to obtain estimates of the rates of dry deposition of sulfur dioxide and sulfate particles. The estimates are eventually to be used in the multi-laboratory effort to evaluate the feasibility of determining a mass balance of airborne sulfur pollutants over the AMBIENS area, and similar areas. The present purpose is to outline the results of the dry deposition work, specifically on the use of the eddy-correlation measurements.

## Field Conditions

The surface conditions of the central site are partially described elsewhere in this Annual Report (Hicks, 1977; Wesely et al., 1977b). It was hoped during planning of the experiment that an early harvest of maize and soybeans would take place, but a rainy autumn prevented this and so most of the micro-meteorological work was performed over cornstalks (senescent maize). Figure 1 shows the condition of the maize canopy. The surrounding fields were devoted about one half to maize and the remainder to soybeans, which were being harvested during the AMBIENS experiment. Figure 2 shows the area in the immediate vicinity of the AMBIENS central site. There were a few small scattered fields of pasture for grazing by domestic livestock. These pastures presented a discontinuity in surface energy balance because they were seeded to

---

[*]Atmospheric Mass Balance of Industrially Emitted and Natural Sulfur
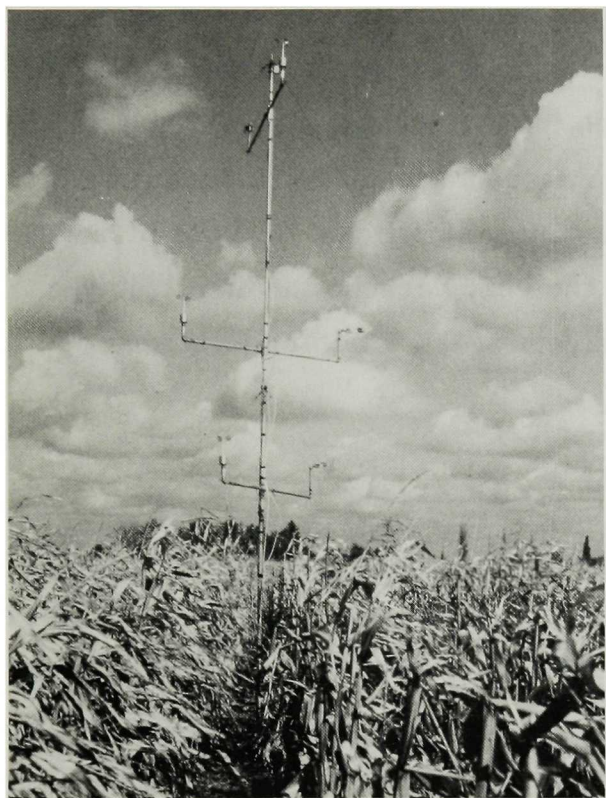
FIG. 1.--View of the maize canopy and a mast that supports cup anemometers and thermometer apparatus.



FIG. 2.--Aerial view of the AMBIENS central site and surrounding fields. The micrometeorological instrumentation was deployed at a location near the left center of the photograph in a maize field.

cool-season grasses, mainly brome grass, which continued to grow and transpire and thus allowed greater evaporation rates than in the fields of bare soil and senescent field crops. Although the differences in latent and sensible heat fluxes were not determined by direct measurement, the disturbances of surface energy balance are considered not very significant in terms of modifications of the fluxes that affect flow in the PBL, because the area that was pasture was quite small, perhaps ten percent of the total AMBIENS area (about $10^4$ km$^2$).

### Eddy Fluxes

Only a few brief examples will be given here. Figure 3 shows the friction velocity $u_*$ and the sensible heat flux H measured on October 5 above the maize. These were measured with eddy-correlation equipment frequently used by this Section. The rather high values of $u_*$ on October 5 correspond to moderately high values of wind speed, which occurred on several days. By examination of near-neutral wind-speed profiles obtained with the three cup anemometers shown in Figure 1, the displacement height was calculated to be $123 \pm 12.5$ cm and the surface roughness to be $9.8 \pm 1.8$ cm. The Bowen ratio (H/LE) of sensible-to-latent heat flux was found to be near 0.5 during most of the daytime, where LE was assumed equal to the net radiation minus the sensible heat flux. Such estimates of LE, however, are probably too large, because the crop was not transpiring and the source of the water vapor was primarily the moist soil beneath the maize canopy. Also, in places the canopy was sparse and allowed much of the insolation to penetrate to the soil surface, so that the soil storage term was probably large. Thus, incorporation of the soil heat flux into the evaluation of LE would result in smaller and more acceptable estimates of LE.

Particle fluxes were measured as has been done previously by use of the "charger" from Washington University (Wesely et al., 1977a). The fluxes at times indicated that the surface was effectively an efficient sink for particles. Surprisingly, though, the particle flux often changed sign. The surface appeared to be a source of small particles (0.05—0.1 μm in diameter) during late
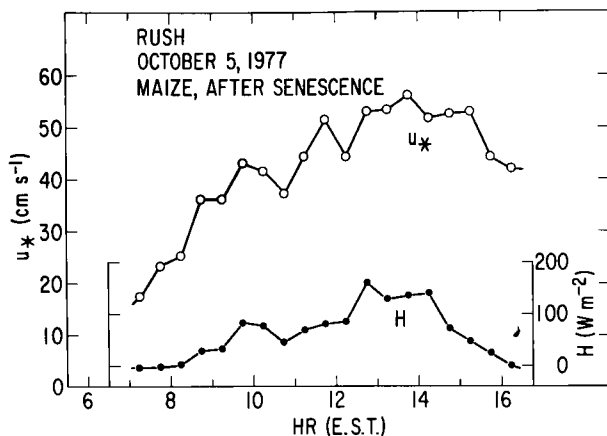
FIG. 3.--Example of momentum and heat fluxes measured by eddy correlation. (ANL Neg. 149-78-9)

morning and most of the afternoon; this corresponded to surface warming and to ozone concentrations exceeding about 25 ppb.

These particle fluxes are certainly not a good indication of the fluxes of particulate sulfur. Mean concentrations measured with the charger were poorly correlated with concentrations of particles greater than 0.3 μm measured at the AMBIENS site. Hence, for the purposes of AMBIENS, the particle eddy fluxes cannot necessarily be used directly to estimate sulfate dry deposition. Parameterizations derived for occasions when the ozone concentrations were small will be relied on at present. On the basis of charger data collected at this experiment and others, the best guess currently for the deposition velocity for sulfate particles is

$$v_d = ku_*[\ln(z/z_0) + ku_* - \psi_H]^{-1} , \qquad (1)$$

where z is the height in the atmospheric surface layer, k is the von Karman constant, and $\psi_H$ is the familiar diabatic correction. This relationship will be revised when more adequate data are obtained.

Ozone fluxes were also measured at the AMBIENS site. Instrumentation is described elsewhere in this report (Cook and Wesely, 1977; Eastman et al., 1977), as are some of the results (Wesely et al., 1977b). Unfortunately, information on the relationship of ozone fluxes to sulfur dioxide fluxes for such a surface is lacking, so we can only guess that the resistances to uptake are about the same. Recent field data collected by this Section indicate that this

19

is probably the case for maize in midseason, but the mechanisms that control uptakes by the soil and senescent maize are surely not the same as for a dense, green maize canopy.

## Conclusions

The eddy-correlation measurements at the AMBIENS central site should give some indication of the heat flux and stress near the surface, but they should not be considered truly representative of the surrounding area unless other data are confirmatory. The stress over fields smoother than the senescent maize is probably less, and a reasonable estimate might be made on the basis of estimated surface roughnesses. Past experiments (Hicks and Wesely, 1977) may provide some insight. For heat flux, a comparison will be made with estimates derived from acoustic sounder measurements (Coulter, 1977), so that a corrective factor can be determined for atmospherically unstable conditions. The data on particle and ozone fluxes can be used to estimate the fluxes of sulfate particles and sulfur dioxide only with considerable speculation. Nevertheless, rough estimates will be made as a contribution to the overall AMBIENS effort.

## References

Cook, D. R. and M. L. Wesely, 1977: Modifications of an ozone sensor to permit eddy-correlation measurements of vertical flux. This report.

Coulter, R. L., 1977: Digital acoustic data from the Rush experiment. This report.

Eastman, J. A., M. L. Wesely, and D. R. Cook, 1977: A comparison of two chemiluminescent ozone detectors used in eddy-correlation measurements. This report.

Hicks, B. B., 1977: The AMBIENS experiment. This report.

_____, and M. L. Wesely, 1977: Momentum fluxes over adjacent soybean and maize fields: Sangamon 1975. This report.

Wesely, M. L., B. B. Hicks, W. P. Dannevik, S. Frisella, and R. B. Husar, 1977a: An eddy-correlation measurement of particulate deposition from the atmosphere. Atmos. Environ. 11, 561–563.

_____, J. A. Eastman, D. R. Cook, and B. B. Hicks, 1977b: A comparison of aerodynamic-to-canopy resistance for ozone uptake by maize. This report.

# BOX BUDGET AND TRACER EXPERIMENTS DURING AMBIENS

J. D. Shannon and B. B. Hicks

---

A series of box budget and tracer studies formed a major part of the AMBIENS experiment, described in greater detail elsewhere (Hicks, 1977). The box budget experiments were to a considerable extent feasibility studies, since it was not known whether or not concentrations and corresponding horizontal fluxes could be measured with sufficient accuracy for testing regional-scale surface removal and transformation rate hypotheses. The bases for selection of the AMBIENS site were the absence of significant local pollutant sources and the frequently upwind presence of numerous atmospheric sulfur sources along the Ohio River, which subtends the arc from west-southwest through south to east, relative to the central AMBIENS site.

It was felt that southwesterly flow was the most desirable situation for box budget experiments for several reasons. First, there are numerous sources to the southwest, but at a distance sufficient for the various transformation and removal rates to be representative of the region rather than of a plume. Second, southwesterly flow in Indiana is frequently associated with maritime tropical air, and higher sulfate concentrations generally occur with higher humidity. Third, southwesterly flow is likely to exist through a layer sufficiently deep and to prevail for a period sufficiently long for an experiment to be conducted without the complication of marked wind shifts in space or time. Fourth, the layout of roads in the area is such that arcs of ground samplers for tracer experiments can be easily located on roads perpendicular to southwesterly flow.

Personnel from Brookhaven National Laboratory conducted tracer experiments using releases of sulfur hexafluoride. Sufficient material was available for experiments to be performed on three days. In conjunction with these studies, tests of deuterated ethane as an atmospheric tracer were conducted by workers from this Section, but in this case the number of possible experiments was limited to one by the sampling capability.

Southern Indiana experienced several synoptic cycles during the experimental period. Southwesterly flow occurred during each cycle, but not always during daytime hours. Three days were selected for box budget and tracer experiments, based upon forecasts made the previous evenings.

October 5. The forecast was for steady SW winds lasting throughout the day, preceding a frontal passage by the morning of October 6. During the predawn hours of October 5, a band of light rain from middle level clouds passed across southern Indiana. This unforecast rain discouraged the tracer release personnel, and they cancelled their release. However, after the rain moved eastward the weather was as forecast, and the aircraft proceeded with the box budget experiment during the day.

October 7. Light southeasterly flow was forecast. Since the experiment was nearing the halfway point, an $SF_6$ (but not heavy ethane) release was made in order to test capabilities and ground/aircraft coordination. The flow was indeed southeasterly, but considerably stronger than expected, and the aircraft box, which was limited in size by the presence of Indianapolis to the northwest, was smaller than desired for sufficient $SO_2$-sulfate transformation.

October 10. The forecast was for south-southwesterly flow changing to southwesterly and strengthening as a front approached. Both $SF_6$ and heavy ethane were released. The initial period was as forecast; however, the development of a depression along the front and the resulting convergence into the low pressure center caused the winds to back and the flow to become southerly to south-southeasterly during the afternoon. Since the line of $SF_6$ and heavy ethane samplers had been positioned on the basis of the forecast and early observations, the arc was not properly centered about the tracer plume. However, the western end of the sampling arc did detect the $SF_6$, and the aircraft sampling patterns were shifted westward.

October 14 also was an occasion of southwesterly flow. However, this was the planned final day of the experiment, and operations were limited by accumulated equipment breakdowns and other technical problems.

Expected tracer trajectories, based upon the release times and the ventilation winds measured at the central AMBIENS site, are shown in

Figures 1 and 2 for October 7 and 10, respectively. Analysis of the data is in progress.
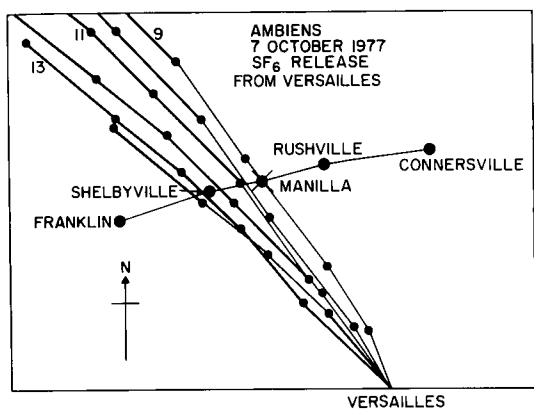


FIG. 1.--Estimated trajectories of tracer material on 7 October 1977. Tracer release is assumed to commence at 0900, and trajectories are calculated on the basis of ventilation winds obtained every hour at the Manilla site. Heavy lines indicate the expected location of tracer material during the period 1300 to 1800, the approximate time that samplers were open along the indicated highways.
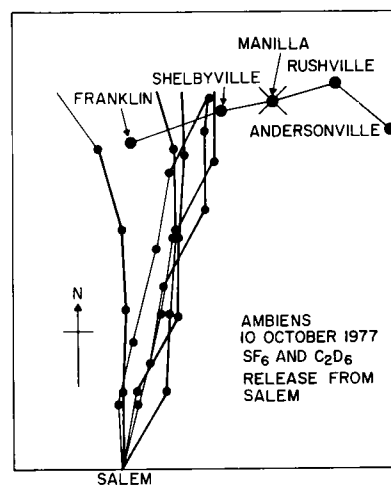


FIG. 2.--Same as Figure 1, except for 10 October 1977.

Reference

Hicks, B. B., 1977: The AMBIENS experiment. This report.

# PRELIMINARY WIND AND TEMPERATURE PROFILES IN THE PLANETARY BOUNDARY LAYER OBSERVED NEAR MANILLA, INDIANA

T. Yamada and P. E. Hess

---

Field experiments were conducted near Manilla in Rush County, Indiana, in conjunction with the AMBIENS study investigating the mass balance of sulfur oxides. As part of this observational program, wind and temperature profiles within the Planetary Boundary Layer (PBL) were obtained using the WHAT system (Frenzen and Prucha, 1974). Measurements were taken every hour from 0700 to 1700 EST on days without rain during the period of investigation (3-14 October 1977); a total of 100 hours of wind data and 84 hours of temperature data are available. Hourly variations of horizontal wind-speed profiles on 10 October are shown in Figure 1. As expected, wind profiles in the afternoon are much more uniform than those in the morning because of strong vertical mixing due to afternoon turbulence.

Evolution of the mixed-layer height (defined as the height where the temperature profile departs from dry adiabatic) on 5 October is depicted in
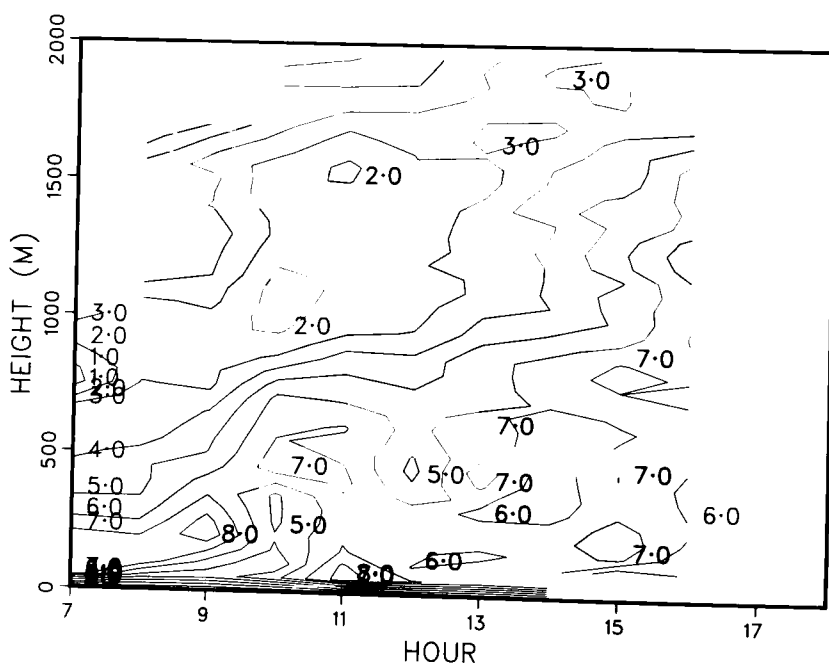


FIG. 1.--Hourly horizontal wind-speed profiles on 10 October 1977 near Manilla, Indiana. Units are m s$^{-1}$.

Figure 2. Although slightly lower, mixed-layer heights obtained from the temperature profiles are generally comparable to those obtained from an acoustic sounder also located at the Manilla site (see Coulter, 1977). The difference may be due to the fact that the acoustic sounder receives a maximum return from the region of maximum temperature variance. This region may be higher than the mixed-layer height obtained from temperature profiles alone, due to penetration of turbulence into the inversion layer above. Wind and temperature data will be used in computing trajectories for box budget studies of sulphur dioxide and sulfate, and in evaluating atmospheric tracers tested during the AMBIENS study. Also, complete analyses of the wind and temperature data according to similarity theory for the PBL will be conducted as soon as the surface turbulent-flux analyses are completed.
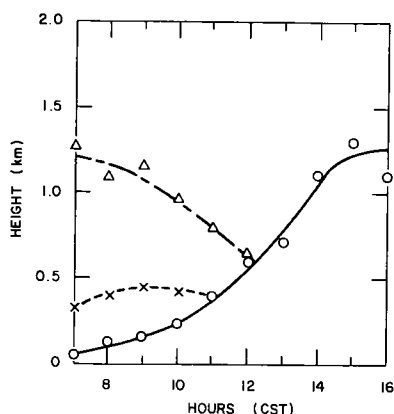


FIG. 2.--Evolution of the mixed layer heights on 5 October 1977 near Manilla, Indiana. x, o, and Δ represent the top of the nocturnal inversion layer, the mixed-layer height, and the base of an upper inversion, respectively.

References

Coulter, R. L., 1977: Mixing-layer heights from the Rush experiment. This report.
Frenzen, P. and L. L. Prucha, 1974: The WHAT system: A digitized radio-sonde and double-theodolite balloon-tracking system for planetary boundary-layer investigations. Atmos. Technol. 6, 129-134.

# DIGITAL ACOUSTIC DATA FROM THE RUSH EXPERIMENT

R. L. Coulter

## Introduction

Acoustic sounder (sodar) data have commonly been in the form of facsimile records in the field programs of this Section. Digital data from these instruments have been taken only occasionally (Hess and Wesely, 1973; Black and Miller, 1974). During the recent Rush experiment conducted in October 1977 near Manilla, Indiana, digital sodar data were again taken, with the aim of making this a permanent part of the Section's experimental capability. The results of this experiment are discussed in this report.

## Data Collection

The amplitude of the signal detected by the sodar (proportional to the intensity of the scattered acoustic wave) was digitized using a TMC pulse height analyzer. Samples were taken every 0.028 or 0.044 seconds (equivalent to 5 and 7.5 meters in the vertical, respectively), beginning 0.1 second after the acoustic pulse was transmitted, until 200 storage locations were filled (equivalent to approximately 1000 to 1500 meters, respectively, in maximum height). Thus, the sequential storage locations represent height above the surface. Successive values detected for 45 pulses were added to each storage location, resulting in a 15-minute integrated "pulse." These integrated pulses were then stored on paper tape. Unfortunately, the data transfer was not always successful, and some data were unusable. As noted by Hess and Wesely (1973), this method of data storage is not very reliable or efficient, but it was all that was available at the time.

## Discussion

Using the retrievable digitized data, a reconstruction of the facsimile chart record in integrated form is easily done using the computer facilities available at ANL. Figure 1 is a three-dimensional (height, time, amplitude)
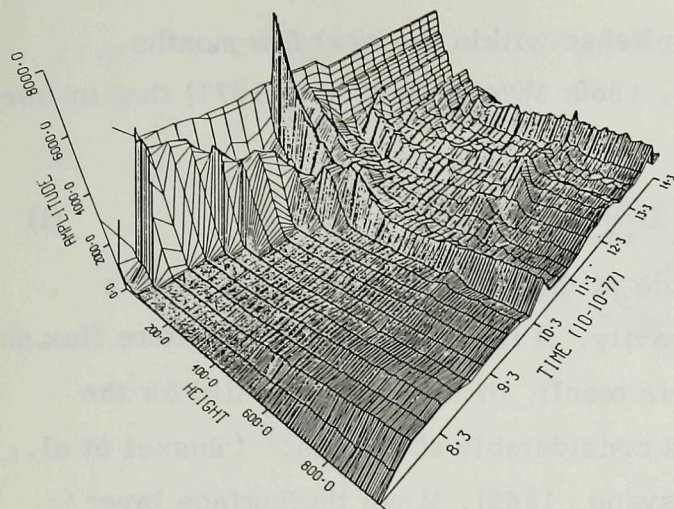
FIG. 1.--A three-dimensional picture of the atmospheric structure as detected by sodar. The x axis is height in the atmosphere. The y axis (into the paper) is elapsed time, and the z axis is amplitude.

depiction of the atmospheric structure as detected by the sodar on October 10. The z axis in this representation is proportional to the signal amplitude, with arbitrary magnitude. In addition to the 15-minute integration along the time axis (into the paper) done on line by the pulse-height analyzer, the data have been passed through a five-weight binary filter along the height axis. This filter has the effect of a low pass filter on the data and has no inherent phase shift, which can be present in simple averaging.

The mixing layer height is easily recognizable, rising rapidly from the surface to approximately 700 m by 1100 hours and becomes quasi-stationary (see Coulter, this report). In addition, we can see the relative magnitude of the temperature fluctuations occurring at the top of the mixing layer and the decrease through the day as the strength of the capping inversion gradually decreases. The signal amplitude at the top of the mixing layer in the morning is three times that in the afternoon. However, a large part of this difference is probably due to the height difference of the returns at the two times. Also, the "bumpy" character of the returns within the mixing layer gives evidence of the strength of the thermals within this layer, their frequency of occurrence, and their decreasing intensity with height. If the sodar system were calibrated, that is, if the relationship between output voltage and acoustic pressure level were know, and the acoustic energy transmitted into the atmosphere were known, then the z axis could be stated in terms of $C_T^2$, the temperature structure constant, and knowledge gained directly of the level of thermal turbulence

27

within the PBL. This will be accomplished within the next few months.

It has been shown (Obukhov, 1960; Wyngaard et al., 1971) that in free convection

$$C_T^2 = [4/3\,k^{-2/3}]\;[\overline{T}/g]^{2/3}\;H^{4/3}\,z^{-4/3}\;, \tag{1}$$

where $\overline{T}$ is the average air temperature at the surface, k is von Karman's constant, g is the acceleration of gravity, H is the surface temperature flux and z is the height above the surface. This result, though strictly valid for the surface layer only, apparently holds considerably above that  ( Russel et al., 1974; Wyngaard et al., 1971; and Tsvang, 1969). When the surface layer is stable, $C_T^2$ should vary more slowly than $z^{-2/3}$ and increase to $z^{-2/3}$ under neutral conditions (Wyngaard et al., 1971). If we assume that the detected signal voltage is directly proportional to the backscattered acoustic energy (Coulter, 1976), then we can plot the log of the digitized signal amplitude versus the log of the height, as in Figure 2A and 2B, and test this relationship. Each curve represents one integrated pulse (15 minutes, or 45 samples at each height). Those in Figure 2A were taken during unstable conditions and illustrate a slope quite close to -4/3 for heights less than 300 m (mixing layer height approximately 800 m). Those in Figure 2B show a transition from stable to unstable conditions in the morning hours. The stable data (A,B) have a slope considerably less than -4/3, dropping off very rapidly above 160 m where there is no discernable scattered signal. The third curve (C) has a steeper slope quite close to -4/3, as unstable conditions are established below the mixing layer height.

In any discussion concerning turbulence variables, the averaging time is very important. It should be as long as possible and yet be subject to little or no change in the mean conditions within which it exists. Thus, there are many instances on a short time scale in which this relationship does not hold (Wyngaard et al., 1971). In fact, for the data taken in this experiment, some of the data exhibited slopes closer to -1 than -4/3. The averaging time for these data was 15 minutes, which may be too short in some instances, particularly if a well developed thermal passes over the sodar. Note also that the
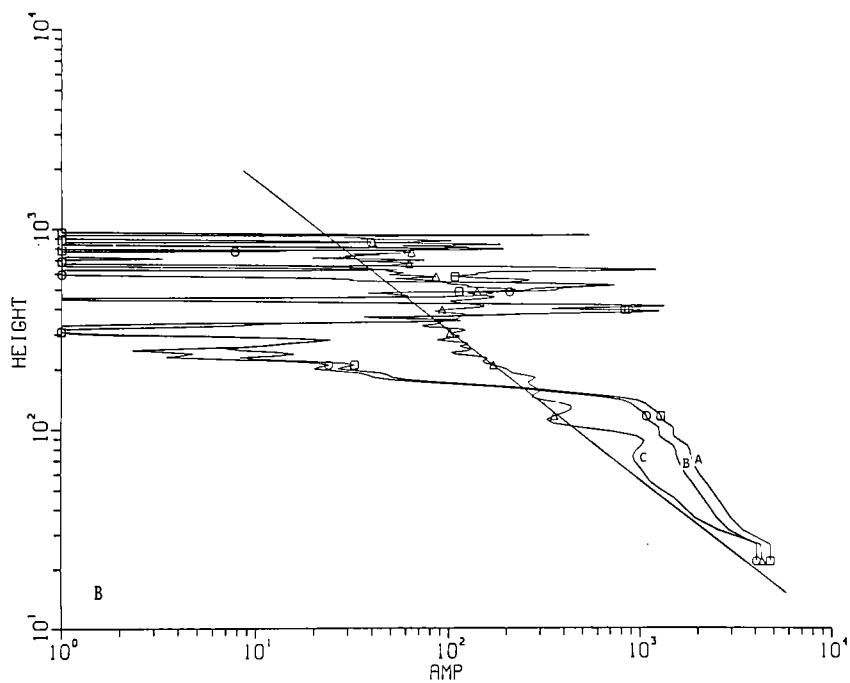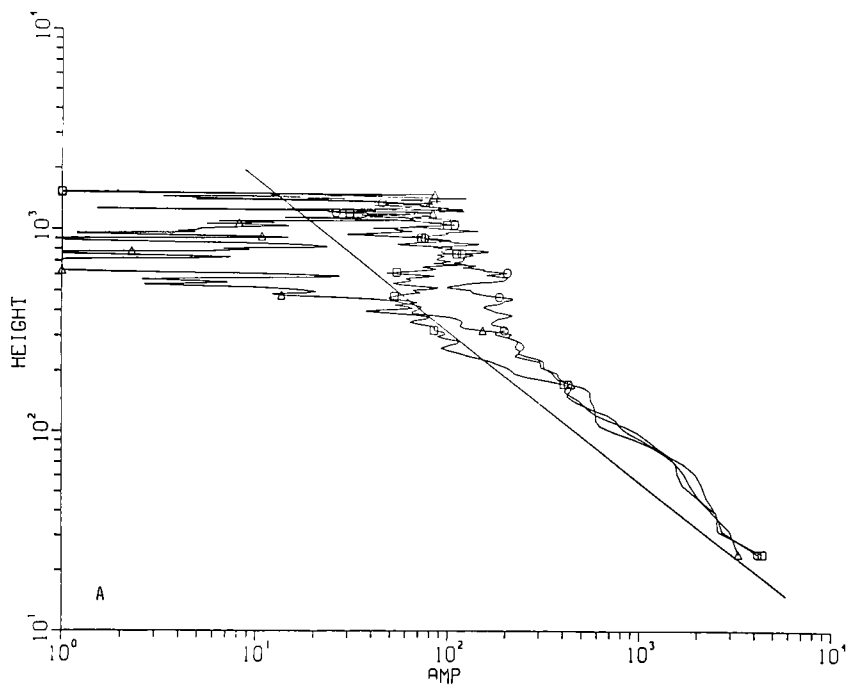
FIG. 2.--Plots of the variation of returned signal strength with height in the atmosphere. Each plot represents a 15-minute average; $\triangle$'s, $\square$'s, and o's delineate separate averages, one symbol every 20 points.

-4/3 slope does not exist up to the top of the mixing layer but flattens out at approximately half the mixing layer height. Frisch and Ochs (1975) observed agreement up to 0.1 of the mixing layer height under marine conditions, while the data of Neff (1975) show agreement up to 0.3 times the mixing layer height.

Under convective conditions, with a well-defined -4/3 slope, Eq. 1 indicates that the surface heat flux can be calculated if the temperature is known. Following the calibration of the sodar system, this will be done, and the results will be compared with the simultaneous eddy correlation heat flux measurements made during the Rush experiment. The comparison should be informative, for the sodar estimate is an areal average while the eddy correlation is a point estimate.

## Conclusions

Digital sodar data taken during field experiments can be used to give a good picture of the evolution of the Planetary Boundary Layer. With proper calibration of the sodar and care in handling of the data, values for surface heat flux can potentially be obtained under free convection conditions.

The system used in the present experiment for digitizing and storing the data was cumbersome at best. With the recent addition of a minicomputer, this capability has been considerably enhanced by using the computer-controlled A-D converter and plotting capabilities available with this system. It is now possible to collect digital acoustic data directly during the Section field experiments.

## References

Black, William C. and Edward L. Miller, 1974: Real-Time Processing of Acoustic-Sounder Data with a Microcomputer. Radiological and Environmental Research Division Annual Report, January-December 1974, Part IV, pp. 80—86.

Coulter, R. L., 1976: System geometry and interpretation of sodar data. Ph.D. Thesis, Penn State University, pp. 90—100.

——————————, Mixing layer heights from the Rush experiment. This report.

Frisch, A. S. and G. R. Ochs, 1975: A note on the behavior of the temperature structure parameter in a convective layer capped by a marine inversion. J. Appl. Meteorol. 14, 415—419.

Hess, P. E. and M. L. Wesely, 1973: Digitization of acoustic-sounder data, Radiological and Environmental Research Division Annual Report, Part IV, pp. 85–92.

Neff, W. D., 1975: Quantitative evaluation of acoustic echoes from the planetary boundary layer. NOAA Technical Report TR ERL 322-WPL 38.

Obukhov, A. M., 1960: The structure of the temperature and velocity fields in free convection, Izv. Akad. Nauk. USSR, Ser. Geofiz. No. 9, English translation pp. 928–930.

Russel, P. B., E. E. Uthe, F. L. Ludwig, and N. A. Shaw, 1974: A comparison of atmospheric structure as observed with monostatic acoustic sounder and lidar techniques. J. Geophys. Res. 79(36), 5555–5566.

Tsvang, L. R., 1969: Microstructure of temperature fields in the free atmosphere. Radio Sci. 4, 1175–1177.

Wyngaard, J. C., J. Izumi, and S. A. Collins, Jr., 1971: Behavior of the refractive index structure parameter near the ground. J. Opt. Soc. Am. 61, 1646–1650.

# MIXING LAYER HEIGHTS FROM THE RUSH EXPERIMENT

R. L. Coulter

## Introduction

Evaluation of pollutant transport and diffusion is highly dependent upon the structure of the Planetary Boundary Layer (PBL), in particular the height of the well-mixed layer. By its very name this parameter indicates its importance: passive quantities (e.g., particles and aerosols) are more or less uniformly mixed throughout this layer by turbulence forced by strong surface heating during the daytime hours; thus, its variation with large scale weather systems and local terrain helps determine the amount and distance of pollutant transport. The ability of acoustic sounders (sodars) to monitor the mixing layer height has been demonstrated many times (Beran and Hall, 1973; Wycoff et al., 1973). During the recent Rush experiment conducted near Manilla, Indiana in October 1977, mixing layer heights were determined by an ANL sodar, as well as by a Stanford Research Institute (SRI) lidar and the ANL WHAT system (Frenzen and Prucha, 1974). The mixing layer heights determined by the three methods are compared in this report.

## Mixing Layer Heights

Figures 1a and 1b illustrate the variation of the mixing layer height detected by the acoustic sounder during several days of the Rush experiment. In Figure 1a, the cases in which the mixing layer height increased rapidly with time and soon became greater than the detectable limit of the sodar (approximately 1 km) are depicted. In each case the mixing layer height exceeded the detectable limit before 1100 hours, and the rate of increase was as large as 650 m hr$^{-1}$ for an hour or more in mid-morning. If there is no large-scale vertical velocity, this indicates turbulent velocities at least as large as 20 cm/s near the top of the mixing layer. In contrast, Figure 1b illustrates the cases when the mixing layer height never rose above the detectable limit, in spite of relatively strong heating at the surface on at least one day (October 10). In these cases, while rapid rise rates are seen, they are of much shorter

32

duration (approximately 20–30 minutes), and the overall rise rate for the first two hours is approximately 200 m hr$^{-1}$. Inspection of the corresponding temperature profiles (taken as early as possible for each date) for both figures shows that in almost all cases there is a strong elevated inversion 700 m or more above the surface (it should be noted that the absolute value of temperature is not yet known; however, the temperature differences are known and thus the profiles are correct). For the cases illustrated in Figure 1a, this elevated inversion varies between 1000 and 1500 meters, and the mixing layer rapidly increases in height during the early hours until it reaches the elevated inversion beyond the detectable limit of the sodar. For cases in Figure 1b, the base of the elevated inversion is lower, ranging from 700 to 1000 meters; thus, the rise of the mixing layer is rapidly cut off. On October 5, the elevated inversion began the day at 1250 m but dropped suddenly around 1100 hours to approximately 800 m for a short time, and prevented further increase of the mixing layer height.

Comparison of temperature profiles from the two cases reveals much stronger surface-based nocturnal inversions in the cases of Figure 1b. Thus, it is more difficult for surface heating to cause penetration and lifting of this layer. Note that the rapid rise rate for these cases begins approximately when the inversion layer is lifted to the height of the beginning of the adiabatic portion of the temperature profile. It is interesting to note something of a paradox: those days with strong heating in the morning hours because of clear skies are likely to have the slower rise rates for mixing layer heights early in the day, for if the preceding night was also clear, the nocturnal inversion will be considerably stronger on those days, thus slowing down the rise rate, particularly in the early morning hours.

At this time of year the strength and duration of solar radiation is much reduced relative to summer conditions; thus, the thermals are often too weak to penetrate through an elevated inversion, and the mixing layer effectively reaches a limit there. This is illustrated very well on October 10, 1977, when the mixing layer begins to deepen very rapidly with strong solar forcing, but upon reaching the height of the elevated inversion, stops quickly and oscillates

33
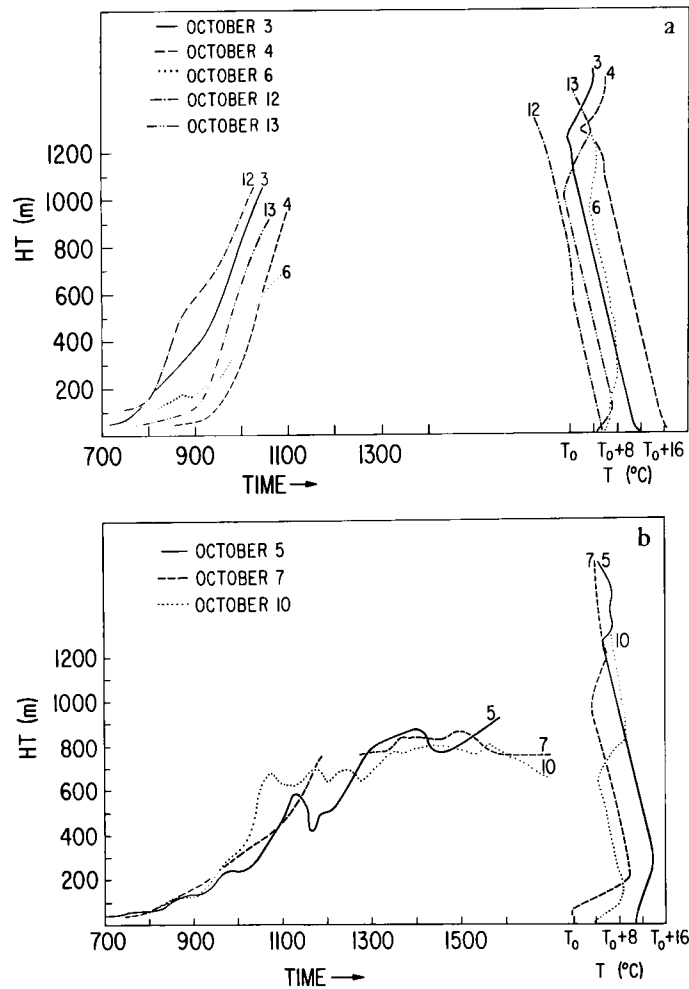
FIG. 1.--(a) Variation of mixing layer height with time as detected by sodar for days with rapid rise rates and (b) days with slow rise rates. Temperature profiles are on the right side
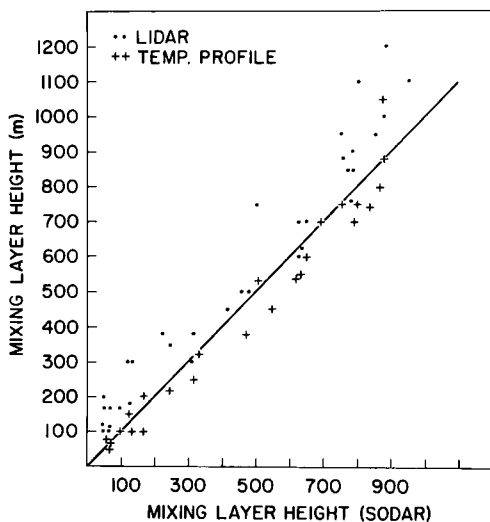


FIG. 2.--Comparison of the mixing layer height as detected by sodar, lidar, and temperature profile.

34

for two hours as the thermal forcing from below is opposed by a descending elevated inversion. Perusal of the sodar returns from the hours before dawn shows faintly the elevated layer descending from aloft until it merges with the rising top of the mixing layer.

Mixing layer heights were also determined by the SRI lidar and the ANL WHAT system. Both these systems were able to monitor mixing layer heights greater than 1 km and thus completed the record. However, the values determined by the three systems did not completely agree. Figure 2 illustrates that the lidar values are consistently higher than the sodar, while the values from temperature profiles are consistently lower. In each case there appears to be little height dependence in the differences, although the lidar differences may be greater at large and again at small heights. One should note that the values for lidar mixing height reported here are preliminary, and have not yet undergone thorough analysis.

The three systems are responsive to different parameters; the lidar to particles, the sodar to small-scale temperature differences, and the WHAT system to temperature. Thus, the three systems have different physical definitions of the mixing layer height: the temperature profile definition is that height at which the temperature profile first becomes stable, the lidar definition is that height at which there is no longer any detectable particle concentration, and the sodar definition is that height at which small-scale temperature differences show a sudden increase. Evidently these three heights are not exactly the same, although they are certainly very well correlated.

The differences between sodar and temperature profile determinations are small (average difference less than 50 m) and constant with height. The point at which turbulent temperature fluctuations become strong enough, in comparison to the overall background noise levels, to be detectable by the sodar is slightly higher than the lower boundary of the stable layer (presumably turbulent fluctuations exist at the beginning of the layer, but are too weak to be detected).

Aerosols and particles are transported vertically by thermals. It is possible that upon reaching the point at which the temperature profile becomes

stable, the rising particles will penetrate into the stable layer for some distance because they have non-zero vertical velocity at that point. One might expect, then, that the lidar could detect a higher value for mixing layer height than the other two methods. In addition, there may be some thermals which have enough energy to penetrate completely through the stable capping layer (or the capping layer "disappears" for a short time and reforms), particularly if it is thin, and carry particles above the capping inversion. These particles will then be trapped above, leading to a higher determined mixing layer height. Thus, later in the day, as more particles become trapped above the capping inversion, the values may tend to become significantly higher as the trapped particles diffuse upward. Higher values for lidar determinations at the greater heights are reasonable; particularly if the capping inversion does not break down during the day. At lower levels, just as the nocturnal inversion is lifting, the lidar (which has a 100 m minimum detectable height) will be sensitive to particles that have been trapped within the nocturnal inversion. Particles emitted through the night within the nocturnal inversion remain within the inversion. Thus, as the nocturnal inversion begins to lift, the lidar will have returns not related directly to the mixing layer height, resulting in values greater than those of sodar. It is not surprising, then, to see the largest differences between lidar and sodar occurring near the lowest and highest levels (Figure 2). The comparisons of Russel et al. (1974) support this, although it is less apparent in those cases due to the limited resolution.

Inasmuch as lidar is sensitive to polluted layer directly, it may provide the most accurate measurement of the true mixing height of pollutants. However, sodar is easier to use and is less expensive. When cognizance is taken of the relative difference among the three methods, a thorough description of the mixing layer heights can be garnered from the sodar returns.

References

Beran, D. W., and F. Hall, 1973: Remote sensing applications in air pollution meteorology. Preprints, 2nd Joint Conference on Sensing of Environmental Pollutants, Washington, D.C., Dec. 10-12, 1973, pp. 241-245.

Frenzen, P. and L. L. Prucha, 1974: The WHAT System: A digitized radio-sonce and double-theodolite balloon tracking system for atmospheric boundary-layer investigations. Atmos. Technol. 6, 129−134.

Russel, P. B., E. E. Uthe, F. L. Ludwig, and N. A. Shaw, 1974: A comparison of atmospheric structure as observed with monostatic acoustic sounder and lidar techniques. J. Geophys. Res. 79(36), 5555−5566.

Wycoff, R. J., D. W. Beran, and F. Hall, 1973: A comparison of the low level radiosonde and acoustic echo sounder for monitoring atmospheric stability. J. Appl. Meteorol. 12, 1196−1204.

# MOMENTUM FLUXES OVER ADJACENT SOYBEAN AND MAIZE FIELDS, SANGAMON 1975

B. B. Hicks and M. L. Wesely

## Introduction

The Sangamon series of Planetary Boundary Layer (PBL) field investigations has been reported in some detail in our previous annual reports. Emphasis has been placed on the behavior of the PBL with regard to the transport of pollutants; supportive surface layer studies conducted during the Sangamon experiments remain to be described fully. The studies in question were conducted during 1975 and 1976 in Sangamon County in central Illinois. In one important way, these investigations represent a departure from earlier PBL studies (e.g., the Wangara experiment reported by Clarke and Hess, 1973, and the Minnesota experiment of Kaimal et al., 1976) in that the surface was not spatially homogeneous. Instead, the experiments were conducted over relatively flat but randomly distributed fields of soybeans and maize. Thus, representative values of momentum and sensible heat had to be obtained by spatial averaging not necessary in such previous experiments. Spatial averaging of this kind is a problem which must be addressed for studies of flow over a nonuniform surface, and thus is clearly relevant to the regional-scale modeling studies of MAP3S. Here, some results of the micrometeorological studies conducted in the first of the Sangamon experiments will be presented. The interpretation of friction velocities will be emphasized, since accurate determination of average momentum fluxes is crucial in studies of PBL flow characteristics.

## Site Description

Figures 1 and 2 show the distribution of equipment at the main Sangamon site during the 1975 and 1976 experiments, respectively. On both occasions, micrometeorological data were collected over both soybeans and maize; however, the distribution of equipment in 1976 was quite different from that in 1975. This was necessitated by the changes in vegetation that occurred as a
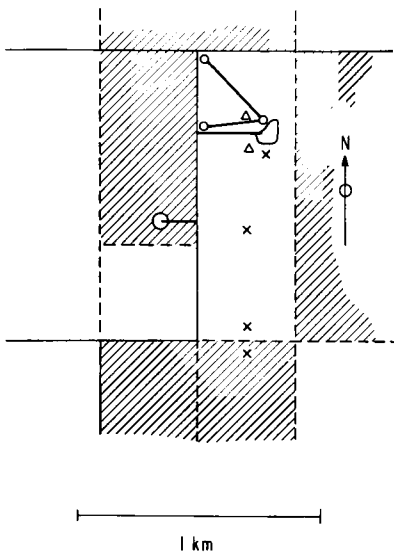
FIG. 1.--Layout of the 1975
Sangamon experiment PBL field
site, showing the locations of
WHAT-system theodolites (circles)
and preferred baselines, the sites
of micrometeorological investiga-
tions (crosses) and the area used
as a base for kytoon operation
(triangles). Hatching indicates
surfaces bearing a maize crop.
Soybeans were grown in all other
areas. (ANL Neg. 149-78-143)
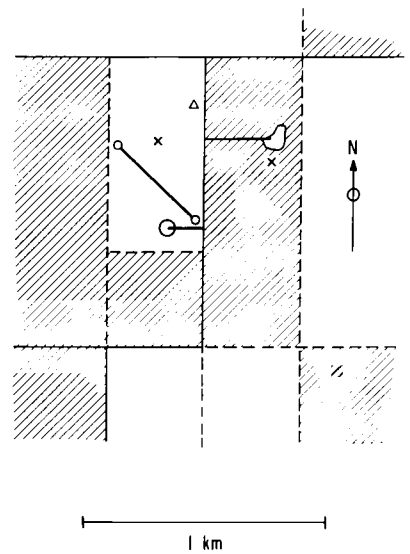
FIG. 2.--Layout of the 1976
field site, using the same symbols
as in Figure 1. (ANL Neg. 149-78-
144)

result of the normal practice of crop rotation in this area.

The distribution of equipment was constrained somewhat by the desire
to concentrate on conditions of southerly flow; in part, this preference was a
reflection of the wish to cooperate with other research efforts in the same area,
especially the MISTT* program. Thus, during the 1975 experiment wind profile
masts were set up in locations selected to give good fetches over both soybean
and maize in southerly flow. Momentum fluxes were measured by eddy cor-
relation whenever suitable fetches could be utilized. In order to maximize use,
the eddy flux equipment was operated on a mast on a mobile platform that was

---

*The Midwest Interstate Sulfur Transformation and Transport experiment of the
U.S. Environmental Protection Agency.

moved whenever changes in wind direction occurred. The specific intent was to evaluate the distribution of surface stress between the two types of surface, and to determine the roughness length and displacement height of each canopy. In this way, spatially averaged momentum fluxes can be derived from single wind observations and rather simple flux-gradient relationships. To a considerable extent, these aims were accomplished during the 1975 experiment, and accordingly a less complicated micrometeorological experiment was designed for the 1976 study.

## Momentum Fluxes over Soybeans

Here we will consider only data obtained in unstable conditions during the 1975 experiment. The 1976 data set was heavily weighted towards stable conditions, and interpretation is considerably more difficult.

As is shown in Figure 3, the soybean canopy grew rapidly during the 1975 study. In the early part of the experiment, the soybeans were relatively small, and bare soil was exposed between the rows. By the end of the study, no bare soil remained exposed. Inspection of the crop-height measurements plotted in Figure 3 shows that the soybean canopy was extremely uniform in height. The growth of the crop during the period of observation is described by the relation

$$h = 1.32 \, (1 - \exp(0.056(190 - T))) \tag{1}$$

between the crop height h (in meters) and the Julian date T.

It was assumed that the roughness length and zero-plane displacement height would both change during the experiment. Thus, a large number of eddy-correlation measurements were made over the soybean canopy in order to determine the change with time of $z_0$ and d. However, fetch considerations regarding the soybean wind profile tower resulted in the elimination of all data except those obtained on 28 and 31 July and 6 August. This limited data set proved insufficient to quantify the changes in $z_0$ and d with time, although the geometric mean roughness length derived from data obtained in July ($3.5 \pm 0.6$ cm from 11 evaluations) was significantly different than the mean value obtained on 6 August ($5.9 \pm 0.8$ cm from 19 evaluations). The earlier value corresponds
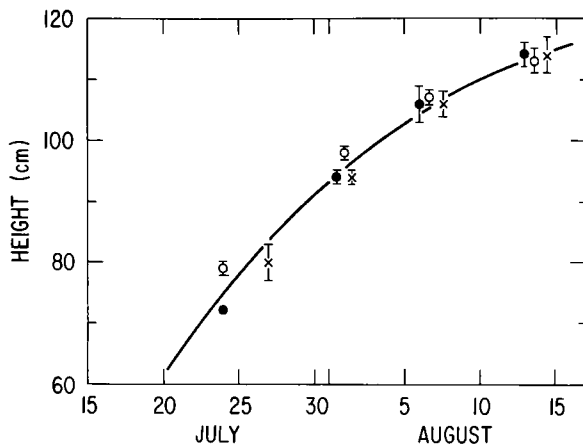
FIG. 3.--The growth of the soybeans during the 1975 Sangamon study. The data show no significant differences between different locations in the soybean field studied (solid circles indicate the northern end of the field, open circles the soutnern end, and crosses the center). The curve drawn through the data is given by Eq. 1. (ANL Neg. 149-78-146)

to a roughness length about 4% of the crop height, whereas the later average is about 6%. The mean value of 5 cm will be used in the following comparisons with flow conditions over the maize surface.

The average zero-plane displacement measured above the soybeans was d = 90 ± 7 cm (i.e., 90% of the average crop height).

In obtaining these results, eddy fluxes have been corrected for the effects of high frequency sensor inadequacy (following the procedures set down by Hicks, 1972) and stability corrections have been applied (as recommended by Dyer, 1974). The effect of water vapor buoyancy has been included in the evaluation of atmospheric stability, through inclusion of the latent heat flux, estimated from net radiation data as $(R_n - H)$, in the usual notation.

## Momentum Fluxes over Maize

The larger, upper leaves of the mature maize crop of the 1975 experiment had an average maximum height of about 2.25 m, whereas tassels extended to about 2.85 m. The average crop height was thus about 2.55 m. No change with time was detected.

After eliminating a number of measurements made in extremely light wind conditions, the remaining 21 observations yield an average roughness length of 17 ± 2 cm (i.e., about 6.5% of the average crop height, h) and an average displacement height of 151 ± 12 cm (about 60% of h).

41

## The Distribution of Stress Between Crops

A comparison between simultaneous momentum fluxes over the two canopies can be obtained by consideration of occasions of southerly wind in which mean wind measurements were made over both surfaces and net radiation and sensible heat fluxes were measured directly, so that friction coefficients could be properly corrected for the effects of atmospheric stability. For purposes of evaluating this stability correction, it is assumed that sensible heat fluxes over both canopies are the same. The spatial distribution of the sensible heat flux is addressed later in this report (Hicks and Wesely, 1977); the 10% errors which arise in the present assumption of equality will have only a minor influence upon the evaluation of friction velocities.

Figure 4 is a comparison between the two sets of friction velocities derived in this manner. It is clear that a close relationship exists (as expected), and it seems that a simple proportionality provides an adequate description of the data. Analysis of the data which contribute to Figure 4 shows that the average ratio of the friction velocities, maize/soybean is 1.17 ± 0.03 (29 values). Maize and soybean fields were evenly distributed on the farmland surrounding the Sangamon field site during both the 1975 and 1976 studies. Thus, the analysis presented above can be extended to address the question of how to derive spatial averages of the friction velocity from observations made over one type of surface only. Measurements made over soybeans should be increased by about 9%, and measurements made over the maize should be
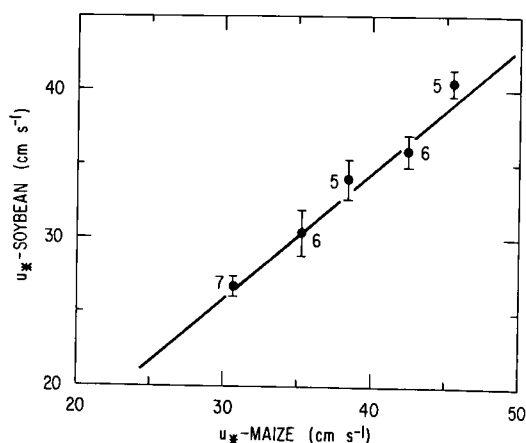


FIG. 4.--A comparison between simultaneous estimates of friction velocity over adjacent soybean and maize surfaces. The line has a slope of 1.17. (ANL Neg. 149-78-145)

decreased by about the same amount.

## Conclusions

Friction velocities over the maize crop during the 1975 experiment were found to be about 17% greater than over an adjacent soybean field. The maize was much taller than the soybeans (2.55 m versus about 1 m) and was considerably rougher ($z_0 = 17$ cm versus about 5 cm at the time of this experiment). The displacement height of the maize crop was about 151 cm, i.e., 60% of h. In the case of the soybeans, which were growing rapidly during the experiment, the displacement height was about 90% of h.

Thus, it seems that spatially averaged friction velocities suitable for use in PBL scaling studies can be estimated from single wind observations made at a single location close to the surface. Estimates made on the basis of wind speeds measured over the soybeans should be increased by about 9%, and those derived from observations over maize should be reduced by the same amount. This assumes that d, $z_0$ and H are known. For other PBL studies over maize and soybeans when $u_*$ and H are not measured directly, we may use values of d and $z_0$ estimated from crop heights. Wind measurements should be made quite close to the surface in order to minimize the effect of atmospheric stability.

## References

Clarke, R. H. and G. D. Hess, 1973; On the appropriate scaling for velocity and temperature in the planetary boundary layer. J. Atmos. Sci. 30, 1346–1353.

Dyer, A. J., 1974; A review of flux-profile relationships. Boundary-Layer Meteorol. 7, 363–372.

Hicks, B. B., 1972; Propeller anemometers as sensors of atmospheric turbulence. Boundary-Layer Meteorol. 3, 215–228.

—————— and M. L. Wesely, 1978; Thermal characteristics of adjacent soybean and maize crops: Sangamon 1975. This report.

Kaimal, J. C., J. C. Wyngaard, D. A. Huagen, O. R. Cote, Y. Izumi, S. J. Caughey, and C. J. Readings, 1976; Turbulence structure in the convective boundary layer. J. Atmos. Sci. 33, 2152–2169.

# THERMAL CHARACTERISTICS OF ADJACENT SOYBEAN AND MAIZE CROPS, SANGAMON 1975

B. B. Hicks and M. L. Wesely

---

## Introduction

The need to derive spatially averaged surface fluxes during the Sangamon experiments of 1975 and 1976 has been explained elsewhere in this report (Hicks and Wesely, 1977). In the analysis, it was found that the momentum fluxes to the soybean canopy were about 34% less than those to the maize canopy (each surface accounted for about 50% of the area surrounding the main field site). A simple correction factor was found to be sufficient for evaluating spatially averaged friction velocities from observations made over one particular canopy. Here, similar questions will be addressed in the case of the sensible heat flux, which is another crucial quantity in parameterizations of the evolution of the mixed layer of the lower atmosphere. Since the magnitude of the sensible heat flux above a vegetated surface results from a number of sometimes counteracting factors, special attention will be given to such related matters as net radiation and surface temperature.

## Net Radiation and Surface Temperature

Miniature net radiometers placed above each surface were used to compare the radiation balance above the two types of vegetation. Figure 1 shows that the net radiation values recorded over the maize exceeded simultaneous readings above the soybeans during the mornings and late afternoons, but the difference averages less than 10%. The curve drawn by eye through the plotted averages and standard errors appears to be roughly symmetrical about noon.

A slight difference in thermal properties is also indicated by surface temperature data, obtained during the 1975 experiment by the use of a hand-held infrared thermometer. On the average, infrared temperatures of the maize were about 0.4°C higher than those of the soybeans during the morning, but by noon they were about 0.4°C lower. The nature of the similarity between the
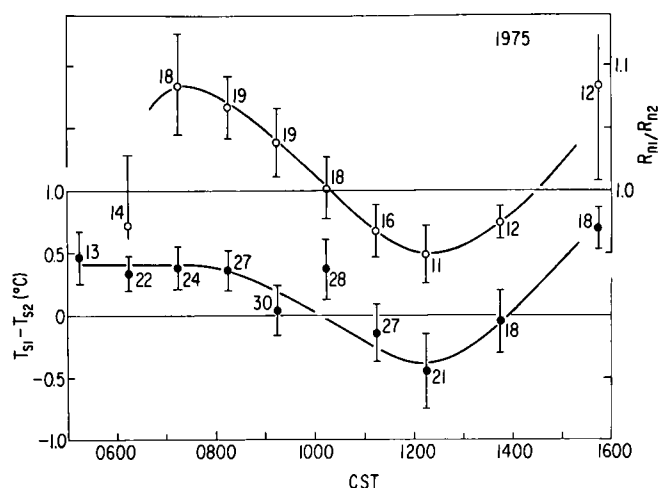
FIG. 1.--Cycles of the average differences between net radiation over the maize crop (subscript 1) and over adjacent soybeans (subscript 2), and of the corresponding differences in surface temperature detected by infrared thermometry. Averages and standard errors are plotted; numbers indicate sample size.
(ANL Neg. 149-78-76)

surface temperature and net radiation data plotted in Figure 1 is quite surprising. In situations in which albedos and emissivities are identical, lower values of net radiation should be detected above the warmer surface, but the opposite behavior is apparent in Figure 1. Albedo differences between the two crops may have varied diurnally, mainly as a result of greater wilting of the soybean leaves, such as was clearly visible by late morning on a number of occasions. Differences in the amount of dewfall might also have occurred, and it seems likely that dew was distributed more evenly through the less dense maize canopy; thus differences in the surface albedo may have been important in the morning hours also. It seems likely, however, that a major factor might have been the bare soil exposed between the rows of soybeans during the early part of the experiment. Patches of soil were exposed to direct insolation during the period centered about noon; the amount of soil exposed in this way decreased uniformly with increasing time difference from solar noon. The matter is by no means simple, and the present body of information is insufficient to address the problem properly.

## Sensible Heat Fluxes

Average diurnal cycles of net radiation and sensible heat flux (corrected for the effects of inadequate sensor performance) are given in Figure 2. In the case of the sensible heat fluxes, results obtained over the two surfaces are displayed separately, in order to show that the average fluxes measured above
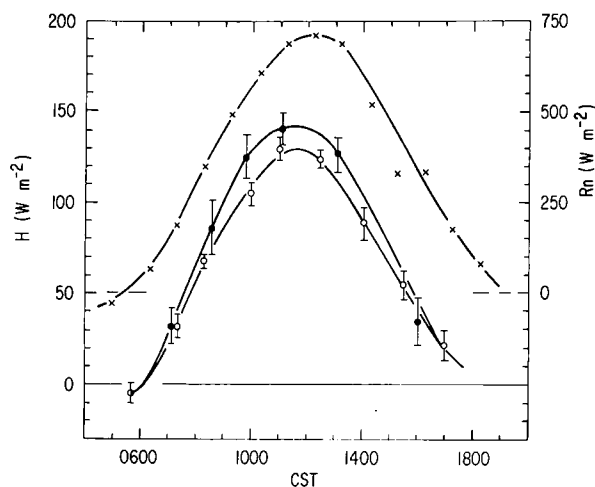
FIG. 2.--Average diurnal cycles of net radiation (upper curve) and sensible heat flux (lower curves) measured during the 1975 experiment. Two sets of sensible heat flux data are illustrated. Open circles represent data obtained over soybeans, solid circles indicate results obtained over maize. (ANL Neg. 149-78-151)

the soybeans were slightly smaller than those over the maize. On the average, the difference is about 10%. Thus, the problem of how to derive spatial averages of the sensible heat flux seems to have an answer as simple as that which was obtained elsewhere (q.v., Hicks and Wesely, 1977) for the case of friction velocities: heat fluxes measured over the soybeans should be increased by about 5%, and observations made over the maize should be decreased by the same amount.

It is of some interest to compare the roughness length for sensible heat transfer with the value derived earlier for the case of momentum. There are insufficient data (and those available are too highly scattered) to warrant discussion of the maize surface in this context. However, a large body of relevant data was obtained over the soybean canopy on 21 July (10 values) and on 31 July (12 values). After omitting two unusually high and two low values, the mean value of $z_H$ derived from these data is 2.5 cm, with a large standard error (about 55%). For the same occasions, the earlier study of momentum fluxes yielded $z_0$ = 4.7 cm. This is largely in accord with the pattern presented by Garratt and Hicks (1973), who suggest that the property $\ln(z_0/z_H)$ is a single-valued function of the roughness Reynolds number $Re_* = u_* z_0 / \nu$, where $\nu$ is kinematic viscosity. The present value of $\ln(z_0/z_H)$ is $0.6 \pm 0.5$, which should be compared with a value of about 1.5 suggested by Garratt and Hicks for the case of an even canopy with fibrous elements at the appropriate roughness Reynolds number (about 800).

46

## Thermal Structure of the Maize Canopy

The matter of flux-gradient relationships over tall crops is of some interest, since it has been claimed that penetration of the canopy by deep thermal eddies in convective conditions leads to substantially increased diffusivities that might not transfer momentum very well; thus $K_H$ near the top of a deep canopy appears to be much greater than predicted by the usual flux-gradient relationships. However, it seems possible that much of the explanation lies in the manner in which the sun heats the foliage. Before sunrise, all turbulent transfer is mechanically induced. Thermal and mechanical diffusivities would be the same, and displacement heights for momentum and sensible heat transfer would be expected to be about the same. After sunrise, convection commences, and $K_H$ starts to exceed $K_M$. But as the sun rises above the horizon, radiation will first warm the very top of the canopy. Later, solar radiation will gradually penetrate more deeply, and the zero plane for heat transfer might be expected to move downward from the top of the canopy. Meanwhile, the zero plane for momentum transfer (visualized by Thom, 1971, as the mean level of action of the drag force) would not be so affected.

Thus, the apparent discrepancy in the applicability of flux-gradient relations may not be a result of deep penetration by convective cells aloft so much as a consequence of a consistent change in the height of the effective source of sensible heat.

In order to investigate this possibility, hand-held infrared thermometry was used during the 1975 Sangamon experiment to locate the height of maximum foliage temperature within the maize canopy. This task proved relatively simple at most times, and Figure 3 shows that a quite consistent picture was obtained. Although the number of values contributing to the diagram is small, the trend in the level of temperature maximum seems clearly defined. The line drawn through the plotted values indicates that the level of maximum foliage temperature moved to below the momentum zero plane at about 0800 CST, on the average. It should be emphasized that the present radiometric data do not provide a direct determination of the level of the zero plane itself, however, they do illustrate the manner in which the effective source of sensible heat moves
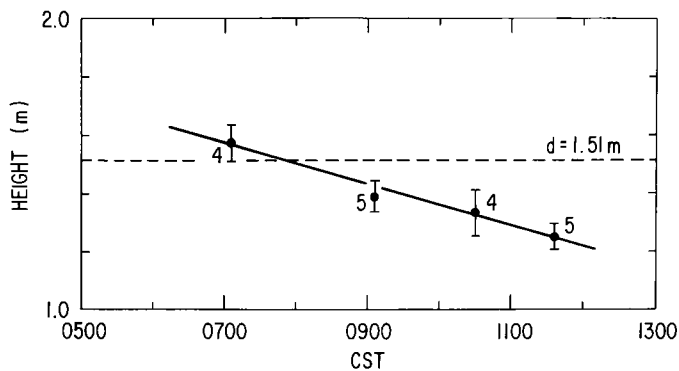
FIG. 3.--The variation with time of day of the height of the level of maximum foliage temperature within the maize canopy. The dashed line indicates the height of the zero plane for momentum transfer.
(ANL Neg. 149-78-147)

during a typical diurnal cycle.

## Conclusions

Evaluations of net radiation over adjacent fields of soybeans and mature maize show less than 10% difference between the two surfaces. Differences in infrared surface temperature were also small (usually less than 0.4°C), but were counter to the differences that would be expected by simple interpretation of the net radiation data alone. It seems likely that the thermal properties of the soybean field could have been influenced considerably by the bare patches of soil which were exposed between the rows during the early part of the experiment. Finally, sensible heat fluxes measured over the maize averaged about 10% greater than over the soybeans.

## References

Garratt, J. R. and B. B. Hicks, 1973: Momentum, heat and water vapour tranfer to and from natural and artificial surfaces. Q. J. R. Meteorol. Soc. 99, 680-687.
Hicks, B. B. and M. L. Wesely, 1977: Momentm fluxes over adjacent soybean and maize fields. This report.
Thom, A. S., 1971: Momentum absorption by vegetation. Q. J. R. Meteorol. Soc. 97, 414-428.

# ANALYSES OF THE SANGAMON DATA

T. Yamada

---

For prediction of air pollution dispersion over regional scales, knowledge of temporal and spatial variations of wind and turbulence profiles in the Planetary Boundary Layer (PBL) is essential. During the day, wind above the surface boundary layer becomes almost uniform with height due to turbulent vertical mixing, but at night, wind profiles often exhibit considerable shear in both direction and speed. The speed maxima can be significantly greater than the corresponding geostrophic winds and are referred to as nocturnal low-level jets. These complex wind variations should be simulated for realistic numerical modeling of dispersion.

Similarly theory for the PBL suggests that wind profiles can be reduced to a universal form if wind and height are appropriately scaled, and universal velocity profiles are then empirically derived from observational data. The most commonly accepted scaling parameters are the geostrophic wind, the Coriolis parameter, and the friction velocity. Data obtained from the Sangamon field experiments have been used to investigate the validity of similarity theory for the PBL. Description of the experiment site, measurement procedures, instrumentation and preliminary results have been previously reported (Hess and Hicks, 1975; Sisterson et al., 1976). Totals of 150 and 95 hours of wind and temperature data, respectively, were obtained during the 1975 experiment, which investigated the evolution of the mixed-layer height during the period between 0400 and 1200 CST. The following year the formation and development of the surface inversion layer during the period between 1600 and 2400 CST was investigated, producing 80 and 59 hours of wind and temperature data, respectively. Magnetic tapes and microfiche cards containing the data are available.

In order to obtain geostrophic wind and friction velocities from the observed wind profiles, a method proposed by Lettau (1950) and modified by Johnson (1965) has been employed (details of the method may be found in Yamada et al., 1976). Strictly speaking, this method applies only for stationary

49

and horizontally homogeneous conditions, and the real atmosphere never completely satisfies such conditions. Nevertheless, we have employed this method because of its simplicity. The method requires knowledge of the mixed-layer height, most conveniently defined as the height where the temperature lapse rate changes from dry adiabatic. About 30% of the temperature soundings made during the Sangamon experiments were not completed for various reasons, such as a poor signal from the radiosonde or visual loss of the balloon in clouds. An additional 40% of the data were not used in this study because the computed friction velocities were found to be either much too small or excessively large. The results reported here are based on 28 and 23 hours of data for the 1975 and 1976 experiments, respectively. Surface geostrophic winds thus obtained have been compared with those obtained from the pressure records at National Weather Service installations and those from three micro-barograph stations temporarily operated during the observational period. Agreement is surprisingly good (see Yamada et al., 1977). The difference between the actual wind and the geostrophic wind, scaled by friction velocity, has been plotted against height scaled by the mixed-layer height. Wind profiles under approximately the same atmospheric stability conditions agree reasonably well. On the other hand, distinguishable differences have been found between the profiles in the early morning, 0300 to 0700 CST (see Figure 1) and those in the late morning, 1000 to 1200 CST (see Figure 2). These results appear to support the existence of universal profiles suggested by similarity theory.

An important result from the same analysis is illustrated in Figure 3, which shows two vertical profiles of eddy viscosity coefficients under different atmospheric stability conditions. Values in late morning are approximately one order of magnitude greater than the counterparts in early morning. The differences between the calculated values and the curves fitted by eye may be due in large part to inclusion of data from several days and times. Parameterization of the eddy viscosity coefficient (or the approximately equivalent eddy diffusivity) is extremely important in the modeling of air pollution.
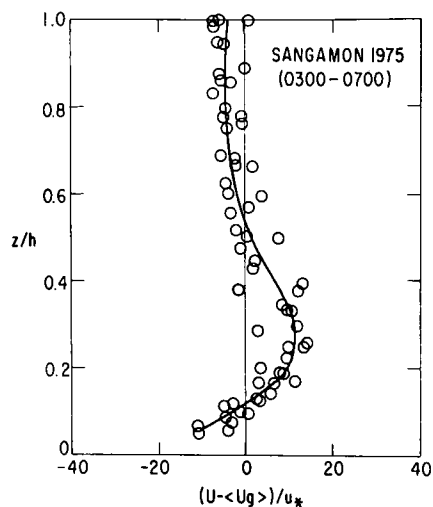
FIG. 1.--Normalized wind departure $(U - \langle U_g \rangle)/u_*$ vs. $z/h$ during early morning, 0300 to 0700 CST, where $\langle U_g \rangle$ is a vertically averaged geostrophic wind, $u_*$ is friction velocity, and h is the mixed-layer height as defined in the text.
(ANL Neg. 149-77-448)
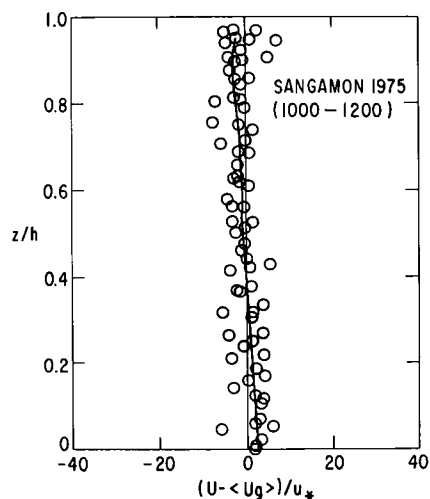


FIG. 2.--Same as for Figure 1 but for late morning, 1000 to 1200 CST.
(ANL Neg. 149-77-450)
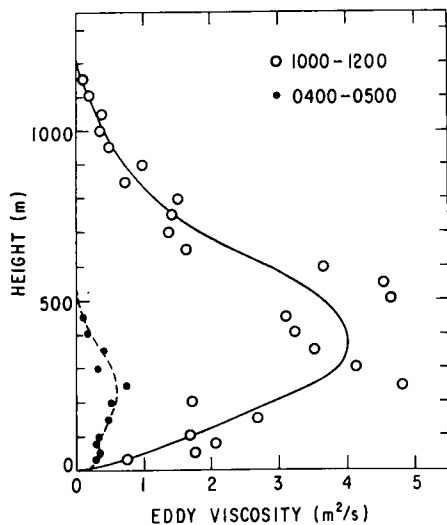


FIG. 3.--Eddy viscosity profiles obtained from geostrophic departure analysis.
(ANL Neg. 149-77-449)

References

Hess, G. D. and B. B. Hicks, 1975: A study of PBL structure: The Sangamon experiment of 1975. Argonne National Laboratory Radiological and Environmental Research Division Annual Report, ANL-75-60, Part IV, pp. 1-4.

Johnson, W. B., Jr., 1965: Atmospheric boundary-layer dynamics over the forests of northeastern Wisconsin. Final report 1965: Studies of the effects of variations in boundary conditions on the atmospheric boundary layer. University of Wisconsin, Dept. of Meteorology, Contract DA-36-039-AMC-00878 (E), pp. 45-145.

Lettau, H. H., 1950: A re-examination of the "Leipzig Wind Profile" considering some relations between wind and turbulence in the friction layer. Tellus 2, 125-129.

Sisterson, D. L., B. B. Hicks, and M. L. Wesely, 1976. An outline of the 1976 Sangamon field experiment. Argonne National Laboratory Radiological and Environmental Research Division Annual Report, ANL-76-88, Part IV, pp. 1-6.

Yamada, T., D. L. Sisterson, and G. D. Hess, 1976: A preliminary analysis of the Sangamon data. Argonne National Laboratory Radiological and Environmental Research Division Annual Report, ANL-76-88, Part IV, pp. 7-13.

Yamada, T., R. G. Everett, and S. Berman, 1977: Surface geostrophic winds during the 1975, 1976, and 1977 experiments. This report.

# SURFACE GEOSTROPHIC WINDS DURING THE 1975, 1976, AND 1977 EXPERIMENTS

T. Yamada, R. G. Everett, and S. Berman[*]

The geostrophic wind is defined as the wind that results when pressure and Coriolis forces are in balance (geostrophic equilibrium); such equilibrium is considered to be a valid approximation above the Planetary Boundary Layer (PBL). From the equation of motion for the mean wind, the following relations may be obtained:

$$U_g \equiv -(1/f\rho)\, \partial p/\partial y \tag{1a}$$

$$V_g \equiv (1/f\rho)\, \partial p/\partial x , \tag{1b}$$

where $U_g$ and $V_g$ are geostrophic wind components along x (positive eastward) and y (positive northward), respectively; p is the pressure, $\rho$ is the air density, and f is the Coriolis parameter. This geostrophic equilibrium should, however, be modified in the PBL where vertical momentum transfer due to turbulent mixing becomes important. Consequently, observed wind profiles in the PBL often differ considerably from the corresponding geostrophic wind profiles. Similarity theory for the PBL assumes that the departure of the observed wind from the geostrophic wind is a universal function of height and atmospheric stability. This assumption appears to be supported, to some extent, by existing observations (e.g., see discussions in Yamada, 1976). Currently the validity of similarity theory is being investigated with the data obtained during the Sangamon experiment (Hess and Hicks, 1975) and the Rush experiment (Hicks, 1977).

In numerical simulations of the PBL, geostrophic winds have been frequently used as approximations of the pressure-gradient terms that appear in the equation of motion. Such approximations have been used in the turbulence-closure model of Mellor and Yamada (1974), which is currently being

applied to simulate the evolution of the mixed-layer during the Sangamon experiment. Geostrophic winds analyzed as shown here will be used in that simulation as an external forcing function.

The geostrophic wind becomes constant with height if hydrostatic equilibrium and horizontal homogeneity are assumed, although the latter assumption may be only approximately true during either the Sangamon or Rush experiments. These two assumptions permit the pressure in Eqs. 1a and 1b to be replaced by the mean sea level pressure, obtained by reducing the surface pressure measured by standard pressure sensors. Henceforth, "surface" refers to values at mean sea level. The surface geostrophic wind components $(U_{g_O}, V_{g_O})$ are computed from the pressure records collected at 1) a network consisting of three microbarograph stations (see Lipschutz, 1975 for discussion) and 14 National Weather Service (NWS) stations, and 2) the three microbarograph stations alone (see Figure 1).

Following Clarke, et al. (1971) the surface pressure distribution is approximated by

$$p_i = c_1 x_i + c_2 y_i + c_3 x_i^2 + c_4 y_i^2 + c_5 x_i y_i + c_6 , \qquad (2)$$

where $p_i$ is the deviation of the pressure from the mean of the values measured at all stations considered, and $x_i$ and $y_i$ are the distances from the geometric mean of the stations to each station. The coefficients, $c_j$, $j = 1-6$, in Eq. 2 are constants that are obtained by applying a least squares method to the hourly data obtained at the network of microbarograph and NWS stations.

For the case of the microbarograph data alone, the following linear regression is employed:

$$p_i = a_1 x_1 + a_2 y_i + a_3 . \qquad (3)$$

The coefficients, $a_j$, $j = 1-3$, are obtained by solving the simultaneous equations constructed from Eq. 3 for the three microbarograph stations ($i = 1, 2,$ and 3).

Once the coefficients in either Eq. 2 or Eq. 3 are determined, the geostrophic wind is easily obtained from Eqs. 1a and 1b. In addition to the
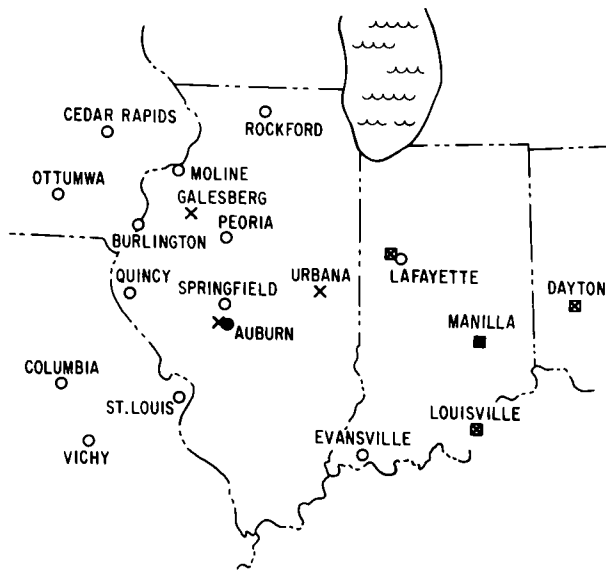
FIG. 1.--Locations of the National Weather Service (o) and microbarograph stations (X), at which pressures were recorded and used to obtain the surface geostrophic winds for the 1975 and 1976 Sangamon experiments at Auburn (●), Illinois. The microbarograph stations (⊠) during the 1977 Rush experiment at Manilla (■), Indiana are also shown. (ANL Neg. 149-78-81)

two methods discussed above, the geostrophic wind may be obtained directly by using the equation of motion for the mean wind and the wind profiles observed at the experimental sites. This method is referred to as a geostrophic departure method (Johnson, 1965), a summary of which may be found in Yamada et al. (1976).

Temporal variations of the surface geostrophic winds during the 1975 Sangamon experiment are shown in Figure 2. The geostrophic winds computed from the three different methods agree reasonably well. The geostrophic winds appear to have a period of 3 to 4 days and an amplitude of approximately 5 m $s^{-1}$. Figure 3 shows the corresponding results for the 1976 experiment at the same site. Agreement between the geostrophic winds computed from the microbarograph stations and from the geostrophic departure analysis is again quite reasonable. The NWS data are currently being analyzed. The amplitude of the variations during 1976 appears to be slightly greater than that during 1975, but the frequency appears to remain the same. Finally, the surface geostrophic winds calculated from the microbarograph station data during the 1977 Rush experiment are shown in Figure 4. The other two methods will be applied in the near future. The amplitude of the variations in Figure 4 appears to be significantly larger than that of the previous two experiments, probably due to the fact that the 1977 experiment was conducted in October, while the other
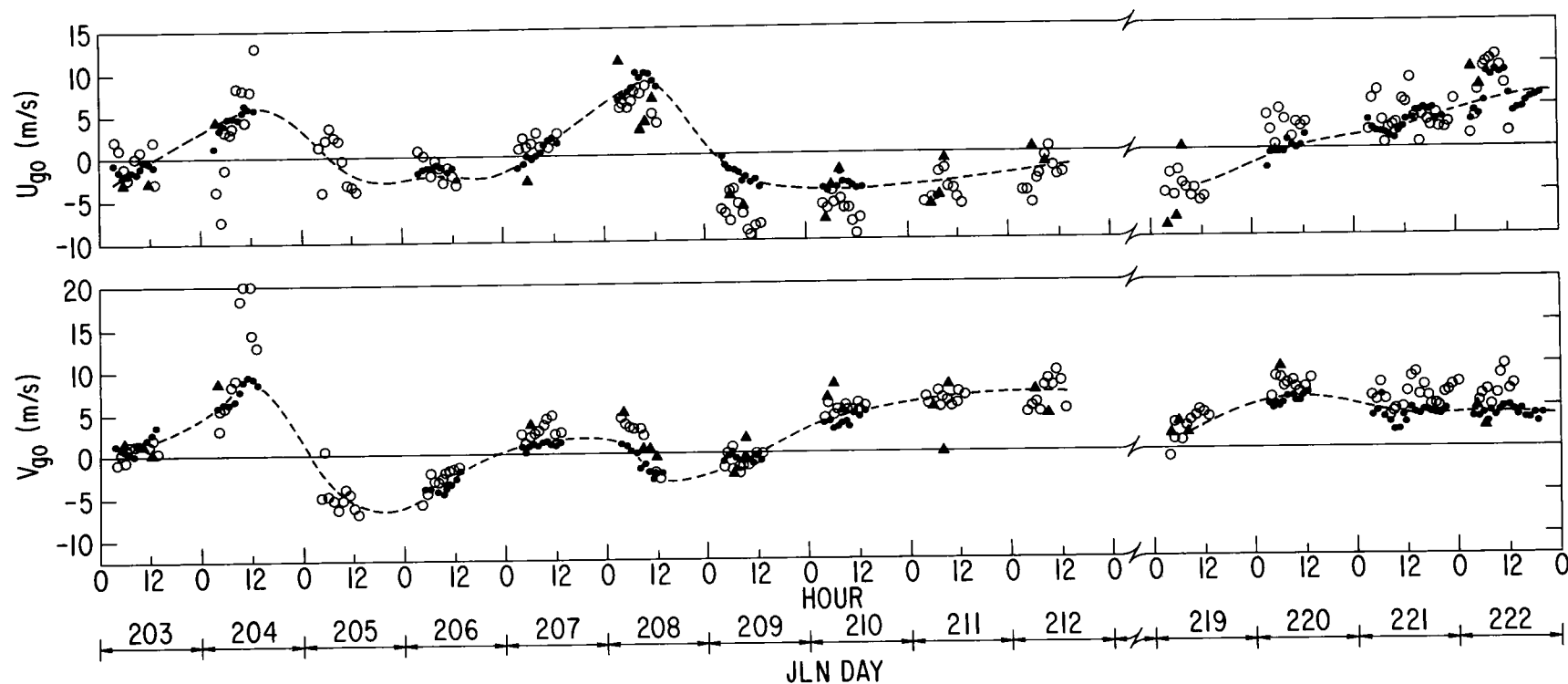
FIG. 2.--Surface geostrophic wind components $U_g$ and $V_g$ computed from the NWS/microbarograph network (•), microbarograph stations (o), and a geostrophic departure analysis (▲) for the 1975 Sangamon experiment. The dotted lines are drawn by hand to connect the values computed from the NWS/microbarograph network for comparison. JLN day refers to the Julian day.
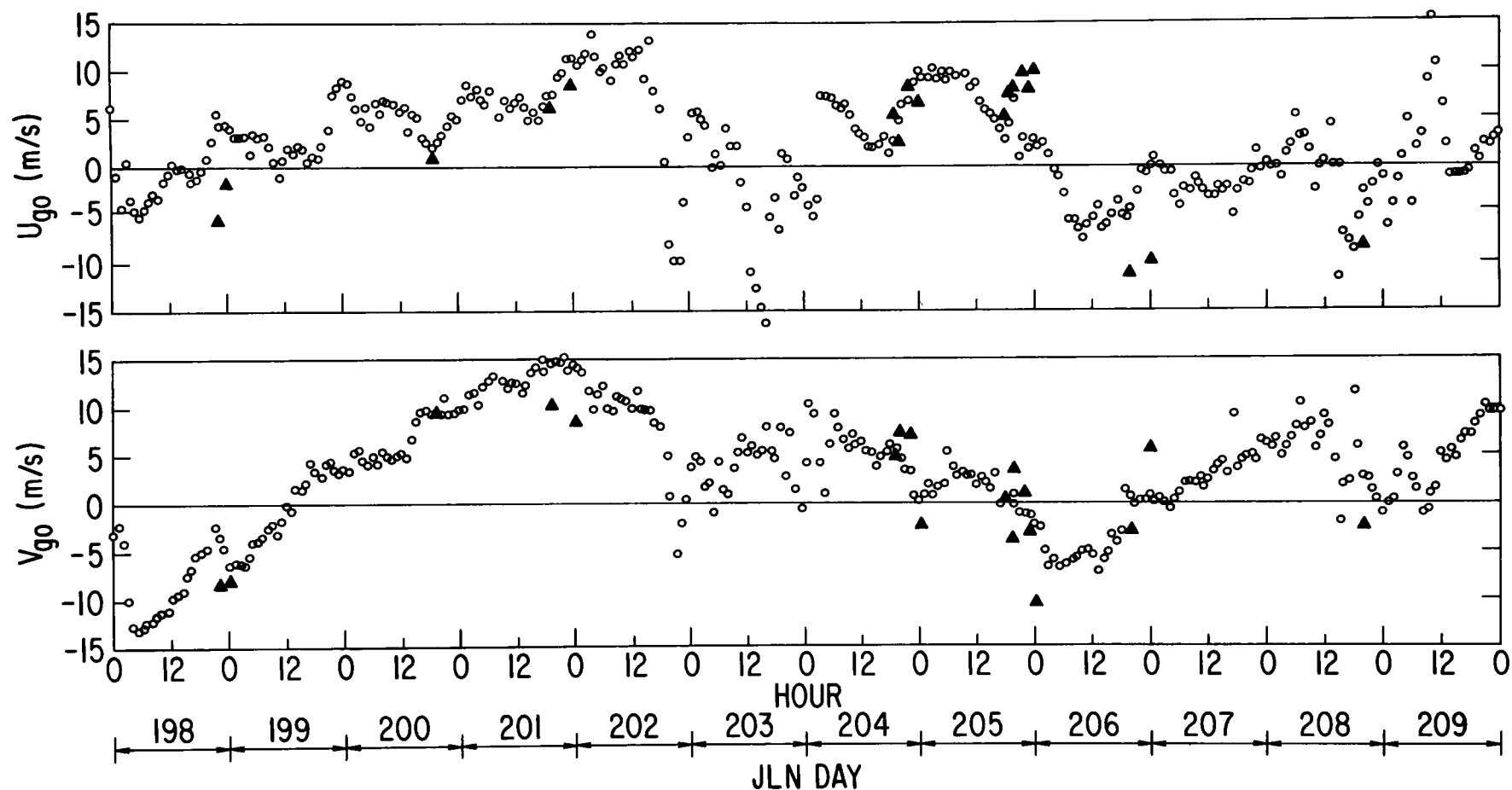
FIG. 3.--Surface geostrophic wind components computed from the microbarograph stations (o) and a geostrophic departure analysis (▲) for the 1976 Sangamon experiment.

57
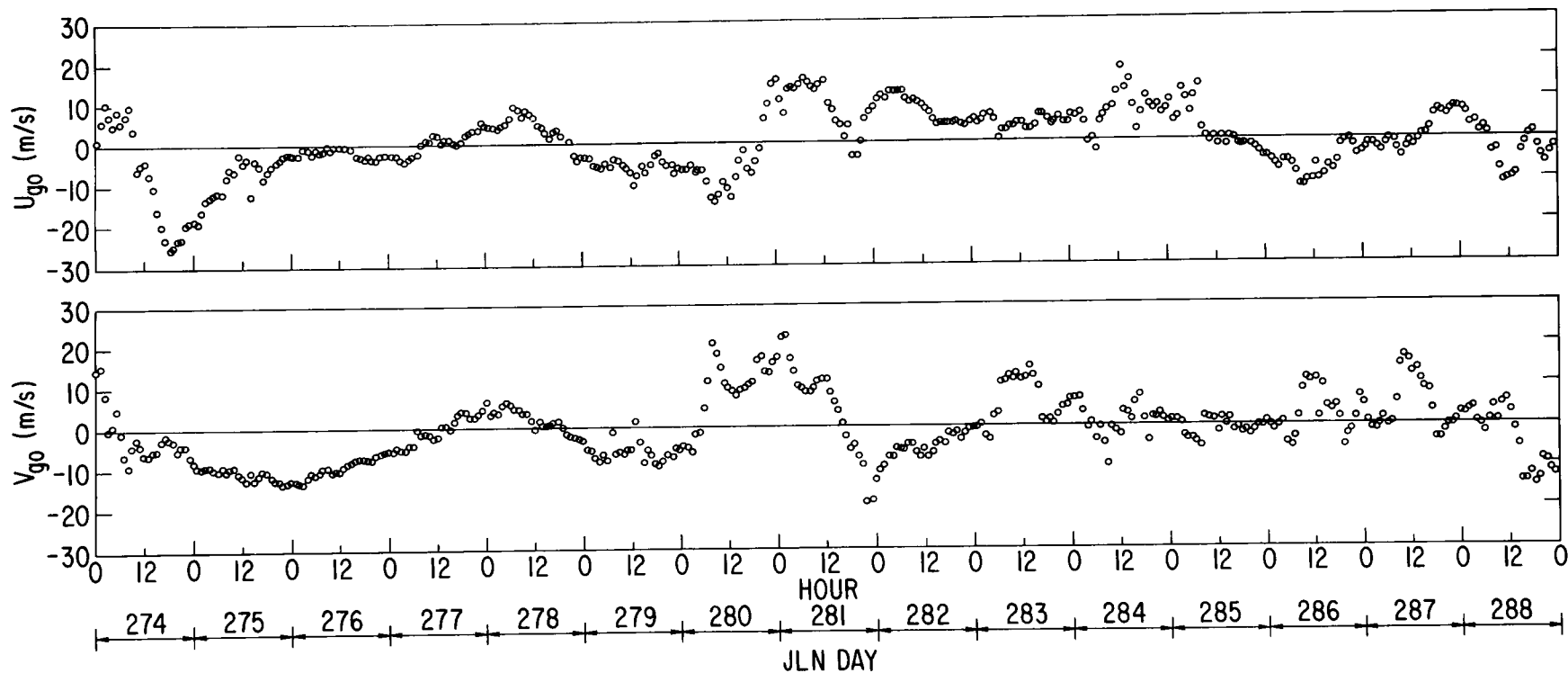
FIG. 4.--Surface geostrophic wind components computed from the microbarograph stations (o) for the 1977 Rush experiment.

58

two experiments were conducted in July and August. Pressure gradients are normally stronger in October and frontal passages are more frequent.

The authors would like to express their thanks to the personnel at the various microbarograph sites who assisted in the data collection processes and to the NWS for supplying the surface network data.

References

Clarke, R. H., A. J. Dyer, R. R. Brook, D. G. Reid, and A. J. Troup, 1971: The Wangara experiment: Boundary layer data. Division Meteorological Physics, CSIRO, Australia, Tech. Paper 19.

Hess, G. D. and B. B. Hicks, 1975: A study of PBL structure: The Sangamon experiment of 1975. Argonne National Laboratory Radiological and Environmental Research Division Annual Report ANL-75-60, Part IV, pp. 1−4.

Hicks, B. B., 1977: The AMBIENS experiment. This report.

Johnson, W. B., Jr., 1965: Atmospheric boundary-layer dynamics over the forests of northeastern Wisconsin. Final report 1965: Studies of the effects of variations in boundary conditions on the atmospheric boundary layer. University of Wisconsin, Dept. of Meteorology, Contract DA-36-039-AMC-00878 (E), pp. 45−145.

Lipschutz, R. C., 1975: Sangamon experiment—geostrophic wind profiles. Argonne National Laboratory Radiological and Environmental Research Division Annual Report ANL-75-60, Part IV, pp. 16−21.

Mellor, G. L. and T. Yamada, 1974: A hierarchy of turbulence closure models for planetary boundary layers. J. Atmos. Sci. $\underline{31}$, 179−1806.

Yamada, T., 1976: On the similarity functions A, B, and C of the planetary boundary layer. J. Atmos. Sci. $\underline{33}$, 781−793.

_____, D. L. Sisterson, and G. D. Hess, 1976: A preliminary analysis of the Sangamon data. Argonne National Laboratory Radiological and Environmental Research Division Annual Report ANL-76-88, Part IV, pp. 7−13.

# ESTIMATING THE GROWTH OF THE MIXING LAYER WITH THE MODEL SUGGESTED BY TENNEKES

S. Berman[*] and T. Yamada

## Introduction

Diffusion in the lower atmosphere varies widely during a typical diurnal cycle. Within an early morning surface inversion, vertical mixing is weak. As surface heating increases, a well-mixed layer forms at the surface and gradually deepens. By mid-afternoon the mixed layer may extend to a height of several kilometers. Subsequent cooling of the ground re-forms the surface inversion, and mixing is reduced once more. Since profiles of meteorological variables and low-level dispersion of pollutants are dependent on the height of this mixed layer, prediction of the height is of practical importance.

Simulations of the growth of the mixed layer during the morning hours by a relatively simple model proposed by Tennekes (1973) are compared below with observations made during the 1967 Wangara experiment (Clarke et al., 1971) and the 1975 Sangamon field experiments (Hess and Hicks, 1975).

## The Model

The equations of the Tennekes model, as summarized by Tennekes and van Ulden (1974) are as follows:

$$-(\overline{\theta w})_i = C_1 (\overline{\theta w})_s + C_2 \frac{T_s u_*^2}{gh} \quad , \tag{1}$$

$$\Delta \frac{dh}{dt} = -(\overline{\theta w})_i \quad , \tag{2}$$

$$h \frac{d\Delta}{dt} + \Delta \frac{dh}{dt} = \gamma h \frac{dh}{dt} - (\overline{\theta w})_s \quad , \text{ and} \tag{3}$$

$$(\overline{\theta w})_s - (\overline{\theta w})_i = h \frac{d\theta}{dt} \quad , \tag{4}$$

where $(\overline{\theta w})_i$ = turbulent sensible vertical heat flux at the top of the mixed

layer ("i" stands for inversion base) ($°C \ m \ s^{-1}$),

$(\overline{\theta w})_s$ = turbulent sensible vertical heat flux at the earth's surface ($°C \ m \ s^{-1}$),

$T_s$ = surface temperature,

$g$ = acceleration of gravity,

$u_*$ = friction velocity

$\Delta$ = inversion strength ($°C$),

$h$ = height of the mixed layer (m),

$\theta$ = potential temperature in the mixed layer (K),

$\gamma = (\frac{d\theta}{dz})_{h+}$ = lapse rate of potential temperature above the mixed layer.

Following Tennekes (1973), it is justifiable to ignore the last term in Eq. 1 if the wind speed is relatively low and the inversion height is greater than 100 m. The coefficient $C_1$ is chosen to be 0.2 on the basis of an average of 35 observed and theoretical values reported by Stull (1976a). Stull (1976b) also shows that $C_1$ is fairly constant from about an hour after sunrise to about an hour before sunset. As modified, Eq. 1 states that downward heat flux at the inversion base equals 20% of the upward heat flux at the surface.

It should be noted that Tennekes' equations do not account for advective changes, the presence of moisture, or large-scale subsidence. These effects have been included by other modelers, but add greatly to the complexity of the system and thus are omitted in this simplified model. Tennekes' set of four independent equations contain six unknown variables. To close this system, we further assume that $\gamma$ is known from an initial morning sounding, and that the surface heat flux $(\overline{\theta w}_s)$ is observed as a function of the time of day. The system can now be solved for variables $(\overline{\theta w}_i)$, h, $\Delta$, and $\theta$ as functions of time provided that initial conditions are specified.

## Results and Discussions

### Sensitivity Studies

Tennekes' model was subjected first to a series of tests designed to study the sensitivity of the height of the mixed layer to variations in $(\theta w_s)$, $\gamma$,

$\Delta_o$, and $h_o$ (subscript "o" refers to an initial value), where each of these parameters was varied while the others were held fixed. No tests of sensitivity to $\theta_o$ were necessary because the mixed-layer height does not depend on $\theta_o$. The results of these tests suggest that sensitivity to variations in stable-layer lapse rate is strong, with mixed-layer height decreased by a factor of 2 when $\gamma$ is increased from 0.001 °C m$^{-1}$ to 0.005 °C m$^{-1}$ (see Figure 1). Sensitivity to the surface heat flux is much less pronounced. These conclusions have been reported also by Mahrt and Lenschow (1976). Dependence of mixed-layer height on its initial value and on the initial strength of the inversion is considerably weaker. These variables modify the initial values of h, but have little influence several hours after sunrise.

### Comparison with 1975 Sangamon Data

The 1975 Sangamon experiment was designed to study the evolution of the planetary boundary layer between 0400 and 1200 CST (Hess and Hicks, 1975). Preliminary values of the surface heat flux for four of the sixteen days of observations were used to test Tennekes' model. Initial values of h, $\Delta$, and $\gamma$ were estimated from soundings at 0800 CST. Model predictions and observed heights for the day with most complete data are plotted in Figure 2 for comparison. In general, agreement is fair, with the average error between observation and prediction approximately 150 m.

### Comparison with the 1967 Wangara Data

A most extensive test of Tennekes' model was made with the wealth of micrometeorological observations available from the Wangara experiment (Clarke et al., 1971) at Hay, New South Wales, Australia. Twelve days of unstable conditions were analyzed for use in the present study. Morning potential temperature profiles at 0900 LST were derived from temperature soundings using the relation

$$\theta \approx T + \Gamma_d z ,\qquad (5)$$

where

T = observed temperature

$\Gamma_d$ = dry adiabatic lapse rate

62
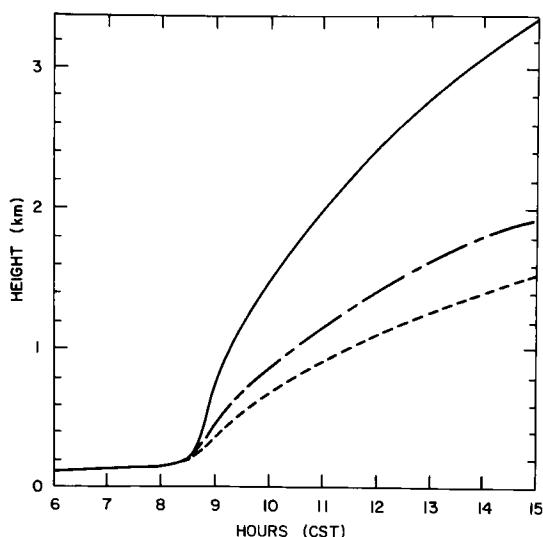
FIG. 1.--Sensitivity of mixed-layer height to variations in stable-layer lapse rate, where $h_0 = 10$ m and $\Delta_0 = 6°C$. The solid line is for $\gamma = 0.001$ °C m$^{-1}$, the dot-dash line is for $\gamma = 0.003$ °C m$^{-1}$, and the dashed line is for $\gamma = 0.005$ °C m$^{-1}$.
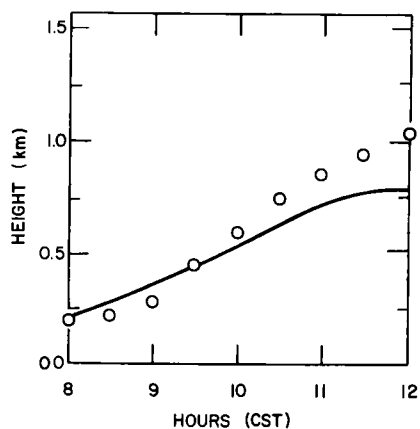
FIG. 2.--Predictions of mixed-layer height (curve) vs. observations (circles) on 27 July 1975 during the Sangamon experiment.

$z$ = height.

Equation 5 is accurate to within 5% in the lowest three kilometers of the atmosphere. Values of $h_0$, $\Delta_0$, and $\gamma$ were determined from the plotted potential temperature soundings. In general, results were mixed for twelve cases tested here. For six cases, agreement between predictions and observations was acceptable, with an average discrepancy of about 100 m. For the remaining six cases, agreement was poor, with an average discrepancy of about 300 m. Although the reasons for such a wide range of results have not yet been completely analyzed, the following features should be noted: (1) Morning temperature (or potential temperature) soundings often do not reveal a simple, "classical" shape with a clearly defined mixed layer. This makes $h_0$, $\Delta_0$, and $\gamma$ particularly hard (if not impossible) to estimate meaningfully. (2) Even when a mixed layer is clearly distinguishable, a stable layer in which $\gamma$ varies widely is often found above the mixed layer. This difficulty might be resolved by selecting two or three different values for $\gamma$, as suggested by Mahrt and

Lenschow (1976), instead of using only one averaged value. (3) Advective changes may make the initial morning sounding a poor predictor of late-morning and afternoon soundings. (4) The omission of moisture and latent heat effects may lead to errors, particularly over wet surfaces.

## References

Clarke, H. H., A. J. Dyer, R. R. Brook, D. G. Reid, and A. J. Troup, 1971: The Wangara experiment: Boundary layer data. Division of Meteorological Physics, CSIRO, Australia, Tech. Paper 19.

Hess, G. D. and B. B. Nicks, 1975: A study of PBL structure: The Sangamon experiment of 1975. Argonne National Laboratory Radiological and Environmental Research Division Annual Report ANL-75-60, Part IV, pp. 1−4.

Mahrt, L. and D. H. Lenschow, 1976: Growth dynamics of the convectively mixed layer. J. Atmos. Sci. 33, 41−51.

Stull, R. B., 1976a: The energetics of entrainment across a density interface. J. Atmos. Sci. 33, 1260−1267.

_____, 1976b: Mixed-layer depth model based on turbulent energetics. J. Atmos. Sci. 33, 1268−1277.

Tennekes, H., 1973: A model for the dynamics of the inversion above a convective boundary layer. J. Atmos. Sci. 30, 558−567.

_____, and A. P. van Ulden, 1974: Short-term forecasts of temperature and mixing height on sunny days. Symposium on Atmospheric Diffusion and Air Pollution, Santa Barbara, Calif., Sept. 9−13, 1974. Am. Meteorol. Soc., pp. 35−40.

# A PRELIMINARY NUMERICAL STUDY OF THE AIRFLOW OVER COMPLEX TERRAIN

T. Yamada

## Introduction

Atmospheric perturbations associated with mountains have been investigated extensively, both theoretically and observationally (e.g., see World Meteorological Organization, Tech. Note, 1967). Unfortunately, observations of wind and temperature with sufficient detail and accuracy can be prohibitively expensive in highly inhomogeneous areas. On the other hand, analytical solutions and wind-tunnel simulations are limited to idealized conditions, which are too restrictive for many applications. A more realistic approach may be to obtain approximate solutions of the finite-difference forms of the hydrodynamic equations through numerical modeling, and to use observations for initial and boundary conditions and verification of selected aspects of the simulations.

There are several existing three-dimensional mesoscale numerical models that include the effects of topography. Most of the models are based on the eddy-viscosity method for parameterizing turbulent fluxes. Turbulence-closure models, which are based on the second-moment turbulence equations, seem to be less restrictive than the eddy-viscosity parameterizations. The closure hypotheses have been discussed in detail elsewhere (e.g., see Mellor, 1973; Mellor and Yamada, 1977). This model has been used in simulating a number of geophysical processes, including atmospheric surface and planetary boundary layers, oceanic surface and bottom boundary layers, pollutant dispersion from a continuous point source and cloud formation over a large cooling pond. As a first step toward realistic treatment of terrain effects by turbulence-closure methods, the airflow over single and multiple Gaussian mountains has been simulated. Detailed discussions on the mathematical formulation and numerical procedures of the basic model, as applied over a flat surface, are given in Yamada (1978a). Thus, only a brief description of the model is given below.

## Description of the Model

The governing equations are 1) equations of motion for the horizontal wind components; 2) conservation equations for the liquid water potential temperature and total water, which are quasi-conservative quantities even when condensation occurs; 3) conservation equations for turbulence energy and a master length scale; and 4) the hydrostatic equation.

These basic equations are transformed into a terrain-following coordinate system $(x, y, z*, t)$ by

$$z* = \bar{H} \frac{z - z_g(x,y)}{H(x,y,t) - z_g(x,y)} , \qquad (1)$$

where $(x, y, z)$ and $(x, y, z*)$ are the original and transformed coordinate systems, respectively; $z_g(x,y)$ is the terrain height above sea level; $H(x,y,t)$ is the height of the computational domain which can be a function of time; and $\bar{H}$ is the initial value of H. The governing equations, after transformation, are given in Yamada (1978b).

## Preliminary Simulations

The mountain used in preliminary simulations is assumed to be Gaussian,

$$z_g(x,y) = M \exp \left\{ -\frac{1}{2} \left[ \left( \frac{x - x_c}{\sigma_x} \right)^2 + \left( \frac{y - y_c}{\sigma_y} \right)^2 \right] \right\} , \qquad (2)$$

where M is the maximum height of the mountain, $(x_c, y_c)$ is the center of the mountain, and $\sigma_x$ and $\sigma_y$ are the horizontal standard deviations. The mountain is placed in a computational domain of 600 km $\times$ 600 km $\times$ 9 km, with M = 499 m, $(x_c, y_c) = (200$ km, 200 km) and $(\sigma_x, \sigma_y) = (50$ km, 50 km). The grid is 13 $\times$ 13 $\times$ 10, with a constant horizontal grid increment (50 km), and a vertical grid increment varying from 10 m at the surface to 2 km at the top. Initial temperature and pressure profiles are constructed from the U.S. Standard Atmosphere. The wind profile is logarithmic near the surface; the wind at the top level is 20 m s$^{-1}$. Water vapor profiles are constructed from the temperature and pressure profiles by assuming the relative humidity to be 90%. The mountain is introduced gradually with time in order to avoid numerical "shock;" thus, all
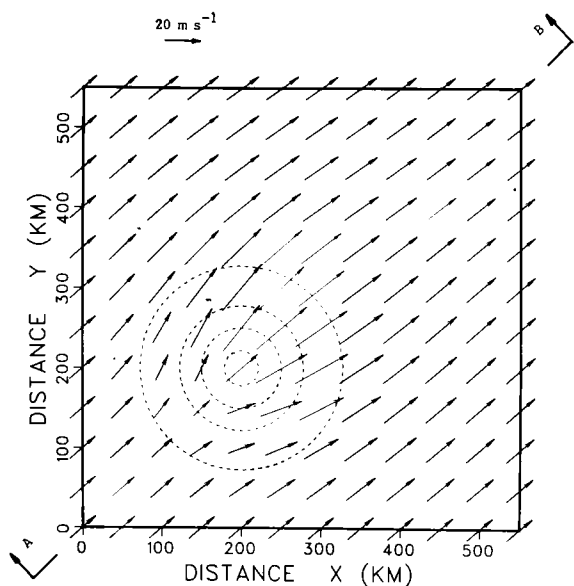
FIG. 1.--Horizontal wind vectors at 1000 m above sea level for a single mountain. Terrain is contoured by dashed lines with an increment of 150 m. The lowest contour is at z = 20 m.
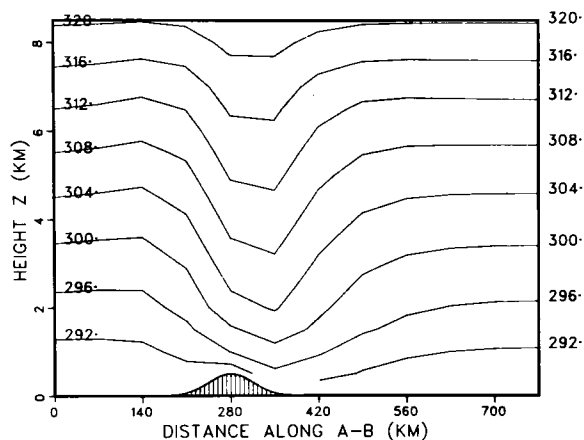
FIG. 2.--Distribution of the potential temperature (K) in a vertical plane through the diagonal A-B shown in Figure 1.
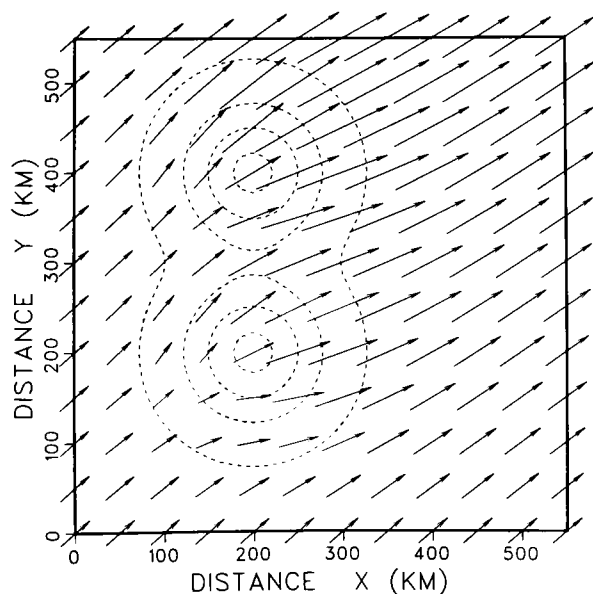
FIG. 3.--Horizontal wind vectors at 1000 m above sea level for twin mountains. Terrain is contoured by dashed lines with an increment of 150 m. The lowest contour is at z = 20 m.

variables are initially horizontally homogeneous. Integrations are performed for 50 time steps with a 10-min time increment.

Figure 1 shows the final horizontal wind distribution at 1000 m. Acceleration and deceleration are seen in the lee and upwind sides, respectively, of the mountain. At the same time the airflow diverges strongly as it approaches the mountain and converges at the lee side of the mountain. Features of the horizontal wind distributions in the layers higher than 4 km are almost the reverse. The convergence and divergence in the horizontal wind fields result in vertical motions, which can be computed from the continuity equation. A maximum downward motion of 2 m s$^{-1}$ is obtained approximately 3.5 km above the mountain and slightly downstream; the maximum upward motion is only 0.35 m s$^{-1}$, as upward motion occurs over a greater volume. The potential temperature in a vertical plane through the diagonal A-B in Figure 1 is shown in Figure 2. The potential temperature is increased by 8°C in the lee of the peak, and the air is much drier than at the inflow boundaries, due to the maximum subsidence, slightly to the lee side of the mountain, bringing down air of higher potential temperature and lower moisture content. A more complex terrain may be constructed by superimposing several Gaussian mountains. Figure 3 shows the horizontal wind distribution at 1000 m for a system of two mountains.

## References

Mellor, G. L., 1973: Analytical prediction of the properties of stratified planetary surface layers. J. Atmos. Sci. 30, 1061—1069.

_____ and T. Yamada: 1977. A turbulence model applied to geophysical fluid problems. Symposium on Turbulent Shear Flows, Pennsylvania State University, University Park, Pennsylvania, 18—20 April 1977, Vol. 1, pp. 6.1—6.14.

World Meteorological Organization, 1967: The airflow over mountains. World Meteorological Organization, Geneva, Switzerland, Tech. Note No. 34, WMO-No.98.TP.43.

Yamada, T., 1978a: A three-dimensional, second-order closure numerical model of mesoscale circulations in the lower atmosphere. Argonne National Laboratory Report ANL/RER-78-1.

_____, 1978b: A three-dimensional numerical study of complex atmospheric circulations produced by terrain. In Proceedings of Conference on Sierra Nevada Meteorology, June 19-21, 1978, Lake Tahoe, Calif., pp.61-67.

# A GAUSSIAN MOMENT-CONSERVATION DIFFUSION MODEL

J. D. Shannon

## Introduction

Development of numerical grid models of regional pollution dispersion is one of the major goals of MAP3S (MacCracken, 1978). The advantage of numerical methods over conventional plume modeling lies in the fact that the effects of temporal and spatial variations of such parameters as wind and stability can be simulated conveniently. A problem in grid models, however, is numerical pseudo-diffusion, which results from finite-difference approximations and limitations in grid resolution.

A one-dimensional numerical diffusion model, known as the puff-on-cell model (Sheih, 1978), has been used with Lagrangian trajectory simulations for the MAP3S area (Sheih, 1977). In his results, Sheih simulated no temporal change of stability (expressed in terms of eddy diffusivity) and little vertical change. For a uniform eddy diffusivity field, the concentration profile predicted by the puff-on-cell method, after constants were adjusted, closely approximated the analytical solution. Further work with the puff-on-cell model, however, revealed that a non-zero minimum of diffusion occurred even when the stability was so strong that the eddy diffusivity was zero.

Since barriers to mixing, such as the nocturnal surface inversion, may be extremely important to dispersion on the regional scale, the puff-on-cell concept has been combined with the conservation-of-moments concept of Egan and Mahoney (1972) as the basis for the Gaussian Moment-Conservation (GMC) model, which reduces the pseudo-diffusion of the original puff-on-cell model in most cases. Egan and Mahoney assume rectangular subgrid-scale distributions; the puff-on-cell and GMC models assume Gaussian distributions within grid cells. The assumptions are arbitrary, since in a grid model a single number must describe the distribution within a grid cell. Both rectangular and Gaussian distributions have well-behaved and easily-calculated moments, and are thus suitable for conservation of moments.

## The Model

The discussion that follows applies to a one-dimensional version of the GMC model. Extension to two or three dimensions is straightforward.

The pollutant mass represented by the single number per grid cell is assumed to be distributed in a Gaussian manner, with the mean $\mu$ at the center of the cell and the variance such that one standard deviation $\sigma$ is half a grid increment. Transport and diffusion during a time step change $\mu$ and $\sigma$. After the time step, which is constrained such that $\mu$ and $\sigma$ change by less than half a grid increment, the temporarily Lagrangian puff must be allocated to the underlying Eulerian grid system; in one dimension the mass of the single puff is allocated to the initial cell and the cells to either side as three Gaussian puffs, defined in such a fashion that the mean and variance of the single puff are approximately conserved. The allocations of different initial puffs are additive in determining the initial field for the next time step.

Diffusion is simulated by an artificial wind, the diffusive velocity (Sklarew et al., 1971), which is calculated at the edges of the grid cell (the $\pm \sigma$ positions). The diffusive velocity is defined as

$$\xi = \frac{-K_x}{C} \frac{\partial C}{\partial x} \, ,$$  (1)

where $K_x$ is the component of eddy-diffusivity along x and C is the concentration. The effect of the diffusive velocity is to shift and spread the $\pm \sigma$ positions and thus the puff. If $\xi_i^+$ and $\xi_i^-$ indicate the diffusive velocities at the $\pm \sigma$ positions, respectively, of the puff in the i-th cell, and $u_i^+$ and $u_i^-$ indicate the corresponding mean wind components, then

$$\overset{*}{\mu}_i = \left( \frac{u_i^+ + \xi_i^+}{2} + \frac{u_i^- + \xi_i^-}{2} \right) \Delta t$$  (2)

and

$$\overset{*}{\sigma}_i = \frac{\Delta x}{2} + \left( \frac{u_i^+ + \xi_i^+}{2} - \frac{u_i^- + \xi_i^-}{2} \right) \Delta t \, ,$$  (3)

where $\overset{*}{\mu}_i$ and $\overset{*}{\sigma}_i$ are the new mean and standard deviation for the puff, $\Delta t$ is the time increment, $\Delta x$ is the grid length, and $\mu_i = 0$ is the center of the i-th cell.

A set of equations conserving the zero-th, first, and second moments of a puff with a normalized mass can now be written

$$M_{i-1} + M_i + M_{i+1} = 1 \tag{4}$$

$$-M_{i-1}\Delta x + M_{i+1}\Delta x = \overset{*}{\mu}_i \tag{5}$$

$$M_{i-1}\left[\left(\frac{\Delta x}{2}\right)^2 + (\Delta x)^2\right] + M_i\left(\frac{\Delta x}{2}\right)^2 + M_{i+1}\left[\left(\frac{\Delta x}{2}\right)^2 + (\Delta x)^2\right]$$
$$= (\overset{*}{\sigma}_i)^2 + (\overset{*}{\mu}_i)^2 \; . \tag{6}$$

$M_i$, $M_{i-1}$, and $M_{i+1}$ are the masses to be allotted to the initial and adjacent cells. Equations 4–6 would conserve moments exactly, except that each mass must be non-negative in order to have a physical meaning. After the calculations are made for every cell, any negative mass in the grid system is set equal to zero, and the positive mass is reduced by the equivalent amount. The total mass of pollutant in the grid system is unchanged, but moments are now only approximately conserved. It can be seen from the equations that there can be no pseudo-diffusion when both $K_x$ and u are zero (such as the limiting case for a strong inversion). If an expanding grid system is used, in order to provide better resolution in some part of the grid system, then Eqs. 5 and 6 become

$$-M_{i-1}\left(\frac{\Delta x_{i-1} + \Delta x_i}{2}\right) + M_{i+1}\left(\frac{\Delta x_i + \Delta x_{i+1}}{2}\right) = \overset{*}{\mu}_i \tag{7}$$

and

$$M_{i-1}\left[\left(\frac{\Delta x_{i-1}}{2}\right)^2 + \left(\frac{\Delta x_{i-1} + \Delta x_i}{2}\right)^2\right] + M_i\left(\frac{\Delta x_i}{2}\right)^2$$
$$+ M_{i+1}\left[\left(\frac{\Delta x_{i+1}}{2}\right)^2 + \left(\frac{\Delta x_i + \Delta x_{i+1}}{2}\right)^2\right] = \overset{*}{\sigma}_i^2 + \overset{*}{\mu}_i^2 \; . \tag{8}$$

Results

A numerical diffusion model should be compared to analytical solutions of the diffusion equation when possible. The comparison here is for a much simpler case (no spatial variation and temporal variation only of the mean wind) than the situations for which the model was designed, in order that the analytical solutions can be calculated. In Figure 1, the results of a one-dimensional
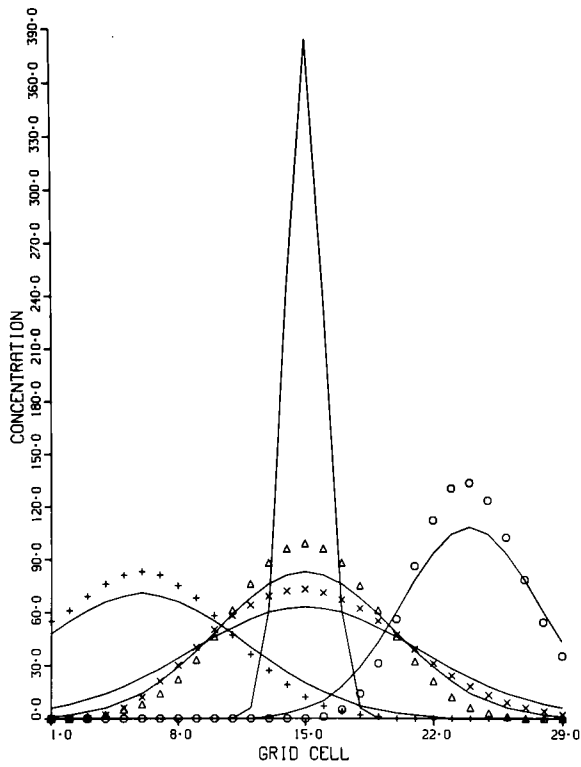
FIG. 1.--Comparison of the GMC method (points) with the corresponding analytical solutions (curves) for the case of $\Delta x = 100$ m, $K_x = 10$ m$^2$ s$^{-1}$, and $u = 0.3925 \cos (2\pi t/4$ hr$)$ m s$^{-1}$. Concentrations are initial and after one (o). two ($\Delta$), three (+), and four (x) hours of advection and diffusion.
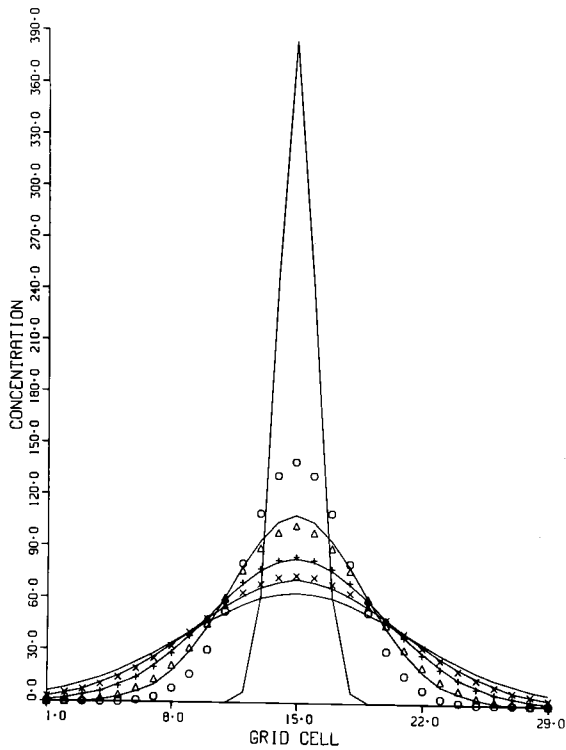


FIG. 2.--GMC results for the case described in Figure 1, without advection (u = 0).
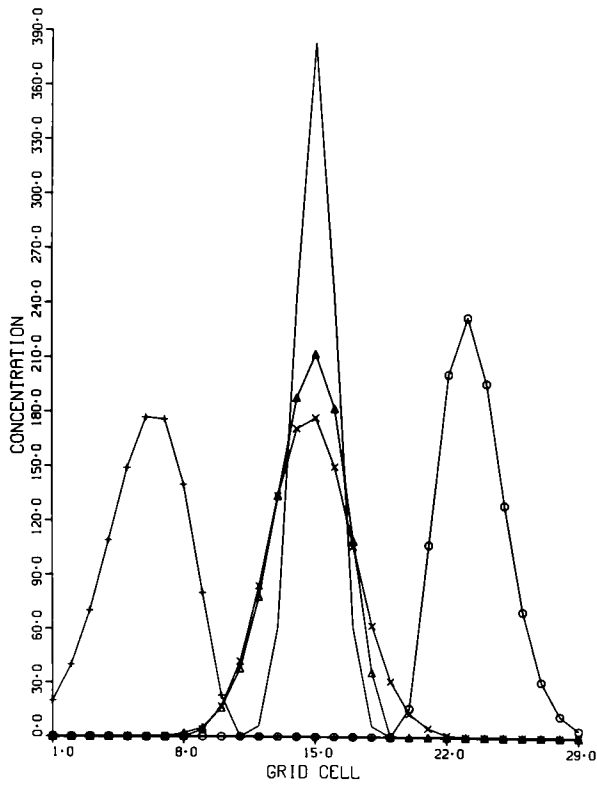
FIG. 3.--GMC results for the case described in Figure 1, without diffusion ($K_x = 0$).
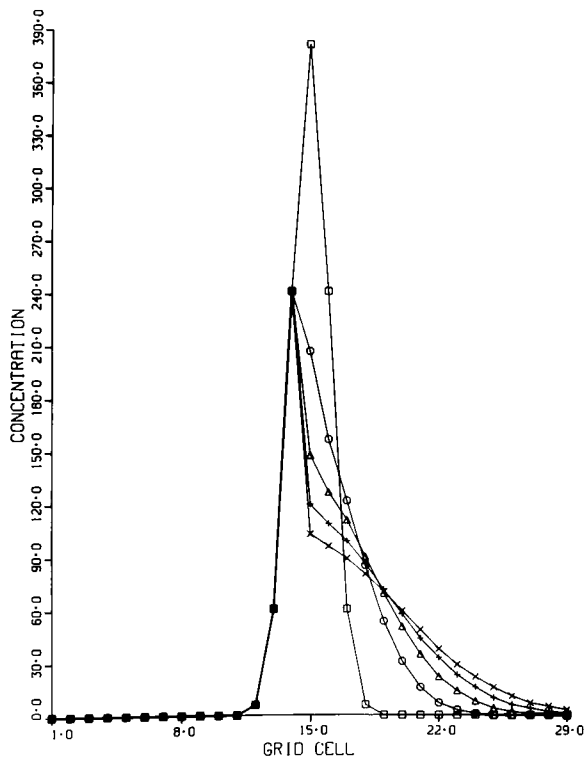


FIG. 4.--GMC results for a case of pure diffusion, with $K_x = 10$ m$^2$ s$^{-1}$ on the right side, and $K_x = 0$ on the left side. Symbols are as described in Figure 1.

version of the GMC model (points) are compared to the corresponding analytical solutions (curves). The test case is an initial Gaussian distribution across seven grid cells. The eddy diffusivity is $10 \text{ m}^2 \text{ s}^{-1}$ and the mean wind velocity is sinusoidal in time with a period of four hours. In this advection-plus-diffusion case, the GMC model diffuses somewhat less than the analytical solution. Figures 2 and 3 show GMC simulations of pure diffusion and pure advection, respectively. The analytical solutions, if centered, correspond to pure diffusion. Again, the GMC method diffuses somewhat less than the analytical solution. The proper analytical solution corresponding to pure advection is the initial distribution (shifted right and left at one and three hours, respectively). The reduction in the peak by the GMC method is due to numerical pseudo-diffusion. The pseudo-diffusion occurs mainly during the first hour when the gradients are steepest. The figures illustrate the fact that the extent of pseudo-diffusion is dependent upon the particular situation being simulated. In a pure diffusion case shown in Figure 4, $K_x = 0$ across the left half of the grid and 10 $\text{m}^2 \text{ s}^{-1}$ across the right half. The pollution in the stable portion of the grid remains highly concentrated. The GMC method can be extended readily to the more complicated situations of realistic simulations of atmospheric structure.

References

Egan, B. A. and J. R. Mahoney, 1972: Numerical modeling of advection and diffusion of urban area source pollutants. J. Appl. Meteorol. 11, 312–322.

MacCracken, M., 1978: MAP3S:An investigation of atmospheric, energy related pollutants in the northeastern United States. Atmos. Environ. 12, 649-659.

Shieh, C. M., 1977: Application of a statistical trajectory model to the simulation of sulfur pollution over northeastern United States. Atmos. Environ. 11, 173–178.

_____, 1978: A puff-on-cell model for computing pollutant transport and diffusion. J. Appl. Meteorol. 17, 140-147.

Sklarew, R. C., A. J. Fabrick, and J. E. Prager, 1971: A Particle-in-cell Method for Numerical Solution of the Atmospheric Diffusion Equation, and Applications to Air Pollusion Problems. Division of Meteorology, National Environmental Research Center, Report 35R-844.

# A POSSIBLE METHOD FOR ESTIMATING THE CONCENTRATION OF SULFUR IN PRECIPITATION

B. B. Hicks

## Introduction

Concern about acid rainfall has led to an increased research effort in a number of related disciplines. At the same time, the need to develop better simulations of air pollution episodes has led to advanced studies of precipitation scavenging as a sink for atmospheric contaminants. Each of the four major programs investigating regional-scale air pollution problems in North America[*] recognizes the importance of precipitation scavenging as a major sink for atmospheric sulfate particles; the other major sink is dry deposition. Several precipitation-sampling networks have been set up in recognition of the need for more comprehensive data on the deposition of pollutants in rain and snow, but simple methods for the estimation of wet removal rates are required immediately.

The complexity of existing numerical schemes and the limited size of available computers result in the requirement that formulations describing both dry and wet deposition processes should be relatively straightforward. For the case of dry deposition, the concept of a deposition velocity has gained considerable favor amongst modelers, although the simple expedient of assuming a surface flux proportional to the appropriate pollutant concentration in air at some conveniently low level is an oversimplification. For wet deposition, there is considerable support for the "washout ratio" approach. This has had a large amount of exposure in recent years, mainly as a consequence of studies of the wet deposition of trace metals. In essence, washout ratios express the relationship between concentrations of material detected in precipitation and

---

those measured in air at the same time. An alternative procedure is to employ some experimentally determined "scavenging rate," usually expressed as a percentage removed per unit of rainfall (or of time) in an exponential decay scheme.

A recent reanalysis of natural radioactivity concentrations measured in rain collected during several storms at Argonne National Laboratory indicated relatively constant values of the scavenging rate, which was assumed to be that appropriate for natural, background aerosol particles (q.v. Hicks, 1978). However, published values of the scavenging rate of sulfate particles vary widely. Part of the apparent scatter can be associated with differences in terminology; some of the reported scavenging rates apply only to the collection of aerosol by falling raindrops (mainly via impaction), whereas other evaluations represent the sum of this and in-cloud processes such as nucleation. The data presented earlier (in Hicks, 1978) suggest, therefore, that sub-cloud and in-cloud scavenging mechanisms combine to produce a relatively constant rate of removal. However, it is well known that the concentration of contaminants in light rains is much greater than in more extensive rainfalls and for this reason a number of relationships describing the dependence of the effective average washout ratio on the amount of rainfall have been developed. Table 1 gives some examples of equations of this kind; these result from studies of radioactive fallout in rain. All of the tabulated formulations yield a net washout ratio which decreases with increasing rainfall amount, but unfortunately there is little agreement otherwise. Some of the relationships are derived from data collected on an event basis, others apply to long-term averages. In order to incorporate wet removal in regional-scale numerical models it is necessary to develop a parameterization procedure similar to those tabulated, but applicable to the short-term precipitation data reported by the National Weather Service and suitable for use in simulations of atmospheric sulfur pollution. It is the present aim to address this need, starting with a review of some relevant results derived in studies of radioactive fallout and ending with a comparison with some recent measurements of sulfate in rainfall collected at ANL (as reported by Tisue and Kacoyannakis, 1978).

Table 1. Some relationships between the amount of material (A) deposited in a rainfall (h); a, b, and c are constants.

| | |
|---|---|
| $A = a[1 - \exp(-bh)]$ | Damon and Kuroda (1954) |
| $A = ah - bh^2$ | Szalay and Bere'nyi (1958) |
| $A = a[1 + bh - \exp(-ch)]$ | Miyake et al. (1960) |
| $A = a(1 + bh^{1.2} - ch^{2.4})$ | Moeken and Alderhout (1963) |

## Total Beta Emitter Concentrations

The period of intensive testing of nuclear weapons during the 1950's provided an opportunity for thorough study of the physical processes associated with the wet removal of atmospheric radioactivity. However, investigations of the factors that control the concentrations in precipitation were hampered by the repeated injection of new material. In the northern hemisphere, injections were sufficiently frequent to make interpretation of observations exceedingly difficult, and even in the southern hemisphere considerable difficulty was encountered. Accordingly, the declaration of a weapons testing moratorium in the early 1960's resulted in a spate of studies intended to capitalize upon the existence of known quantities of trace material held in a reservoir aloft. Figure 1 illustrates the results obtained from an investigation of beta emitters deposited in weekly rainfall at Aspendale, Victoria, Australia, between September 1961 and May 1962. For the present purpose, these moratorium data have been separated into convenient groups and plotted as means and standard errors. Only material deposited in rain is considered. Corrections have been applied for the effects of dry deposition, which was measured in five weeks to be at rates of 28, 29, 30, 23, and 52 $\mu$Ci km$^{-2}$. The data suggest a net dependence upon the half-power of the weekly rainfall amount, as indicated by the line drawn by eye through the data points.

Data suitable for testing the behavior illustrated in Figure 1 are exceedingly rare. We may, however, consider the results published by Hall (1965), who reports on a study of three extensive squall-line storms in Oklahoma in 1964. A network of rain samplers provided about ten separate samples from
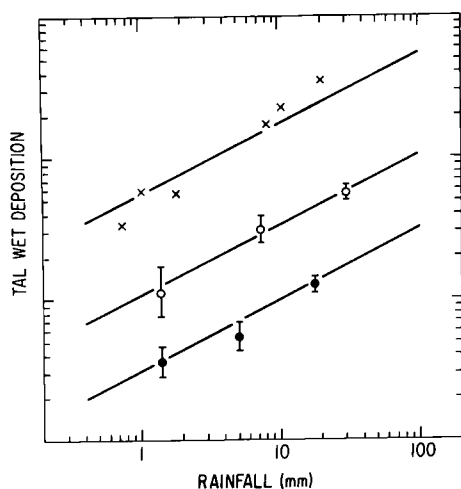
FIG. 1.--The dependence of wet deposition on rainfall amount, using weekly averaged radioactivity data obtained in Australia during 1961 and 1962 (solid circles), pre-event data obtained in Oklahoma during 1964 (open circles, q.v. Hall, 1965), and sulfate measurements made at Argonne during 1975 (crosses, q.v., Tisue and Kacoyannakis, 1978). (ANL Neg. 149-78-80)

each occurrence. The resulting data have also been grouped and plotted in Figure 1. There appears to be excellent support for extending the half-power relationship from weekly averages to events.

## Some Sulfate Data

Recently, Tisue and Kacoyannakis (1978) have analyzed rainfall collected at ANL during 1975. Data collected during a three-week period from October 18 to November 10 are plotted in Figure 1. A value obtained later (November 20) does not fit the overall picture and seems to be representative of an entirely different air mass, but the six plotted sulfate determinations appear to confirm the beta-activity results reasonably well. More data would be required before it could be concluded that the best-fitting power-law relationship is different from that deduced from the beta-activity data.

## A Procedure for Use in Simulations

The considerations above lead to the suggestion of a power-law dependence between the concentration of material deposited in rainfall ($C_r$) and the quantity of rain (h):

$$C_r = A_0 h^{-\frac{1}{2}} \quad . \tag{1}$$

For use in numerical models, it is required to relate the constant $A_0$ to the concentration in air. To this end, we turn again to measurements of radio-

active fallout in rain. Since the intent of this particular study is to suggest an interim parameterization procedure for application in the northeastern USA, we will concentrate on data obtained at ANL, which is located in this region.

Table 2 lists data obtained during a study of rainout at ANL conducted in 1966 (Hicks, 1978). Values of the washout ratio (the ratio of concentration in rain to that in air, $C_a$) are tabulated, as well as estimates of the quantity

$$\xi = C_r h^{\frac{1}{2}} / C_a \qquad (2)$$

suggested by the previous discussion. For these calculations measurements of $C_a$ made near the surface have been employed. Two different fission products have been selected for use here; each is easily identified and measured through the detection of distinctive gamma emissions.

The values listed in Table 2 indicate that for this particular data set there is relatively little statistical benefit to be derived from the use of the present half-power-law relationship instead of the more conventional (linear) washout-ratio method. However, the value of the constant $\xi$ seems to be quite well determined (to ± 30% accuracy). When converted from volumetric to mass units, the value of the constant is found to be about 2000 $mm^{\frac{1}{2}}$. On the other hand, the conventional washout ratio is about 900, which is much the same as would be expected for the case of sulfate rainout (Garland, 1978, presents values ranging from about 500 to 1500, after a single value of 24,000 is omitted; these evaluations are attributed to Cawse, 1974). Thus, the anticipation that radioactivity rainout data will be indicative of sulfate rainout does indeed appear to be verified.

Conclusions

The method described here for the inclusion of precipitation scavenging in regional-scale numerical simulations of atmospheric sulfur pollution is intended mainly as an interim measure. It is fully expected that considerably better relationships will be developed as more data become available. For the present, however, experience in past studies of radioactive fallout indicates

Table 2. Washout ratios and values of the "constant" $\xi$ derived from measurements of $^{141}$Ce and $^{95}$Zr concentrations in air and rain at Argonne during 1966. Values are obtained by direct manipulations of air concentrations in pCi per thousand standard cubic meters, rain concentrations in pCi per litre, and rainfall quantities in millimeters.

| Date | h, mm | Washout Ratios | | $\xi$ | |
| | | $^{141}$Ce | $^{95}$Zr | $^{141}$Ce | $^{95}$Zr |
|---|---|---|---|---|---|
| 20 May | 2.0 | 10.6 | 3.0 | 15.0 | 4.2 |
| 13 June | 1.5 | 1.9 | 1.9 | 2.3 | 2.3 |
| 5 July | 3.1 | 0.2 | 0.5 | 0.4 | 0.8 |
| 11 July | 5.9 | 2.3 | 1.0 | 5.7 | 2.5 |
| 13 July | 4.6 | 0.5 | 0.7 | 1.1 | 1.4 |
| 18 July | 0.8 | 0.3 | 2.3 | 0.3 | 2.0 |
| 26 July | 97.3 | 0.4 | 0.4 | 4.3 | 3.9 |
| 1 August | 6.3 | 0.2 | 0.1 | 0.6 | 0.4 |
| 10 August | 13.6 | 0.6 | 0.3 | 2.3 | 1.0 |
| Geometric mean: | | 0.74 | 0.72 | 1.75 | 1.64 |
| Standard error: | | 56% | 65% | 55% | 29% |
| | | 0.73 ± 32% | | 1.69 ± 28% | |

that the use of a constant washout ratio might be rather misleading, since average concentration will decrease with increasing rainfall amount, following an approximate half-power relationship.

The half-power formulation should be applied with considerable caution, since it is clear that the data on which it is based are very limited. For example, only mid-latitude warm rainfall is considered. Clearly, the results of contemporary precipitation sampling networks will eventually provide the crucial test of this and other models of precipitation scavenging.

Acknowledgements

G. T. Tisue, D. M. Nelson, and J. Kacoyannakis of the Ecological Sciences Section of this Division contributed a significant amount of the data

used here.  This work forms part of the ANL contribution to the U.S. DOE MAP3S program.

## References

Cawse, P. A., 1974:  A survey of atmospheric trace elements in the U.K., (1972–1973):  AERE-R 7669, H.M.S.O., London.

Damon, A. N. and P. K. Kuroda, 1954:  On the natural radioactivity of rainfall. Trans. Am. Geophys. Union, $\underline{35}$, 208.

Garland, J. A., 1978:  Dry and wet removal of sulfur from the atmosphere. Atmos. Environ., in press.

Hall, S. T., 1965:  Radioactivity in precipitation:  Case studies from the 1964 spring season, Radioactive Fallout from Nuclear Weapons Tests. USAEC CONF-765, pp. 532–565.

Hicks, B. B., 1978:  An evaluation of precipitation scavenging rates of background aerosol., J. Appl. Meteorol. $\underline{17}$, 161–165.

Miyake, Y., K. Sarahashi, Y. Katsuragi, and T. Kanagawa, 1960:  Radioactive fallout in Japan and its bearings on meteorological conditions.  Pap. Meteor. Geophys. $\underline{11}$, 151.

Moeken, H. H. Ph., and J. J. H. Alderhout, 1963:  The relationship between the concentration of world-wide fallout in air and in rain.  Int. J. Air Water Poll. $\underline{7}$, 91.

Tisue, G. T. and J. Kacoyannakis, 1978:  Acidity in rainfall:  Analysis and simulations.  In preparation.

Szalay, A. and D. Bere'nye, 1958:  Fission product precipitation from the atmosphere in Debrecen, Hungary between 1952 and 1957.  International Conference on the Peaceful Uses of Atomic Energy, Geneva, 18.

# POLLUTANT TRANSFER ACROSS THE CAVITY REGION BEHIND A TWO-DIMENSIONAL FENCE

C. M. Sheih,[**] P. J. Mulhearn,[***] E. F. Bradley,[***] and J. J. Finnegan[***]

## Introduction

The cavity region or separation bubble in the lee of a structure is known to be isolated from the main flow by a closed-loop streamline. Pollutants can be trapped inside the bubble for extended periods of time, a situation which may cause the pollutants to accumulate to an unacceptable concentration level. The problem has attracted considerable recent interest. For example, Vincent (1977) has studied pollutant transfer across the separation bubbles of rectangular blocks by measuring the decay time constant of pollutant concentration after pollutant emissions inside the bubble are ended. Robins and Castro (1977) have investigated the concentration field in the separation bubble of a cubical model by releasing a continuous pollutant source in the bubble.

In the present investigation, it is felt that better understanding of the transfer processes across the separation bubble might be accomplished by studying a two-dimensional fence. This is because the flow behind a two-dimensional fence is easier to understand and has been studied more extensively (e.g., Chang, 1966; Plate, 1967; Good and Joubert, 1968; and Ranga Raju et al., 1976) than the flow behind cubical structures. A two-dimensional fence also has broad practical applications. It has been used as a shelterbelt to reduce the erosion of soil by wind, and it can also be used to trap radioactive particles from the tailings of uranium mines. Investigation of the transport processes across the separation bubble can help determine optimal arrangements of shelterbelts. Results could also apply to dispersion behind long fence-like buildings. The aspect ratio (height to cross-wind length) required for the existence of a two-dimensional flow section can be estimated from the study

by Mulhearn and Bradley (1977).

In the present investigation a simple mathematical formula for predicting the pollutant flux across the separation bubble in the lee of a two-dimensional fence has been constructed. To determine the constants in the analytical solution, wind tunnel experiments using heat as a tracer to represent the pollutant were conducted with various combinations of fence height, heat input and free-stream mean wind velocity. The study has been extended to the prediction of pollutant concentration inside the separation bubble.

## Theoretical Formulation

Figure 1A shows the configuration of the separation bubble behind a fence and the profiles of wind velocity (u) and pollutant concentration (C). A rigorous treatment of the problem is not possible because of the complexity of the flow. However, if one is interested in the transfer processes in the mixing region, a semi-empirical approach is available. In summarizing Chang's (1966) work, Plate (1971) shows that the velocity and the momentum-flux profiles in the mixing region are very similar to that of the "free-jet-boundary" flow (Schlichting, 1960) and proposes the simplified model shown in Figure 1B for this region. Under such conditions, the equation of motion for the mixing region can be approximated by

$$u\frac{\partial u}{\partial x} + w\frac{\partial u}{\partial z} = \epsilon\frac{\partial^2 u}{\partial z^2} , \qquad (1)$$

$$\epsilon = K_1 x (u_\infty - u_0) , \qquad (2)$$

where x is the horizontal downstream distance from the fence, z is the vertical coordinate, and $z = z' - h$, u and w are the velocity components along x and z, respectively, $\epsilon$ is eddy diffusivity, $K_1$ is a constant, and $u_\infty$ and $u_0$ are wind velocities at the upper and lower boundaries, respectively. The velocity $u_0$ is zero for a solid fence and non-zero for a porous fence. With the flow configuration in Figure 1B the velocity profile in the mixing region can be obtained by solving Eqs. 1 and 2. The result is given by Plate as

A

B
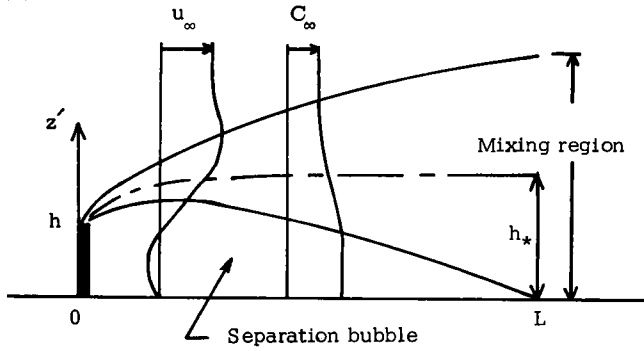
FIG. 1.--A, the configuration of the flow behind a fence and B, the equivalent model of "free-jet-boundary" flow for representing the transfer processes in the mixing region. (ANL Neg. 149-78-85)
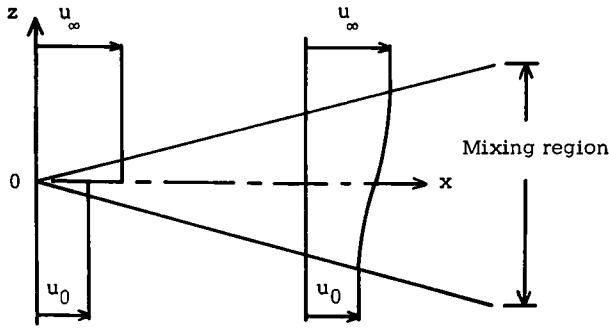
$$u = \frac{u_\infty + u_0}{2} \left\{ 1 + \frac{u_\infty - u_0}{u_\infty + u_0} \ \text{erf}\,(K_2 z/x) \right\} \quad , \tag{3}$$

where $K_2$ is a constant. If one assumes that the eddy diffusivities for the transport of momentum and pollutant are the same, the governing equations for pollutant transport in the mixing region will be similar to Eqs. 1 and 2, and the solution for the pollutant concentration will be

$$C = \frac{C_\infty + C_0}{2} \left\{ 1 + \frac{C_\infty - C_0}{C_\infty + C_0} \ \text{erf}\,(K_2 z/x) \right\} \quad , \tag{4}$$

where $C_0$ and $C_\infty$ are pollutant concentrations at the upper and lower boundaries, respectively. Making use of a flux-gradient relationship and Eqs. 2 and 4, one can formulate the pollutant flux per unit area and integrate the result along the entire boundary of the separation bubble to obtain the following total pollutant flux (Q) leaving the separation bubble,

84

$$Q = K_3 [1 - 2.79 (h/L)^2] (u_\infty - u_0)(C_0 - C_\infty)L , \qquad (5)$$

where $K_3$ is a constant, and L is the length of separation bubble. The equation shows that if the mean wind velocities and pollutant concentrations inside and outside the bubble, the fence height and the separation bubble length are measured, the total pollutant flux leaving the bubble can be computed. On the other hand, if the rate of pollutant injection into the bubble is known, the pollutant concentration inside the bubble can be computed from the equation, provided that fence height, bubble length, wind velocity, and pollutant concentration in the free-stream are measured.

## Wind Tunnel Experiment

The wind tunnel experiment was conducted at the Pye Laboratory of the CSIRO Division of Environmental Mechanics. A detailed description of the wind tunnel has been reported by Wooding (1968). In order to generate a thick boundary layer, a 5-cm tripping fence was installed at the entrance of the test section. For each experiment, one of the model fences was placed 7 m downstream from the tripping fence. The boundary layer thickness at that location was about 20 cm. The free-stream mean wind velocities were in the range of 5 to 25 m s$^{-1}$. The corresponding range of Reynolds numbers for the model fence is $10^4$ to $10^5$. However, it appears that the present results should be applicable to higher Reynolds numbers encountered in full-scale structures. Schlichting (1960) has shown with spheres that if the Reynolds number exceeds about $10^5$, the location of the flow separation around the objects will no longer change enough to affect the dynamic similarity of the flow. Since the location of the flow separation of the present model always occurs at the upstream sharp-edge corner of the fence, the pattern of the forces acting on the fence will remain the same for higher Reynolds numbers.

Instead of a gas, electrically produced heat was chosen as a tracer to represent a pollutant for the experiment. Temperatures inside and outside the separation bubble were measured with a thermistor probe. Measurements of

the length of the separation bubbles were made with a series of loose cotton strings parallel to the fence. The ends of each string were anchored to a pair of metal strips spaced about 40 cm apart. Since wind velocities inside and outside the separation bubble were opposite in direction, the strings were separated into two groups by the flow, and the distance from this division to the fence was the length of the separation bubble.

Since all the other variables in Eq. 5 were measured, the constant $K_3$ could be computed. For 15 cases tested with the bubble temperature $(T_0)$ measured at $x = z' = h/2$ and with various combinations of fence height, free-stream velocity and heating rate, the analysis of the observed data gave $K_3 = 0.0087 \pm 0.00016$.

## Conclusion

The total flux of pollutant leaving the separation bubble can be expressed in terms of fence height, separation-bubble length, free-stream mean velocity and pollutant concentrations in the free-stream inside the separation bubble. The pollutant concentration inside the bubble is taken at a reference location, one half fence height from both the ground and the fence. Obviously, the experimental constant determined for the flux formula is applicable only to the concentration at this location. However, wind-tunnel results, not shown here, indicate that if geometrical similarity is satisfied for two different flows, the concentration fields will be similar if the vertical coordinate, the horizontal coordinate, and the concentration are scaled by the fence height, the separation bubble length, and the product of source strength and the concentration at the reference point, respectively. Using this similarity relationship for the concentration field, one can combine the flux formula with a complete description of the concentration field for a particular case, such as shown in Figure 2, to predict pollutant concentration for other flow conditions and for other locations of the separation bubble.
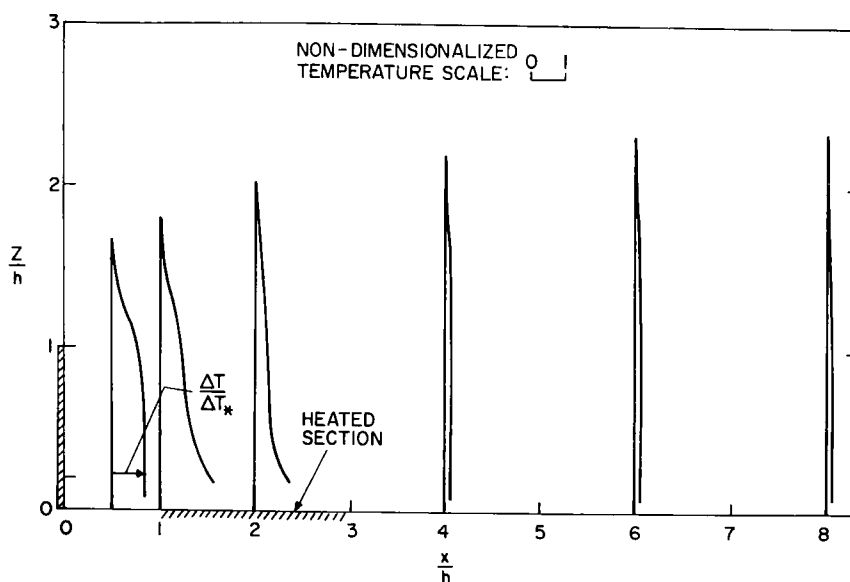
FIG. 2.--Profiles of excess temperature normalized by the excess temperature at $x = z = h/2$, for fence height $h = 6$ cm and free-stream velocity $u = 10$ m s$^{-1}$. (ANL Neg. 149-77-431)

## References

Chang, S. C., 1966: Velocity distributions in the separation flow behind a wedge-shaped model hill, M.S. Thesis, Colorado State University, Fort Collins, Colorado.

Good, M. C. and P. C. Joubert, 1968: The form drag of two-dimensional bluff-plates immersed in turbulent boundary layers. J. Fluid Mech. 31, 547—582.

Mulhearn, P. J. and E. F. Bradley, 1977: Secondary flows in the lee of porous shelterbelts. Boundary-Layer Meteorol., in press.

Plate, E. J., 1967: Diffusion from a ground level line source into the disturbed boundary layer far downstream from a fence. Int. J. Heat Mass Transfer 10, 181—194.

_____, 1971: The aerodynamics of shelterbelts. Agr. Meteorol. 8, 203—222.

Rnage Raju, K. G., J. Loser, and E. J. Plate, 1976: Velocity profiles and fence drag for a turbulent boundary layer along smooth and rough flat plates. J. Fluid Mech. 76, 383—399.

Robins, A. G. and I. P. Castro, 1977: A wind tunnel investigation of plume dispersion in the vicinity of a surface mounted cube-II. The concentration field. Atmos. Environ. 11, 299—311.

Schlichting, H., 1960: Boundary Layer Theory. McGraw-Hill, New York, N.Y., 4th Ed.

Vincent, J. H., 1977: Model experiments on the nature of air pollution transport near buildings. Atmos. Environ. 11, 765—774.

Wooding, R. A., 1968: A low-speed wind tunnel for model studies in micrometeorology, CSIRO Div. Plant Industry Tech. Paper No. 25.

# SOME EFFECTS OF DISPLACEMENT HEIGHT VARIABILITY IN TALL VEGETATION

B. B. Hicks

## Introduction

The micrometeorological data collected during the 1975 Sangamon experiment have been shown to support the contention that the level of maximum foliage temperature in a thick canopy varies with the time of day, presumably according to the depth of penetration of direct solar radiation (Hicks and Wesely, 1977). It seems appropriate to relate this level to the displacement height to which thermal flux gradient measurements should be referred, much in the manner that Thom (1971) identifies the effective level of action of the drag force on crop elements as the conventional zero-plane displacement height d for momentum transfer.

There is no obvious physical reason why the displacement heights relevant to the transfer of any pair of atmospheric quantities should be coincident, even though it is common practice to take all displacement heights to be the same as that for momentum. Equality is usually assumed for the simple reason that information on displacement heights other than d is not available. This assumption is likely to be misleading. For example, if a gas is emitted as a result of decay of organic material at the forest floor, a low value for the appropriate displacement height must be expected. The effective levels of exchange of water vapor and other gases taken up or lost via stomatal apertures are probably controlled by the morphology of the vegetation as well as by stomatal closure; at night, when stomates are closed, displacement heights might be considerably lower than in daytime.

Many of the ideas expressed above are analogous to the concept of "deep thermal penetration" advocated by some forest meteorologists. The consequences of taking $d_H$ to vary with the time of day, which is a convenient way of expressing this concept mathematically, will be explored here. It will be assumed that all other displacement levels are the same as d.

## Formulation of Atmospheric Stability

Micrometeorological flux-gradient relationships are generally formulated in terms of dimensionless atmospheric stability parameters such as $(z-d)/L$, where z is the height of observation and L is the Obukhov scale length of turbulence. At first sight, it might seem that taking $d_H \neq d$ would cause some uncertainty about how to formulate stability in a manner such that there is a one-to-one correspondence with the results obtained over smoother surfaces for which the assumption of equality is appropriate. That this is not the case can be seen from consideration of the fact that $(z-d)/L$ is a measure of the ratio of the production rate of turbulent energy due to buoyancy to that due to mechanical forces. The former term is not a function of height in the constant flux layer, but the latter involves the height above the conventional (momentum) displacement level. No other displacement height enters into the definition of $(z-d)/L$.

However, use of the gradient Richardson number cannot be recommended, since

$$Ri = ((z-d)/L) \cdot ((z-d_H)/(z-d)) \cdot (\phi_H/\phi_M^2) , \tag{1}$$

where $\phi_H$ and $\phi_M$ are correction functions which are strongly dependent on $(z-d)/L$. Equation 1 reverts to the familiar relationship between Ri and $(z-d)/L$ only when $d = d_H$. Thus, use of the gradient Richardson number should be avoided in micrometeorological studies above tall canopies, since otherwise seemingly anomalous flux-gradient relations might be artificially produced. Accordingly, the following analyses will be in terms of $(z-d)/L$.

## Fluxes over a Forest

Consider, for example, the case of flow over a forest canopy of height 20 m and with a known zero plane displacement for momentum transfer of 16 m (i.e., $d = 0.8 h$). Suppose, then, that the displacement height for thermal transfer is located substantially below 16 m, say $d_H = 12$ m, but that all other zero planes are coincident with that for momentum. We will consider the effect of this difference in thermal behavior upon measurements made above the canopy

and upon the interpretation of data obtained.

For purposes of illustration, we will assume that measurements are made at the semi-binary levels 5.66 m, 8 m, 11.31 m, 16 m, etc. above d. In recognition  of the usual desire to analyze only data obtained above the canopy, lower levels will not be considered.

Table 1 presents some examples of what might be measured in typical circumstances.  Starting with assumed values of the friction velocity $u*$ and

TABLE 1. Data and computations used for illustration of the effect of taking $d_H \neq d$. Values of $u_*$, H, and $L_wE$ are assumed and values of L and u are derived from them. Then, finite differences between the heights 5.66, 8, 11.31, and 16 m (levels 1 to 4 respectively) are computed.  These differences are used to determine Bowen ratios on the basis of which erroneous values of H and $L_wE$ are derived.  Wind speeds and friction velocity are in cm s$^{-1}$, heat fluxes are in W m$^{-2}$, temperatures are in °C, humidities are in g kg$^{-1}$ and L is in m.

| Assumptions | | | | | | |
|---|---|---|---|---|---|---|
| $u_*$ | 30 | 30 | 50 | 50 | 70 | 70 |
| H | 100 | 200 | 100 | 200 | 100 | 200 |
| $L_wE$ | 400 | 300 | 400 | 300 | 400 | 300 |
| Obukhov length: -L | 19.1 | 11.1 | 88.3 | 51.3 | 242. | 141. |
| Velocity at 5.61 m | 90 | 74 | 197 | 186 | 289 | 284 |
| Finite differences | | | | | | |
| Levels 1 − 2 | | | | | | |
| $\Delta u$ | 15.9 | 14.1 | 34.8 | 32.0 | 54.3 | 51.6 |
| $\Delta\theta$ | 0.057 | 0.090 | 0.059 | 0.100 | 0.053 | 0.095 |
| $\Delta q$ | 0.148 | 0.087 | 0.153 | 0.097 | 0.136 | 0.092 |
| Levels 2 − 3 | | | | | | |
| $\Delta u$ | 14.7 | 13.0 | 33.1 | 30.1 | 52.7 | 49.5 |
| $\Delta\theta$ | 0.055 | 0.086 | 0.060 | 0.099 | 0.055 | 0.098 |
| $\Delta q$ | 0.127 | 0.074 | 0.138 | 0.086 | 0.128 | 0.085 |
| Levels 3 − 4 | | | | | | |
| $\Delta u$ | 13.6 | 12.0 | 31.2 | 28.1 | 50.7 | 47.2 |
| $\Delta\theta$ | 0.051 | 0.080 | 0.059 | 0.095 | 0.057 | 0.098 |
| $\Delta q$ | 0.109 | 0.063 | 0.123 | 0.075 | 0.119 | 0.077 |
| Average "Bowen ratio" | 0.175 | 0.468 | 0.176 | 0.468 | 0.176 | 0.469 |
| Inferred sensible heat | 74 | 159 | 75 | 159 | 75 | 160 |
| Inferred latent yeat | 426 | 341 | 425 | 341 | 425 | 340 |

the sensible heat flux H, profiles of wind and temperatures have been reconstructed by the use of the flux-gradient relations recommended by Dyer (1974). As required in the present model, gradients of temperature $\theta$ are referred to $d_H = 12$ m, and gradients of wind u are referred to $d = 16$ m.

The examples of Table 1 are constrained so that the sum of sensible and latent heat fluxes $(H + L_w E)$ is 500 W m$^{-2}$. When Bowen ratio methods are used to derive values of H and $L_w E$ from measurements of net radiation R, it is usually assumed that heat storage and photosynthetic terms are small and hence that

$$L_w E = R/(1 + \beta^{-1}) , \qquad (2)$$

where $L_w$ is the latent heat of vaporization of water and $\beta$ is the Bowen ratio:

$$\beta \equiv c_p \Delta\theta/L_w \Delta q , \qquad (3)$$

Equating $\beta$ to the ratio $H/L_w E$ requires that the diffusivities $K_H$ and $K_W$ are equal, which has been found to be true over relatively smooth surfaces, (e.g., Dyer, 1967) but which is clearly inappropriate in the present circumstances. Blind application of the usual Bowen ratio methods to the temperature and humidity data of Table 1 results in underestimation of the sensible heat flux by about 25%.

Analysis of the flux-gradient relations in terms of Richardson number would be similarly misleading. Figure 1 presents the apparent $K_H/K_M$ versus Ri dependence yielded by the values of Table 1. The suggestion that the stability dependence does not follow the conventional flux-gradient relations (as indicated by the solid line) is a direct result of the assumption that $d_H = d$. A plot of $K_H/K_M$ against z/L would be similarly misleading, although possibly compounded by the use of inaccurate estimates of H and $L_w E$ derived from the Bowen ratio method.

Discussion and Conclusions

A number of analyses of flux-gradient relations over rough surfaces have indeed resulted in the suggestion that conventional formulations might be wrong by a considerable amount. For example, an exceedingly thorough
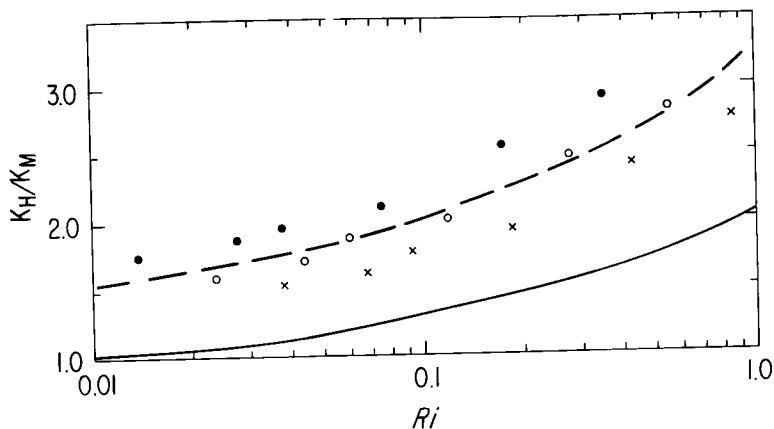
FIG. 1.--The apparent variation of $K_H/K_M$ with Richardson number over a canopy in which $d = 16$ m and $d_H = 12$ m. Gradients from which these values are derived are obtained by application of conventional flux-gradient formulations, so that the appearance of a discrepancy is a direct consequence of taking $d_H = d$ in the reduction of the data. The solid line represents the behavior that would be expected if $d_H = d$; the dashed line is drawn by eye through data points evaluated from Table 1. Solid circles, open circles, and crosses indicate results applicable at levels of 22.7, 25.5 and 29.5 m, respectively. (ANL Neg. 149-78-150)

micrometeorological investigation of a pine forest (Thom et al., 1975) concluded that errors of the order of a factor of two occurred in unstable and near-neutral conditions, but that no such disagreement existed when conditions were stable. Their finding is in complete agreement with the present model, since in stable stratification (at night) the assumption $d_H = d$ is almost certain to be correct (since penetration of the canopy by the solar beam is no longer an active mechanism). Further, Hicks et al.(1975) investigated the relationship between $d$ and $d_H$ in slightly unstable conditions, but under persistent heavy cloud cover, and detected no significant difference.

If the present simple model of flux-gradient relationships above tall vegetation proves correct, some rather intriguing characteristics can be predicted. In tropical areas, the depth of thermal penetration into canopies would be much greater than at higher latitudes (all other matters being the same) and hence relatively large apparent discrepancies might be expected for surfaces near the equator. Distinct differences would be expected between the behavior of atmospheric quantities which are derived from near-surface sources (e.g., hydrogen sulfide from duff and aromatic hydrocarbons from boles) and that of

92

stomatally-controlled quantities (e.g., sulfur dioxide and water vapor).
Finally, and perhaps most importantly, these considerations cause us to
question the validity of a large body of hydrological literature which has ac-
cepted estimates of evaporation rates based on Bowen ratio methods without
recognizing that these estimates might be inaccurate when vegetation is suf-
ficiently tall.

References

Dyer, A. J., 1967: The turbulent transport of heat and water vapour in an
        unstable atmosphere. Q. J. R. Meteorol. Soc. 93, 501−508.
_____, 1974: A review of flux-profile relationships. Boundary-Layer
        Meteorol. 7, 363−372.
Hicks, B. B., P. Hyson, and C. J. Moore, 1975: A study of eddy fluxes
        over a forest. J. Appl. Meteorol. 41, 58−66.
_____ and M. L. Wesely, 1977: Thermal characteristics of adjacent
        soybeans and maize crops: Sangamon 1975. This report.
Thom, A. S., 1971: Momentum absorption by vegetation. Q. J. R. Meteorol.
        Soc. 97, 414−428.
_____, J. B. Stewart, H. R. Oliver, and J. H. C. Gash, 1975: Compari-
        son of aerodynamic and energy budget estimates of fluxes over a pine
        forest. Q. J. R. Meteorol. Soc. 101, 93−105.

# AN ANALYSIS OF PARTICULATE DATA COLLECTED AT ARGONNE

R. G. Everett and B. B. Hicks

## Introduction

During the summer of 1976, particulate air samplers were operated at two heights on the 44.5 m meteorological tower at Argonne. The samplers, usually called streakers, were maintained by ANL personnel as part of a Florida State University (FSU) regional pollution study. In each streaker, a vacuum pump was connected to a moving orifice that was slowly drawn across a Nuclepore filter (0.4 $\mu$m pore diameter). This sample was then analyzed in two-hour increments by Proton Induced X-ray Emission (PIXE). The resulting energy spectra were analyzed by a nonlinear least squares program in order to obtain concentrations of various elements, including sulfur, lead, iron, titanium, silicon, and potassium. A complete, detailed description of the project and analysis techniques may be found elsewhere (Berg et al., 1977a and Berg et al., 1977b).

This paper presents a quantitative analysis of fluxes determined from the ANL tower streaker data previously reported by FSU investigators (Berg et al., 1977a). The horizontal transport of particulate sulfur and lead is investigated through the use of a wind rose and polar plots of normalized fluxes. Finally, data from the two streakers are compared and deposition velocities are estimated.

## Data Analysis

The data used in this study were obtained during the period 6—13 July 1976. As the PIXE technique is capable of two-hour time resolution, there are 84 time steps available for analysis. This imposes some rather severe limitations on any generalizations about long-range transport, and any statements about fluxes or long-range transport should be considered to be specific to this study (q.v., Sheih and Hess, 1977). The streakers were located at 11.5 m and 34.5 m on the tower, but winds used in the analysis were taken at 6 m

94

and 44.5 m. This discrepancy between the levels of measurements probably resulted in small but consistent errors in the analysis which follows.

In the particulate sulfur transport analysis, the first consideration is the relative frequency of wind direction. Figure 1 is a wind rose computed from ANL wind data during the study period. Each 30-degree sector contains one point that represents the normalized frequency distribution of the wind coming from that sector. This agrees quite well with a 15-year average wind rose computed at ANL for the month of July (see Moses and Bogner, 1967, p. 46). A polar plot of wind speed in each sector normalized by the sum of the wind speeds for all the sectors was almost identical to Figure 1. Figures 2 and 3 contain the normalized fluxes of particulate sulfur measured at 11.5 m and 34.5 m, respectively. The fluxes are computed from the equation

$$F_j = \left( \sum_{i=1}^{n_j} u_i C_i \right) / \left( \sum_{i=1}^{N} u_i C_i \right) , \tag{1}$$

where $F_j$ and $n_j$ are the normalized flux and the total number of occurrences of the wind in the j-th sector, respectively, $u_i$ and $C_i$ are wind velocity and particulate sulfur concentration of the i-th sample, respectively, and N is the total number of samples. For example, Figure 2 shows that about 30% of the total amount of particulate sulfur passed by the ANL tower when the winds were between 195° and 225°. The total flux of particulate sulfur for the lower streaker is about 0.6 mg $m^{-2} s^{-1}$ while for the upper unit the value is 1.1 mg $m^{-2} s^{-1}$. From this analysis it is clear that more than 50% of particulate sulfur observed at ANL is associated with winds from the south through west. Chicago contributes a substantially smaller amount of particulate sulfur to Argonne.

The horizontal transport of lead at ANL was studied in a similar manner. Unfortunately, the number of data points available for analysis is much smaller since the concentration of particulate lead was at or below the detection limit about half the time. The wind rose was not modified for analysis of lead flux, since it was felt that points below the detection limit still contained valuable information (i.e., for that two-hour period, and with the winds in that given direction, there was very little lead). The normalized lead fluxes were
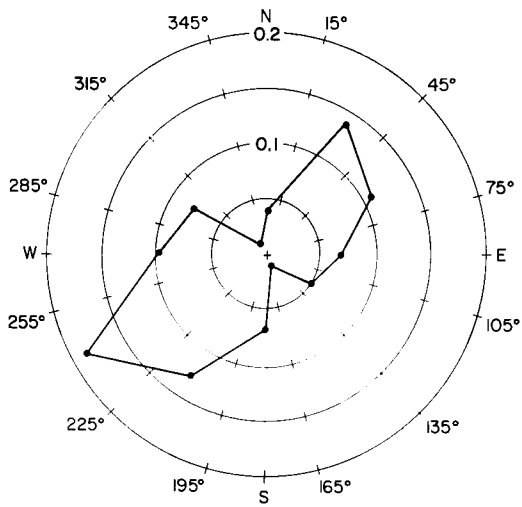
FIG. 1.--Normalized wind rose at ANL
during the week of 6–13 July 1976 at
44.5 m.
(ANL Neg. 149-78-61)
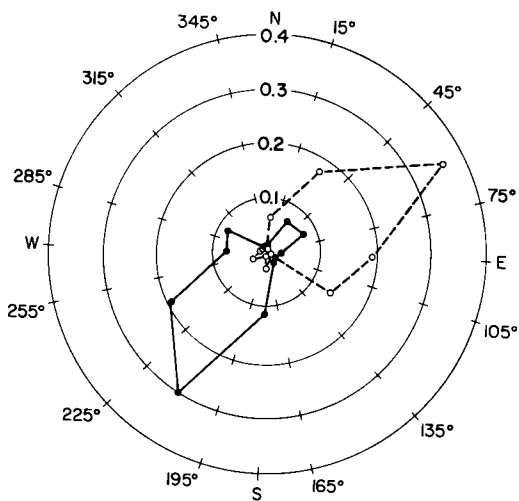
FIG. 2.--Polar plot of normalized
particulate sulfur (solid line) and lead
(dashed line) fluxes during the week of
6–13 July 1976 at 11.5 m on the ANL
tower (center of the plot).
(ANL Neg. 149-78-63)
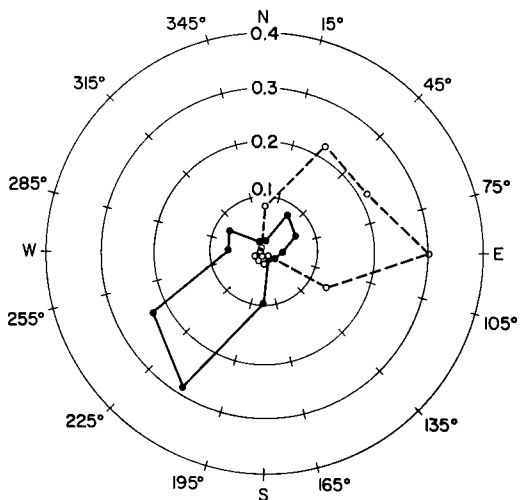
FIG. 3.--Same as above, but at
34.5 m.
(ANL Neg. 149-78-62)

96

computed in a manner similar to Eq. 1 and are shown in Figures 2 and 3 for 11.5 m and 34.5 m, respectively. These show the strong influence of heavy automobile traffic east and northeast of ANL. Total fluxes are 0.04 mg m$^{-2}$s$^{-1}$ and 0.07 mg m$^{-2}$s$^{-1}$ for the lower and upper streakers, respectively.

A comparison of the particle concentrations at the lower and upper streakers produces some interesting results. The mean ratio of particulate sulfur concentration at the top to that at the bottom is 1.206, with a standard error of 0.018. On the other hand, the same analysis for lead results in a mean ratio of 1.150 and a standard error of 0.230; thus, the ratio was not statistically different from unity. Clearly, the case of lead is not well defined; while the concentration ratios seem to yield a similar average to that obtained from the particulate sulfur data (certainly not statistically different), the standard error is sufficiently great that little further analysis is warranted. However, in the case of particulate sulfur, the ratios can be used to obtain some tentative information on deposition velocities $(v_d)$, since it can be shown (q.v., Hicks, 1975) that in near-neutral conditions

$$v_d \simeq (C(z_2)/C(z_1) - 1)(ku_*)/\ln(z_2/z_1) \, , \tag{2}$$

where $C(z_i)$ is the concentration of the appropriate material at height $z_i$, k is the von Karman constant $(\approx 0.41)$, and $u_*$ is the friction velocity. For this study Eq. 2 was corrected for the various atmospheric stabilities during which the data were taken (for discussion, see Wesely and Hicks, 1977). In particular, the 1.5 to 6 m Richardson number, Ri, was used such that for the stable case, $0.0 < Ri < 0.2$, Eq. 2 becomes

$$v_d = \Delta u \left[ \frac{C(z_2)}{C(z_1)} - 1 \right] \left[ \frac{k}{1.10 + (\frac{38.35\, Ri}{1 - 5\, Ri})} \right] \left[ \frac{k}{1.39 + (\frac{7.5\, Ri}{1 - 5\, Ri})} \right] \, , \tag{3}$$

where $\Delta u$ is the difference in wind speeds between 1.5 m and 6 m. For the unstable case, $-2 < Ri < 0.0$, Eq. 2 is changed to

$$v_d \simeq \Delta u \left[ \frac{C(z_2)}{C(z_1)} - 1 \right] \left[ \frac{k}{1.10 - \psi_{H_2} + \psi_{H_1}} \right] \left[ \frac{k}{1.39 - \psi_{M_2} + \psi_{M_1}} \right] ,$$

(4)

where $\psi_{H_i}$ and $\psi_{M_i}$ are stability-dependent correction functions evaluated at the appropriate heights. The results are summarized in Table 1. The limited quantity of information warrants only a coarse sorting according to wind speed and stability; nevertheless, a tendency for $v_d$ to increase with velocity is indeed apparent. Furthermore, $v_d$ is seen to decrease as the atmosphere becomes more stable. Both these findings are in agreement with the predictions of simple turbulence models.

It is clear that the present deposition velocities are substantially greater than the values common in most contemporary numerical models; usually, deposition velocities of about 0.1 cm s$^{-1}$ are used. The adoption

Table 1. Values of the deposition velocity (cm s$^{-1}$) for particulate sulfur and of the momentum transfer velocity yielded by the ANL tower data, sorted according to velocity and stability. Data are restricted to $|L| > 10$ m, and n is the number of samples.

|  |  | $\tilde{u} \le 4.5$ m s$^{-1}$ | $\bar{u} > 4.5$ m s$^{-1}$ | Overall |
|---|---|---|---|---|
| | n | 7 | 8 | 15 |
| Stable | $v_d$ | 1.37 | 1.00 | 1.17 ± 0.25 |
| | $v_u$ | 1.07 | 1.62 | 1.36 ± 0.15 |
| | n | 6 | 6 | 12 |
| Unstable | $v_d$ | 0.98 | 2.32 | 1.65 ± 0.81 |
| | $v_u$ | 0.54 | 2.23 | 1.39 ± 0.35 |
| | n | 13 | 14 | 27 |
| Overall | $v_d$ | 1.19 ± 0.48 | 1.56 ± 0.59 | 1.38 ± 0.38 |
| | $v_u$ | 0.82 ± 0.11 | 1.88 ± 0.25 | 1.37 ± 0.17 |

of low values for the deposition velocity for particulate sulfur is sometimes supported (somewhat heuristically) by the contention that the transfer of particles in the immediate vicinity of the ultimate surface sink will be hindered by their extremely low diffusivity. In essence, this imposes a surface resistance to transfer which is somewhat analogous to that which enters into formulations of the transfer of trace gases such as water vapor and sulfur dioxide. This surface resistance acts in series with the aerodynamic resistance $\bar{u}/u_*^2$ determined by the momentum transfer to the surface in question. In fact, close examination of the present deposition velocities shows them to be remarkably close to the values corresponding to the aerodynamic resistance. To show this, Table 1 also lists values of the momentum transfer velocity, or conductivity, $v_u = u_*^2/\bar{u}$.

The suggestion in Table 1 that $v_d$ sometimes exceeds $v_u$ is of doubtful statistical significance. It seems unlikely that $v_d$ will exceed $v_u$, although it is possible that such a finding might result when the sulfur flux is heavily weighted towards larger particles and is consequently influenced by gravitational sedimentation. The close agreement between $v_d$ and $v_u$ might indeed be fortuitous; however, a considerable amount of confidence in the present numbers is generated by the overall behavior evident in Table 1.

## Conclusions

Clearly, much less particulate sulfur reaches the ANL site from the northeast than from the southwest, a result that is expected. Long and short-range transport are intermingled so that it is difficult to distinguish between the effects of nearby sources located 5 to 40 km SW of Argonne and emissions from St. Louis and other industrial areas to the southwest. Again, particulate sulfur emission data would help solve this problem. On the other hand, lead behaves as if it were solely from local sources. The present analysis of particulate concentration data at ANL yields results which are somewhat surprising, especially insofar as the deposition velocity appropriate for evaluating the flux of sulfur-bearing particles is indistinguishable from that derived from atmospheric turbulence properties alone. In this regard, it appears that the

sulfur particle flux is unaffected by surface considerations, which have some-
times been considered to be the critical and controlling factors. However, it
is obvious that the present results cannot be extended to other situations with-
out great risk. It is important to remember the limitations of the experiment,
and especially the rather poor exposure of the tower on which the measurements
were made.

## References

Berg, W. W., R. Vie le Sage, K. Sato, J. O. Pilotte, S. L. Cohn, J. W.
        Winchester, and J. W. Nelson, 1977a: Time variation of aerosol
        composition in the Great Lakes basin. Submitted to Journal of Great
        Lakes Research.
———, K. Sato, R. Vie le Sage, J. W. Winchester, and S. L. Cohn,
        1977b: Time dependent sulfur and trace metal correlations in nonurban
        aerosols from an eastern U.S. mesoscale network. Proceedings of
        AICHE 70th Annual Meeting, New York, N.Y., November 13—17,
        1977 (in press).
Hicks, B. B., 1975: Instrumental requirements for the measurement of pol-
        lutant fluxes. Argonne National Laboratory Radiological and Environ-
        mental Research Division Annual Report ANL-75-60, Part IV, pp. 51-57.
Moses, H. and M. A. Bogner, 1967: Fifteen-year Climatological Summary:
        January 1, 1950—December 13, 1964. Argonne National Laboratory
        Report ANL-7084.
Sheih, C. M. and G. D. Hess, 1977: Temporal sampling requirements for
        long-term atmospheric pollutant dispersion studies. Submitted to
        Tellus.
Wesely, M. L. and B. B. Hicks, 1977: Some factors that affect the deposition
        rates of sulfur dioxide and similar gases on vegetation. J. Air
        Pollut. Control Assoc. 27, 1110—1116.

# A COMPARISON OF AERODYNAMIC TO CANOPY RESISTANCES FOR OZONE UPTAKE BY MAIZE

M. L. Wesely, J. A. Eastman, D. R. Cook, and B. B. Hicks

## Introduction

In a previous annual report (Wesely and Hicks, 1976), the resistance of vegetation to uptake of sulfur dioxide and similar gases was shown to be significant when compared to aerodynamic resistances within the atmospheric surface layer. Typical values of the bulk canopy resistance were estimated on the basis of numerous investigations of stomatal resistances reported in the scientific literature. The bulk canopy stomatal resistance $r_{cs}$ undergoes strong diurnal variations due to changes in solar radiation and water stress, among other factors. Thus, in numerical models that are to account for the fate of pollutants over long trajectories, the simulated rate of removal at the surface of the earth should be highly variable over the course of a day of travel over vegetation, owing to the highly variable surface properties. Similarly, in studies of the effects of pollutants on plants, the total uptake needed for determining dose-response relationships can be calculated accurately only if variations of canopy resistances are taken into consideration.

In this report, the bulk canopy resistance $r_c$ to ozone uptake is computed for both healthy and senescent maize crops, so that its importance relative to aerodynamic resistances can be assessed. Ozone is quite different from sulfur dioxide in chemical properties, e.g., ozone is more reactive with most substances and is less soluble in pure water. Nevertheless, there is strong evidence, as will be shown, that ozone uptake is mostly controlled by stomatal resistance in the healthy maize canopy in much the same manner as the flux of sulfur dioxide is normally controlled.

## Measurements of $r_c$

Two experiments are partially reported here. The first was performed at the Sangamon site in central Illinois during the summer of 1976 (Sisterson et al., 1976), the second at the AMBIENS site in Rush County of southeastern

Indiana during the autumn of 1977 (Hicks, 1977; Wesely, 1977). At Sangamon the corn crop was full-grown and healthy, while at Rush the canopy was senescent, so that the stomata were not functional.

At both sites, the ozone vertical flux was estimated by eddy-correlation techniques frequently used by this Section, with ozone sensors as described elsewhere (Eastman and Stedman, 1977; Eastman et al., 1977; Cook and Wesely, 1977). The deposition rate was essentially measured directly, and the values of aerodynamic resistance $r_a$ and average leaf boundary-layer resistance $r_s$ were calculated on the basis of eddy-correlation measurements of stress and heat flux, and mean quantities. A full description of the formulations used is given by Wesely and Hicks (1977); we only note here that the deposition velocity is

$$v_d = (r_a + r_s + r_c)^{-1} \, ,$$

(1)

specific to a certain height, usually 4–5 m in the present studies.

The values of $r_c$ and $r_{cs}$ are determined with the use of rather elaborate assumptions. These assumptions include: (1) the eddy diffusivities for heat, water vapor, and ozone are identical; (2) the aerodynamic displacement heights for heat, water vapor, and ozone are equal to that for momentum; (3) there are no sources or sinks for ozone in the air layer between the point of measurement at a height of 4–5 m and the leaf surfaces in the canopy; and (4) the leaf boundary-layer resistance associated with the quasi-laminar flow very close to leaf surfaces can be taken into account for heat and water vapor, as shown, for example, by Garratt and Hicks (1972), and in a similar manner for ozone. Various aspects of the validity of these an other assumptions are discussed by Wesely and Hicks (1977).

Figures 1 and 2 show the results obtained at Sangamon, where the estimates of resistance $r_{cs}$ to water vapor transport are derived on the basis of energy balance estimates of latent heat flux. This $r_{cs}$ should be a measure primarily of the bulk canopy stomatal resistance and is easily converted to the case of any gas of known molecular diffusivity that does not react with leaf surfaces and is taken up with negligible resistance by the mesophylls of leaves.

Obviously $r_c$ and $r_{cs}$ are highly correlated during most of the day. Before about 0900 on each day, dew was present on the surfaces of the leaves, resulting in a failure of $r_{cs}$ to be an accurate measure of stomatal resistance.

If $r_{cs}$ were an accurate measurement of only stomatal resistance, and if stomatal resistance were the only important mechanism that controls uptake, $r_c$ would be greater than $r_{cs}$ as a result of the relatively slow rate of ozone diffusion through stomatal openings. With such conditions, considerations of molecular diffusivities leads to the approximation $r_c \simeq 1.6 \, r_{cs}$. However, the matter is complicated by the need to include a mesophyll resistance, which might not be negligible for ozone because of its relatively low solubility in water (mesophyll resistance to water loss is assumed to be zero). Let us assume for the moment that mesophyll resistance to ozone uptake is extremely small, and that the only site for ozone removal within the canopy, other than via stomatal apertures, is at the leaf surface. Also, because of the dense canopy, transfer to the soil surface is assumed to be very small. Then, with the assumption that the leaf stomatal resistance is $r_{cs}$ and is in parallel with the resistance $r_x$ to ozone transfer at the outer portions of the leaves, $r_c$ can be expressed as

$$r_c = [(1.6 \, r_{cs})^{-1} + r_x^{-1}]^{-1} . \tag{2}$$

With the use of the average values of $r_c$ and $r_{cs}$ found between 0900 and 1500 for the two days at Sangamon, $r_x$ is calculated to be about 7 s cm$^{-1}$. This value is fortuitously close to the likely value of cuticular resistance to water vapor transport. Since $r_{cs}$ already includes the effects of cuticular resistance to water vapor, the actual cuticular resistance to ozone uptake would seem to be significantly less than 7 s cm$^{-1}$, perhaps 3–4 s cm$^{-1}$. Therefore, it appears that a small but significant amount of ozone is lost at the leaf surface. If the mesophyll resistance to ozone uptake were large, $r_x$ would have to be even smaller in order to compensate.

Figure 3 shows some of the results at Rush, which were nearly duplicated on other days. Comparison with Figs. 1 and 2 shows that $r_x$ was greater at Rush than at Sangamon, indicating that the dead canopy was not as good a
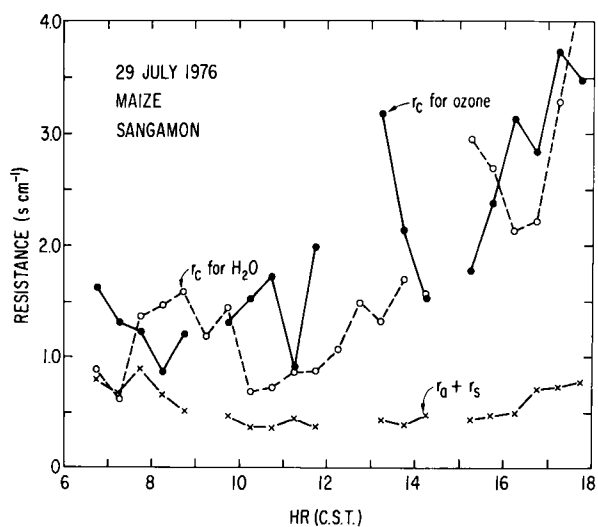
FIG. 1.--Comparison of resistances determined for the full-grown, healthy maize canopy at Sangamon.
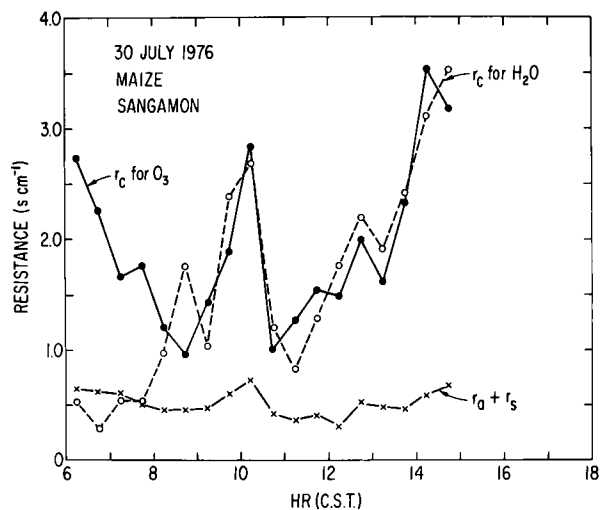
FIG. 2.--Resistances as in Figure 1 for the following day.
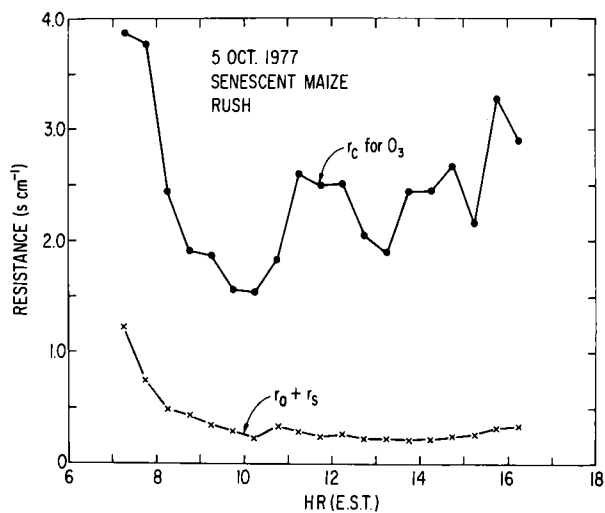
FIG. 3.--Comparison of resistances to ozone transport to the senescent maize canopy at Rush.

104

site for ozone destruction as was the living maize canopy. The midmorning minimum occurs almost simultaneously with the disappearance of dew. Thus, water on the leaves and stalks may have retarded ozone uptake during early morning. After about 1030, $r_c$ seems to increase gradually but not as markedly as at Sangamon. This increase of $r_c$ is difficult to explain, since stomatal effects, which occurred at Sangamon, probably were not present. A few small grassy weeds upwind of the sampling location may have had an effect. Otherwise, a possible explanation is that the surfaces became slightly saturated with the products of ozone reactions with surface materials, thus decreasing the efficiency of uptake. In order to explain the recurrent midmorning minimum, a mechanism causing the surface to become more reactive at night should be postulated. Perhaps the wetting of leaf surfaces by dew somehow allows the surfaces to "recover" over night during periods of very low ozone concentrations.

## Conclusions

The field data presented here support the hypothesis that ozone uptake by maize is controlled largely by resistance to diffusion through leaf stomata in a manner similar to the regulation of water loss. During the daytime, values of $r_c$ are typically 1–5 times larger than aerodynamic resistances calculated for the layer below heights of 4–5 m. A similar result for the uptake of sulfur dioxide by healthy maize is expected.

For surfaces not covered by healthy vegetation, the rates of uptake of ozone are poorly documented at present. This is also true for sulfur dioxide, indicating that a variety of pollutants and types of surfaces need to be investigated.

## References

Cook, D. R. and M. L. Wesely, 1977: Modification of an ozone sensor to permit eddy-correlation measurements of vertical flux. This report.
Eastman, J. A., M. L. Wesely, and D. R. Cook, 1977: A comparison of two chemiluminescent ozone detectors used in eddy-correlation measurements. This report.

Eastman, J. A. and D. H. Stedman, 1977: A fast response sensor for ozone eddy-correlation measurements. Atmos. Environ. $\underline{11}$, 1209−1211.

Garratt, J. R. and B. B. Hicks, 1972: Momentum, heat, and water vapour transfer to and from natural and artificial surfaces. Q. J. R. Meteorol. Soc. $\underline{99}$, 680−687.

Hicks, B. B., 1977: The AMBIENS experiment. This report.

Sisterson, D. L., B. B. Hicks, and M. L. Wesely, 1976: An outline of the 1976 Sangamon field experiment. Argonne National Laboratory Radiological and Environmental Research Division Annual Report ANL-76-88, Part IV, pp. 1−6.

Wesely, M. L. and B. B. Hicks, 1976: Likely effects of plant stomatal resistance on the deposition of sulfur dioxide and ozone on soybeans and maize. Argonne National Laboratory Radiological and Environmental Research Division Annual Report ANL-76-88, Part IV, pp. 76−80.

_____ and B. B. Hicks, 1977: Some factors that affect the deposition rates of sulfur dioxide and similar gases on vegetation. J. Air Pollut. Contol Assoc. $\underline{27}$, 1110−1116.

_____, 1977: Surface characteristics of the 1977 AMBIENS site. This report.

# MODIFICATION OF AN OZONE SENSOR TO PERMIT EDDY-CORRELATION MEASUREMENTS OF VERTICAL FLUX

D. R. Cook and M. L. Wesely

## Introduction

Regional modeling of pollutant dispersion and removal requires knowledge of the rate of removal of pollutants at the surface of the earth. By measurement of the vertical flux of pollutants near the surface, the removal rate can be estimated, and appropriate formulations can be developed. Eddy-correlation techniques have proven quite successful in making such measurements because of the reliability of the sensors and the direct nature of the measurements. Flux determinations over a variety of surfaces can provide a significant data base from which typical fluxes can be estimated and applied in a regional-scale model. Surfaces of interest include agricultural crops, forests, water bodies, bare soil, and snow.

To apply eddy-correlation techniques to the measurement of ozone flux, a commercially available, chemiluminescent ozone sensor similar to that described by Warren and Babcock (1970) was purchased and modified to make a fast-response sensor. In 1977, it was used in conjunction with a fast-response propeller anemometer to measure ozone flux over three surfaces: mature soybeans, loblolly pines, and senescent maize.

## Sensor Characteristics

The principal components of the ozone sensor are a 100 ml reaction chamber, a photomultiplier tube and accompanying electronics for signal processing. A sensitivity selection of 1 ppb to 1 ppm full scale by decades is included, with only the two most sensitive settings having been used so far. Sample air and ethylene simultaneously enter the reaction chamber, mixing at the photomultiplier tube face. Destruction of ozone is assumed to be insignificant as the sample moves 0.5 m from the Teflon sample tube inlet to the photomultiplier tube face. Before entering the reaction chamber, particles are removed from the sample stream by a Teflon filter, preventing accumulation on the photo-

multiplier tube face that could result in reduced sensitivity of the device.

A reaction between ozone in the air sample and the ethylene results in the emission of light in a broad band of wavelengths centered at 435 nm (Fontijn, Golomb, and Hodgeson, 1972). The intensity of light is proportional to the concentration of ozone. A description of the reaction and an example of the emission spectra are included in an article by Finlayson, Pitts, and Akimoto (1972). Factors influencing the sensitivity of the sensor include the temperature of the photomultiplier tube and the flowrates of the ethylene and air sample streams. These factors are monitored with a temperature sensor implanted next to the housing of the photomultiplier tube and flowmeters placed in the exhaust (combined sample air and ethylene leaving the sensor) and ethylene streams. Laboratory calibrations were made at an ethylene flowrate that is a compromise between flowrate and sensor response. This flowrate has been and will be used in all measurements. The calibrations resulted in the calibration equation

$$[O_3] = 794 \ V \ F^{-1} \ (T/273)^{-9} \ ,$$

where    $[O_3]$ is the concentration of ozone in ppb

V is the signal from the sensor in volts DC

T is the temperature of the photomultiplier tube in °K

F is the exhaust flowrate in $l \ min^{-1}$.

Rapid variations of temperature in the photomultiplier tube are prevented by a half inch of polystyrene insulation surrounding the tube. Although the commercially-available sensor is designed to operate at atmospheric pressure, the length of inlet tubing needed produces slightly less than atmospheric pressure in the modified version.

Because eddy-correlation instruments are used near the surface (at about four meters height), they must meet certain criteria for delay and response times. The ozone sensor delay time is approximately 0.4 second, and the response time has been measured to be about 0.6 second. The response time is typical of many eddy-correlation instruments, making the ozone sensor capable of responding to atmospheric fluctuations of frequency near 1 Hz. Adjustments to the ozone flux measurements are necessary because of the

inability of the sensor to respond to all of the atmospheric frequencies that contribute to the net vertical transport of ozone. The adjustments, however, are usually smaller than 30%. The accuracy of the instrument is approximately 10%.


## Examples of Applications

The ozone sensor has been used over a variety of surfaces, including loblolly pines during the Alamance experiment in cooperation with the EPA and Duke University, senescent maize during the AMBIENS experiment (Hicks, 1977) and mature soybeans in Plainfield, Illinois. A typical deployment of the sensors is shown in Figure 1. The Plainfield experiment included a comparison of the ozone sensor and a nitric oxide type chemiluminescent ozone sensor (Eastman et al., 1977). Measurements of mean ozone concentration and ozone flux were made, from which the ozone deposition velocity is easily calculated.

Examples of the adjusted data from the Alamance and AMBIENS experiments appear in Table 1. Even though there is a large difference in the mean concentration of ozone between the summer and the fall experiments, deposition velocities are approximately the same during the daylight hours. This suggests that the two types of vegetation are equally effective in the removal of ozone. Also, the near zero deposition velocities during nighttime hours indicate the importance of high surface resistance to uptake by vegetation at night and poor mixing during atmospherically stable conditions.


## Conclusions and Recommendations

The modified chemiluminescent ozone sensor, using ethylene as a reactant, has proven to be reliable in the field, with ozone flux measurements in 1977 having been made over three surfaces: loblolly pine , mature soybean , and senescent maize. However, the response of the instrument is slightly slower than desired. This could be corrected by reducing the length of time that the sample spends in the reaction chamber. An increase in the sample flowrate, produced by an increase in the exhaust pumping rate, a decrease in the diameter of the sampling tube or a decrease in the length of the exhaust
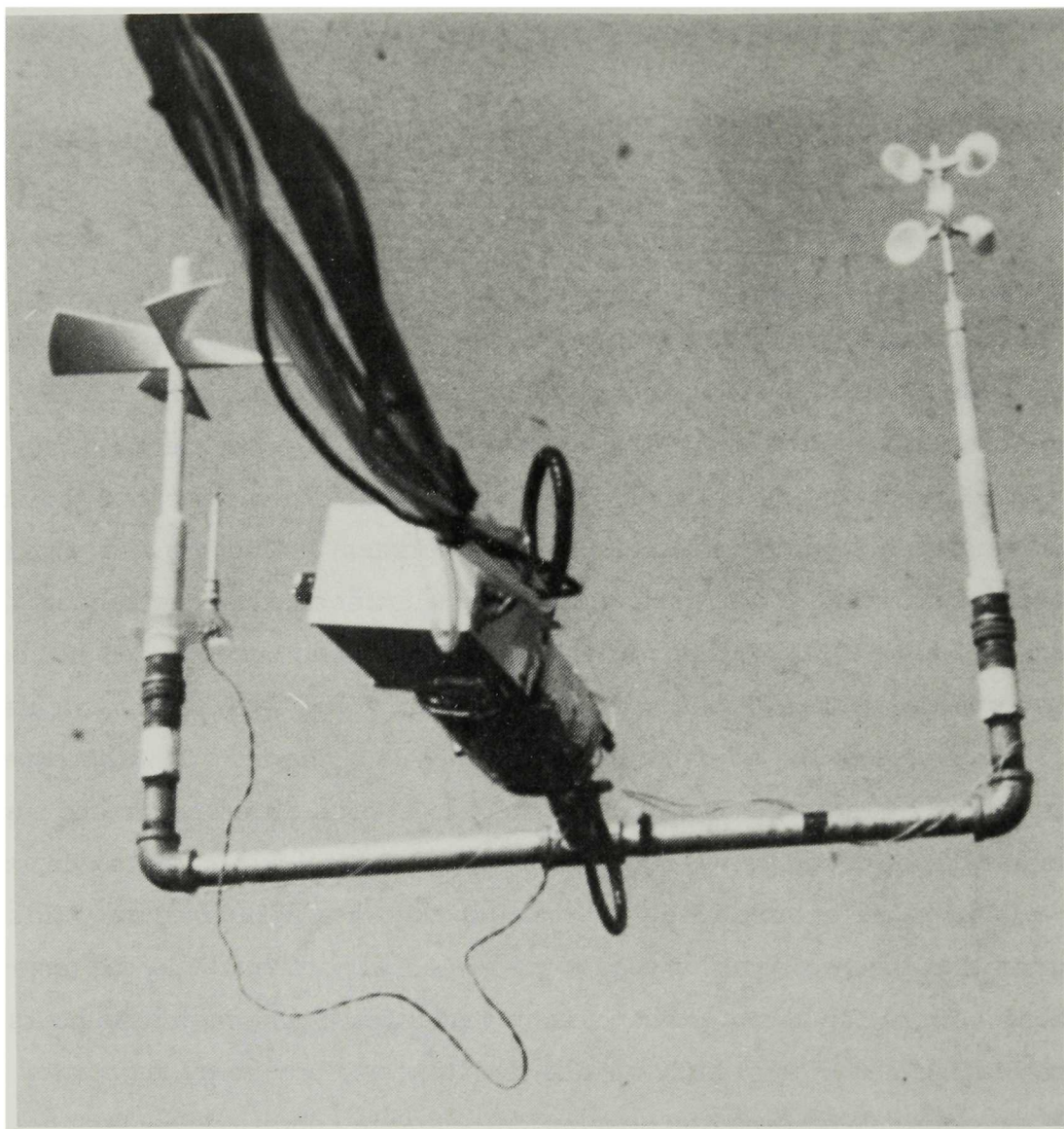
FIG. 1.--Deployment of the ozone sensor at Alamance. The sensing element can be seen attached to the central supporting pipe and is used in conjunction with the propeller anemometer on the left. Also shown, near the propeller, is the support for a fast-response thermometer and, on the right, a fast-response cup anemometer.

tube, would decrease the response time of the sensor. Because of the circum-

stances surrounding the placement of the sensor on a tower at a field site,

most of these improvements are impractical. Even so, the small size, speci-

ficity of the ozone-ethylene reaction and the reliability of the sensor have

made it quite desirable for fast response eddy-correlation measurements in

Table 1. Examples of ozone flux ($\overline{w'c'}$), mean concentration (c), and deposition velocity ($v_d$).

| Date | Time (EST) | $\overline{w'c'}$ $10^{10}$ mol cm$^{-2}$ s$^{-1}$ | $\overline{c}$, ppb | $v_d$, cm s$^{-1}$ | Location |
|------|-----------|------|------|------|----------|
| 16 July | 0015 | 11.6 | 120.8 | -0.04 | Alamance |
|  | 0545 | -11.7 | 69.6 | 0.07 | |
|  | 1145 | -124.5 | 92.6 | 0.56 | |
|  | 1715 | -89.2 | 100.5 | 0.37 | |
|  | 2115 | -13.1 | 136.5 | 0.04 | |
| 17 July | 0015 | -29.7 | 137.5 | 0.09 | |
|  | 0415 | -13.4 | 139.6 | 0.04 | |
| 5 Oct. | 0645 | -9.6 | 16.2 | 0.25 | AMBIENS |
|  | 1145 | -36.5 | 41.8 | 0.36 | |
|  | 1715 | -46.8 | 39.0 | 0.50 | |
| 10 Oct. | 1015 | -18.3 | 23.0 | 0.34 | AMBIENS |
|  | 1145 | -21.0 | 29.2 | 0.30 | |
|  | 1715 | -49.4 | 32.9 | 0.63 | |

comparison to instruments that employ other sensing methods. The present response of the sensor is acceptable because the most important criteria for eddy-correlation instrumentation are nearly satisfied. Adjustments to the ozone flux data must be made to compensate for the inability of the sensor to respond fully to all of the frequencies of atmospheric fluctuations that contribute to the vertical transport of ozone.

It is expected that the sensor will be used to measure ozone flux over other surfaces in the coming year, including snow, bare soil, and various stages of soybean growth.

References

Eastman, J. A., M. L. Wesely, and D. R. Cook, 1977: A comparison of two chemiluminescent ozone detectors used in eddy-correlation measurements. This report.

Finlayson, B. J., J. N. Pitts, and H. Akimoto, 1972: Production of vibrationally excited OH in chemiluminescent ozone-olefin reactions. Chem. Phys. Lett. 12, 495-498.

Fontijn, A., D. Golomb, and J. A. Hodgeson, 1972: A review of experimental measurement methods based on gas-phase chemiluminescence. Chemiluminescence and Bioluminescence, M. J. Cormier, D. M. Hercules, and J. Lee, Eds., Plenum Press, New York, pp. 393—426.

Hicks, B. B., 1977: The AMBIENS experiment. This report.

Warren, G. J. and G. Babcock, 1970: Portable ethylene chemiluminescence ozone monitor, Rev. Sci. Instrum. 41, 280—282.

# A COMPARISON OF TWO CHEMILUMINESCENT OZONE DETECTORS USED IN EDDY-CORRELATION MEASUREMENTS

J. A. Eastman, M. L. Wesely, and D. R. Cook

## Introduction

High ozone concentrations occurring periodically during the summer over large regions of the eastern half of the United States are often associated with transport over distances exceeding 1000 km (e.g., Fankhauser, 1976; White et al., 1976; Samson and Ragland, 1977; Vukovich et al., 1977).

Modeling of these phenomena requires that we understand the sources and sinks of ozone over appropriate time scales, ranging from several hours to several days. Photochemical reactions in the atmosphere both produce and destroy tropospheric ozone, while reactions at the surface of the earth act mainly as a continuous sink. In fact, the amount removed at the surface can be large, sometimes resulting in damaging effects on vegetation. This Section is currently measuring the uptake of ozone by various surfaces, mainly with eddy-correlation techniques employing two fast-response ozone sensors that rely on chemiluminescent reactions, one with nitric oxide (NO) (Eastman and Stedman, 1977) and the other with ethylene ($C_2H_4$) (Cook and Wesely, 1977). Earlier studies have shown that these two chemiluminescent methods can provide accurate, linear measurements of mean ozone concentrations (unpublished report, Eastman and Stedman, 1974). The present report compares the fluxes measured simultaneously by each sensor and examines the restrictions imposed upon that comparison due to sensor response characteristics.

## Principles of Detection

The ozone sensors detect light emitted as a result of the reaction of ozone with NO or $C_2H_4$. In both sensors, the gaseous mixture produces excited molecules and light is emitted as lower energy levels are reached (Fontijn et al., 1970; Kummer et al., 1971). The emitted light has wavelengths between 400 and 900 nm; the light intensity is proportional to the concentration of ozone, provided there is an excess of NO or $C_2H_4$.

113

In both sensors, samples of air are drawn continuously through Teflon tubes into a reaction chamber where mixing with NO or $C_2H_4$ takes place. Reactions take place near the face of a photomultiplier tube that translates the detected light into a measurable current that is proportional to the ozone concentration in the sampled air.

The two devices differ in several ways. The ozone-NO sensor minimizes the dark current of the photomultiplier tube by use of a refrigeration coil, while the ozone-$C_2H_4$ sensor does not use cooling to reduce dark current or thermal noise. The tube of the latter sensor is insulated to avoid rapid thermal changes, and is calibrated as a function of temperature of the tube housing. By use of a vacuum pump and restrictive inlet orifices, the reaction chamber and inlet sample tubing of the ozone-NO sensor are maintained at a pressure of about 500 Pa, whereas the ozone-$C_2H_4$ sensor operates at atmospheric pressure. The use of critical orifices and large pressure differences controls the flow rate in the former, while flowmeters and needle valves near the ethylene inlet and at the end of the exhaust tube regulate flow in the latter. The NO and $C_2H_4$ are supplied through dual regulators attached to pressurized cylinders.

## Comparison of Flux Measurements

In the current study, vertical fluxes of ozone are computed by analog covariance circuitry (Hicks, 1970). A single fast-response propeller anemometer with an assumed distance constant of 2 m measures the vertical wind speed, while the ozone concentration is simultaneously measured with the two ozone sensors. Typical delay times are 0.7 s and 0.4 s and typical response times are 0.2 s and 0.6 s for the sensors using NO and $C_2H_4$, respectively. The rather long delay times are due to the transit time of the air sample down the inlet tubes of length 0.5 m for the ozone-$C_2H_4$ sensor and 5.0 m for the ozone-NO sensor. The flux data were obtained at a height of about 5 m above the soil surface in a field of full-grown soybeans with a momentum zero-plane displacement height of about 1.0 m.

Table 1 shows average values of fluxes, both raw and adjusted for the signal loss caused by the inability of the sensors to measure fully the

114

Table 1.  Comparison of ozone fluxes obtained with two types of fast-response ozone sensors and a shared propeller anemometer for vertical wind.  The wind speeds $\bar{u}$ and values of the stability parameter $z/L$ are appropriate to the height of the eddy-correlation sensors.

| Time (CST) | | $\bar{u}$, m s$^{-1}$ | $z/L$ | Ozone flux $10^{10}$ molecules cm$^{-2}$ s$^{-1}$ | |
|---|---|---|---|---|---|
| | | | | $C_2H_4$ | NO |
| 8/2/77 | | | | | |
| 0600-0800 | raw | 2.4 | | 15.4 | 12.2 |
| | adjusted | | 0.057 | 23.6 | 18.3 |
| 0800-1000 | raw | 3.9 | | 30.2 | 24.2 |
| | adjusted | | -0.014 | 43.3 | 34.1 |
| 1000-1130 | raw | 3.9 | | 31.4 | 42.4 |
| | adjusted | | -0.077 | 44.5 | 55.6 |
| 8/3/77 | | | | | |
| 1300-1500 | raw | 2.2 | | 47.8 | 51.2 |
| | adjusted | | -0.100 | 58.1 | 61.1 |
| 1500-1700 | raw | 3.1 | | 37.5 | 39.5 |
| | adjusted | | -0.025 | 50.8 | 52.3 |
| 2100-2300 | raw | 2.9 | | 5.6 | 5.8 |
| | adjusted | | 0.124 | 11.2 | 12.4 |

relatively high-frequency atmospheric fluctuations that contribute to the eddy flux.  The methods of adjustment will not be described in detail here, except to note that the procedures of Hicks (1972) are used with the cospectra of Kaimal et al. (1972) and Kaimal (1973).  The adjustment factors used in Table 1 are strongly dependent upon atmospheric stability and range from about 1.25 during unstable conditions to nearly 2.2 during stable conditions.  Because such large adjustments are applied to some of the data, large errors are sometimes possible.

The ratio of the adjusted ozone fluxes measured by the $C_2H_4$ method to those obtained by the NO method is 1.03 ± 0.09 for all six cases.  The ratio found for the four unstable cases is 1.00 ± 0.11.  Since these ratios are nearly

equal to the ratios before adjustment, 1.02 for all six cases and 0.97 for the unstable cases, the time response characteristics of the two ozone sensors were evidently nearly the same. It is expected that the total time of response and delay for the ozone-NO sensor will be near 0.1 s when the vacuum system is performing well. However, this was not the case for the data in Table 1 because of a leak in the system; the faster response time will markedly improve performance during stable conditions. The good agreement of the results in Table 1 shows that the two methods can be used interchangeably to determine vertical fluxes of ozone, provided that the response and delay times are well known.

Conclusions

Both the ozone-NO and ozone-$C_2H_4$ sensors can be used to measure fluctuations in ozone concentration for use in eddy-correlation measurements of vertical flux of ozone in the atmospheric surface layer. The fluxes, obtained with a common propeller anemometer to measure vertical wind and adjusted for inadequate frequency response, are nearly equal for simultaneous measurements during unstable conditions. The values appear to be roughly equal during stable conditions also. In future work over a variety of surfaces, the two types of ozone sensors will be used interchangeably at heights of 4−5 m in slightly stable to moderately unstable conditions, thus providing some versatility in field work.

The rather long delay time of 0.7 s for the ozone-NO sensor, found by measurement in the field, is not typical of that expected for this system. If the vacuum system had been operating properly, the combined delay and response times should be near 0.1 s, even with an inlet sampling tube of several meters length. By comparison, the time response of the ozone-$C_2H_4$ sensor is at least 0.5 s in its present configuration, which is unlikely to be changed. Hence, although the ozone-$C_2H_4$ sensor can be easily deployed near the top of a tower in the field because of the small size and light weight of the sensing element, the potential of the ozone-$C_2H_4$ sensor for use as a fast-response eddy-correlation sensor is not as great as that of the ozone-NO sensor when a long,

116

partially-evacuated, sampling tube is successfully employed.

## References

Cook, D. R. and M. L. Wesely, 1977: Modifications of an ozone sensor performed to permit eddy-correlation measurements of vertical flux. This report.

Eastman, J. A. and D. H. Stedman, 1977: A fast response sensor for ozone eddy-correlation flux measurements. Atmos. Environ. 11, 1209–1211.

Fankhauser, R. K., 1976: Ozone levels in the vicinity of 33 cities. J. Air Poll. Control Assoc. 26, 771–777.

Fontijn, A., A. J. Sabadell, and R. J. Ronco, 1970: Homogeneous chemiluminescent measurement of nitric oxide with ozone. Anal. Chem. 42, 575–579.

Hicks, B. B., 1970: The measurement of atmospheric fluxes near the surface: A generalized approach. J. Appl. Meteorol. 9, 386–388.

_____, 1972: Propeller anemometers as sensors of atmospheric turbulence. Boundary-Layer Meteorol. 3, 214–228.

Kaimal, J. C., J. C. Wyngaard, Y. Izumi, and O. R. Cote, 1972: Spectral characteristics of surface-layer turbulence. Q. J. R. Meteorol. Soc. 98, 563–589.

_____, 1973: Turbulence spectra, length scales and structure parameters in the stable surface layer. Boundary-Layer Meteorol. 4, 289–309.

Kummer, W. A., J. N. Pitts, Jr., and R. P. Steer, 1971: Chemiluminescent reactions of ozone with olefins and sulfides. Environ. Sci. Technol. 5, 1045–1047.

Samson, P. J. and K. W. Ragland, 1977: Ozone and visibility reductions in the Midwest: Evidence for large-scale transport. J. Appl. Meteorol. 16, 1101–1106.

Vukovich, F. M., W. D. Bach, Jr., B. W. Cressman, and W. J. King, 1977: On the relationship between high ozone in the rural surface layer and high pressure systems. Atmos. Environ. 11, 967–983.

White, W. H., J. A. Anderson, D. L. Blumenthal, R. B. Husar, N. V. Gillani, J. D. Husar, and W. E. Wilson, Jr., 1976: Formation and transport of secondary air pollutants: Ozone and aerosols in the St. Louis urban plume. Science 175, 187–189.

# ON THE USE OF SILICON PHOTOCELLS IN THE MAP3S TURBIDITY NETWORK

M. L. Wesely, W. W. Nazaroff, [*] and R. G. Everett

## Introduction

Episodes of increased atmospheric turbidity in the Midwest and the Northeast cause the commonly-observed phenomena of reduced visibility and greater whiteness of the sky where cloudless, but such data are not quantitative and objective. When available, data from Volz sunphotometers provide a good measure of the intensity of haze (Flowers et al., 1969). Such data were used in a previous Annual Report (Shannon and Wesely, 1976), to show that the spatial and temporal periodicities associated with increased levels of haze were on the order of 1500 km and 5 d in the MAP3S [†] region during the summers of 1972 and 1973. Numerous other studies have shown that reduced visibility and increased ozone levels are regional-scale phenomena. Thus, the nature of the episodes of increased turbidity are controlled to a great extent by weather patterns, as well as by locations of natural and anthropogenic sources of the gaseous and particulate substances that are precursors of haze. Shannon and Wesely described a network of ten silicon-cell pyranometers that has been established in the MAP3S region and southern Ontario, in order to study quantitatively the spatial and temporal patterns of increased turbidity and to estimate the resulting changes in the amounts of solar radiation absorbed and scattered in the atmosphere and at the surface of the earth.

Both diffuse and direct solar irradiances are measured by the silicon photocell apparatus as described elsewhere (Wesely, 1975). Because of the obvious difficulty in interpreting diffuse radiation measurements under skies with clouds, the direct-beam attenuation is being used as the measure of turbidity. However, the silicon photocell does not have an even spectral response to solar radiation. This report will relate the measurements of direct-beam attenuation by use of the silicon photocell to measurements made

---

with wide-band pyranometers. Also, the potential for using satellite photographs of haze will be discussed briefly.

## Usability of the Turbidity Measurements

The silicon photocell was chosen because of its low cost and ease of operation in the present assembly. As was expected, however, analysis of the strip charts is tedious and time-consuming, which results in a significant delay in the interpretation of data. Also, the strip-chart recorders have not performed flawlessly, about 75 percent of the observations attempted during the summer of 1977 are usable.

The reduction in direct-beam radiation due to haze can be found by reference to the levels of radiation found during cloudless days with very little haze. At Argonne, extremely clean skies occur perhaps 2-4 times each summer. The values of clean-sky direct-beam irradiance $I_0$ measured with both the silicon-cell pyranometer and an Eppley black-and-white pyranometer have been obtained (Wesely, 1975; Wesely and Lipschutz, 1976). The optical depth (extinction coefficient) $\tau_a$ due to the incremental extinction of solar radiation by aerosols in hazy situations can be calculated according to the equation

$$I = I_0 \exp(-m\tau_a) , \tag{1}$$

where I is the value measured under cloudless hazy skies and m is the optical air mass based on the solar zenith angle $\theta$. Both I and $I_0$ are specific to certain values of $\theta$. Figure 1 shows the comparison of extinction coefficients measured with the two solar sensors. It appears that, despite the uneven spectral response of the silicon photocell, the two extinction coefficients are approximately equal for $\tau_a < 0.4$ when $\theta \le 55°$, for $\tau_a < 0.3$ when $\theta = 65°$, and for $\tau_a < 0.2$ when $\theta = 75°$. These limits all correspond to values of $m\tau_a$ of 0.7 or less. One possible explanation for this near equality is that the amount of light scattered and absorbed on a single pass through a moderate amount of haze does not vary appreciably with the wavelength of light. With larger values of $m\tau_a$, the fraction of blue light lost is greater than that of red

light (the sun appears red near sunset), causing overestimates of $\tau_a$ with the silicon cell.

To assess the effects of haze on solar radiation received at the surface of the earth and on the effective albedo of the atmosphere-earth system, diffuse radiation must be considered. As shown in Table 1, silicon-photocell values of diffuse irradiance $D_0$ under very clean cloudless skies are considerably less than those derived by use of an Eppley pyranometer. This indicates that blue light from the sky is poorly detected with the silicon cell. It should be kept in mind that the total irradiance $(D + I)$ for the two devices should be about the same value for clean cloudless conditions and small zenith angles, because this is the method used to calibrate the silicon photocell.

Figure 2 shows the relationship between D and I obtained under cloudless skies during the summers of 1976 and 1977 at Argonne. The straight lines represent a least-squares fit with intercept b and slope $\partial D/\partial I$ given in Table 1. The slopes of the two lines for each value of $\theta$ are almost the same, again suggesting that scattering from the direct beam to form diffuse irradiation takes place rather evenly over all wavelengths of solar radiation.

Table 1. Comparison of the silicon photocell with the Eppley black-and-white pyranometer. The slope $\partial D/\partial I$ and the intercept b result from a linear regression analysis. Irradiances are given in watts per square meter.

| $\theta$ | Eppley | | | | Silicon cell | | | |
|---|---|---|---|---|---|---|---|---|
| | $D_0$ | $I_0$ | $\partial D/\partial I$ | b | $D_0$ | $I_0$ | $\partial D/\partial I$ | b |
| 37.5° | 77 | 707 | −0.68 | 552 | 51 | 728 | −0.64 | 513 |
| 45° | 70 | 621 | −0.62 | 457 | 47 | 636 | −0.62 | 444 |
| 55° | 65 | 487 | −0.59 | 352 | 45 | 487 | −0.63 | 352 |
| 65° | 54 | 331 | −0.57 | 243 | 41 | 331 | −0.62 | 243 |
| 75° | 43 | 170 | −0.49 | 127 | 35 | 167 | −0.56 | 132 |

For cloudless skies, the information given in Table 1, plus the assumption that values of $\tau_a$ derived by use of the two types of sensors are identical, allows computation of D and I as would be measured by a wide-band pyranometer.
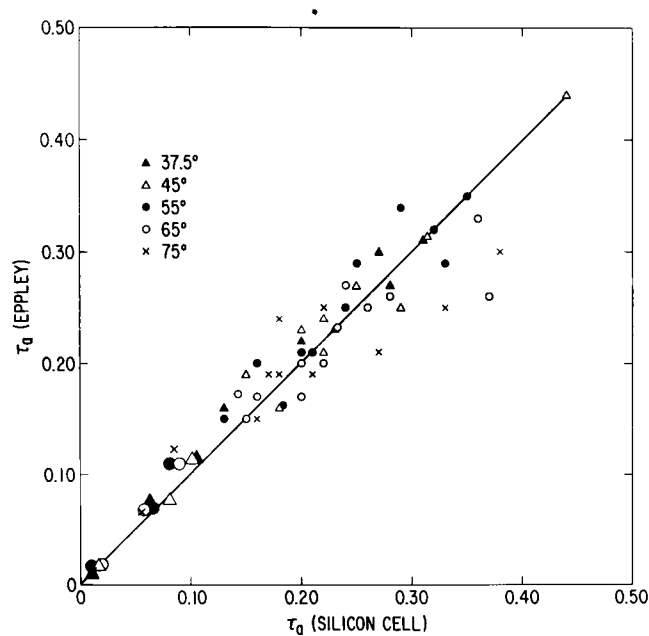
FIG. 1.--Comparison of extinction coefficients obtained by identical techniques applied to simultaneous measurements from silicon-cell and Eppley black-and-white pyranometers. Averages of many points are shown when $\tau_a < 0.12$.
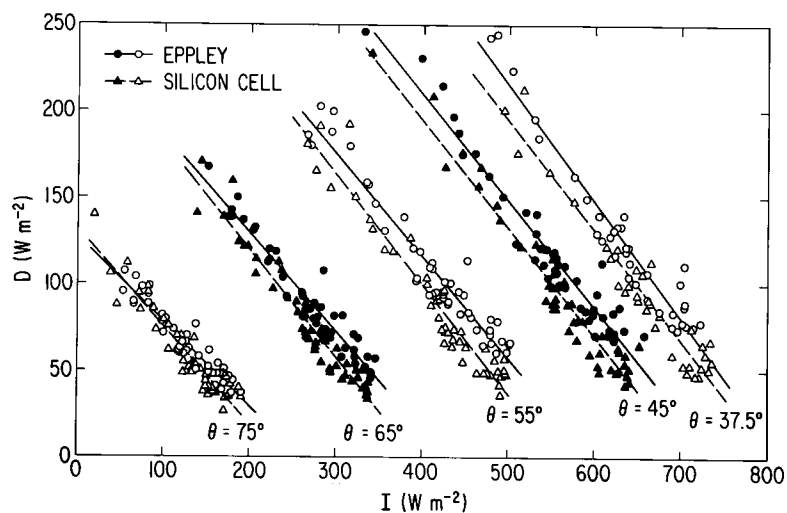
(ANL Neg. 149-77-374)



FIG. 2.--Diffuse versus direct-beam irradiances measured with two types of solar sensors simultaneously.

(ANL Neg. 149-77-373)

121

Only I from the silicon photocell and the corresponding value of $\theta$ need be known. The equations required are Eq. 1 and

$$D = D_0 + (I - I_0) \, \partial D / \partial I \ . \tag{2}$$

For $m\tau_a$ greater than 0.7, the value of $\tau_a$ should be adjusted according to information that can be derived from the data that contributed to Figure 1.

## Satellite Observations

It has been shown that episodes of widespread atmospheric turbidity over the United States can be monitored by satellite observations with the detection of visible radiation (e.g., Lyons and Husar, 1976). Thus, it may be possible to use such observations in conjunction with the MAP3S turbidity network. Simultaneous observations by satellite would improve the spatial resolution and total coverage of haze monitoring. The major problem associated with the detection of haze from satellite photographs arises from the fact that reflections from the surface tend to obscure small changes in scattering caused by varying aerosol concentrations. Over most land surfaces, changes in atmospheric aerosol content must be as large as a factor of three greater than the normal background level (corresponding to $\tau_a > 0.25$) to be detected (L. Stowe[*], personal communication). Thus, techniques of analyzing satellite imagery primarily allow qualitative but not quantitative analysis of particulate concentrations over land. Over water, the surface albedo is significantly lower than over most land surfaces, allowing easier detection of haze relative to the dark surface. In this case, work can be more quantitative.

Ideally, early morning satellite pictures would be used in the analysis since 1) fair-weather cumulus clouds typically do not form until late morning and 2) haze and smog are most clearly seen when the sun is low on the horizon and the resulting scattering is maximized (Parmenter, 1977). Such pictures with 1.6 km resolution from a SMS/GOES (Synchronous Meteorological Satellite/Geostationary Operational Environmental Satellite) spacecraft are

---

[*] U.S. Department of Commerce, NOAA, Rockville, Maryland.

available on a daily basis. A disadvantage of utilizing this satellite is that the angle at which the picture is taken varies from day to day—a situation which greatly complicates both the analysis and the comparison of photographs from two or more days. Using photographs from the Landsat (Land Satellite) series helps overcome some of these problems since the horizontal resolution is 0.2 km and the camera is pointing straight down for all of the photographs. The major drawback of Landsat is its infrequent rate of passage over the United States, once every nine days. Nevertheless, attempts will be made to use imagery from SMS/GOES and Landsat (if available), through correlations of derived information with data from the MAP3S network during especially turbid situations.

## Conclusions

The silicon photocell used as a pyranometer provides quantitative estimates of atmospheric turbidity due to haze in the MAP3S region. Measurements of direct-beam irradiance extracted from strip-chart recordings lead directly to estimates of the aerosol optical depth. The consistent linearity of the relationship between D and I for various amounts of particulate loading suggests that aerosol characteristics, such as the shape of the particle size spectrum and the refractive index of airborne particles, remain fairly constant from episode to episode. Since D and I can both be related explicitly to the extinction coefficient, it should be a direct measure of the total particulate matter suspended in the lower troposphere. The turbidity data can be combined with other, less quantitative information, such as that obtained from satellite imagery or surface visibility observations, in order to increase coverage in the MAP3S region.

## References

Flowers, E. C., R. A. McCormick, and K. R. Kurfis, 1969: Atmospheric turbidity over the United States, 1961–1966. J. Appl. Meteorol. 8, 955–962.

Lyons, W. A. and R. B. Husar, 1976: SMS/GOES visible images detect a synoptic-scale air pollution episode. Mon. Weather Rev. 104, 1623–1626.

Parmenter, F. C., 1977: Delineating haze and pollution boundaries from satellite data. Satellite Applications Information Note 77/15, National Weather Service and National Environmental Satellite Service.

Shannon, J. D. and M. L. Wesely, 1976: Optimal selection of sites in a regional turbidity network. Argonne National Laboratory Radiological and Environmental Research Division Annual Report ANL-76-88, Part IV, pp. 32–37.

Wesely, M. L., 1975: Measurements of atmospheric turbidity in an arc downwind of St. Louis. Argonne National Laboratory Radiological and Environmental Research Division Annual Report ANL-76-3, Part IV, pp. 22–30.

_____ and R. C. Lipschutz, 1976: An experimental study of the effects of aerosols on diffuse and direct solar radiation received during the summer near Chicago. Atmos. Environ. 10, 981–987.

# POSSIBILITIES FOR USING THE ARGONNE ACOUSTIC SOUNDERS IN A PHASED ARRAY

R. L. Coulter

The concentration and transport of pollutants in the lowest portion of the atmosphere is strongly affected by the height of the surface-based mixed layer, for it is within this layer that most of the pollutants are trapped. Many researchers have demonstrated the ability of acoustic sounders to monitor this height (Beran and Hall, 1973; Wycoff et al., 1973). Several experiments conducted by this Section (Miller, 1975; Miller, 1976; Shaw, 1974) have utilized sodar (sound detection and ranging, the presently accepted acronym) in monitoring the height of the inversion that caps the mixed layer. The height of the mixed layer in autumn, winter, and spring has not often exceeded one kilometer at Argonne (see Coulter, 1977). During previous experiments in midsummer, however, mixing layer heights often exceeded the range (approximately 1 km) of the sodars used. Obviously it is desirable to increase the effective probing of the Argonne sodars in order to obtain continuous estimates of this parameter.

At present the Atmospheric Physics Section has two identical operational sodars (Aerovironment model 300), each of which is mobile to some degree. One of these sodars runs continuously at the Argonne meteorology field site, while the second is deployed in various field projects whenever desired. Thus the potential exists for the two to be operated simultaneously when both are at Argonne, which may significantly increase the range and information content of the returned signals. The possibilities and problems for this type of operation are discussed in this report.

## Interference Patterns

Whenever transmitters of radiation are placed close to one another, the radiation emitted by each interferes with the other, producing maxima and minima in the amplitude of the resultant radiation pattern. The present case considers two identical point transmitters separated by a distance d, trans-

mitting acoustic energy at wavelength $\lambda$, with no phase differences between them. The resultant amplitude at some distant point in the far field (where the signal amplitude decreases linearly with distance, approximately 20 times the diameter of the source for this case) is given by

$$A_R = A_1 \{1 + \cos [2\pi (d/\lambda) \sin (\theta)]\} , \tag{1}$$

where $A_1$ = amplitude of a single transmitter

$\theta$ = angle between a perpendicular bisector of the line between transmitters and the line to the point from the midpoint between transmitters.

Clearly the effective amplitude for $\theta = 0$ is doubled, and the power increased by a factor of four. Equation 1 describes an interference pattern, which has the effect of redistributing the energy in space, with the maxima for $\theta = \arc \sin (n/2)(\lambda/d)$ and minima (received power = 0) for $\theta = \arc \sin (2n-1)(\lambda/4d)$. We see that both position and width of the maxima are also critically related to the ratio of separation distance to wavelength; the smaller the values of $(d/\lambda)$, the wider the peak and larger the separation in space of successive maxima.

However, a true point source is never actually achieved, particularly in the case of sodar. The sources in the present system are parabolic dishes, 1.31 meters in diameter, which are surrounded by enclosures that increase the effective width to about 1.5 m. The use of a parabolic dish creates a beam pattern for each individual transmitter that is an axially symmetric interference pattern in its own right and decreases in intensity with deviation from the pointing angle of the antenna. For most cases only the main, or center, lobe need be considered, for the secondary lobes are usually reduced in intensity by about 20 db. The intention here is to consider using two of these antennae side by side with little or no modification, thus limiting the practical values of $d/\lambda$.

Effective Power

Mathematically the power received at any instant in a monostatic sodar system can be written (Thomson and Coulter, 1974)

$$P(r) = P_0 A_r \ell \, r^{-2} \exp(-2\delta r)\beta , \qquad (2)$$

where $A_r$ is the effective receiving area of the receiver, $\ell$ is the length of the scattering volume, r is the distance to the scattering, $\delta$ is the attenuating co-efficient, and $\beta$ is the scattering cross section. The coefficient $P_0$ is the effective integrated power input into the atmosphere within the solid angle de-fined by the halfwidth of the antenna beam. An axially symmetric beam is as-sumed so that the solid angle associated with the halfwidth is defined by an angle $\alpha_0$ in a plane including the beam axis. That is, it is assumed that most of the detected backscattered signals occur within $\alpha_0$ of the axis of the antenna because the incident power (and sensitivity of the receiver) is concentrated in this region. Equation 2 shows that there is a one-to-one correspondence be-tween $P_0$ and P(r) for a certain system. In changing from a single- to two-element array, it is $P_0$ which changes, leading directly to changes in P(r). The power incident at a given point in space can be expressed as

$$dP_{0I} = I \left\{ 1 + \cos \left[ 2\pi \, (d/\lambda) \sin(x/r) \right] \right\}^2 f(\alpha) \, dA , \qquad (3)$$

where I is the power per unit area or energy flux per second along the beam axis with no attenuation, x is the distance from the axis of the beam along the direction of the line between the two antennae, and $\alpha$ is the angle from the axis to the point in question (see Figure 1a). Now it can be seen that the energy at a given location is the result of the product of the interference pattern (a one-dimensional function) and the beam pattern (f(x,y)) of an individual antenna. For the case of the Argonne system, f(x,y) is not yet known. However, approximations can be used with reasonable accuracy (Coulter, 1976; Kristenson, 1977), namely

$$f_1(\alpha) = \exp \left[ -\ln(2) \, \alpha^2/\alpha_0^2 \right] , \quad \text{or} \qquad (4a)$$

$$f_2(\alpha) = \sin^2 (k\alpha)/k\alpha_0)^2 , \qquad (4b)$$

with $f_2$ being more realistic. Assuming a value for the halfwidth angle $(\alpha_0)$ allows determination of k (since $f_2(\alpha_0) = 1/2$). Figures 1b and 1c illustrate
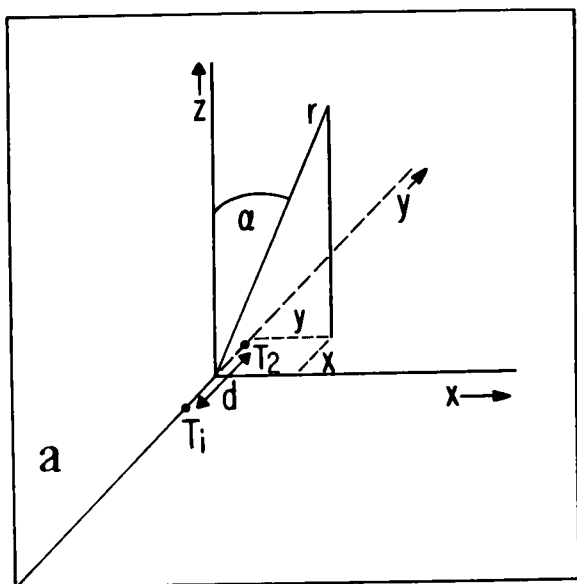
FIG. 1a.--Description of co-
ordinate system and position
of antennae (T1 and T2) for
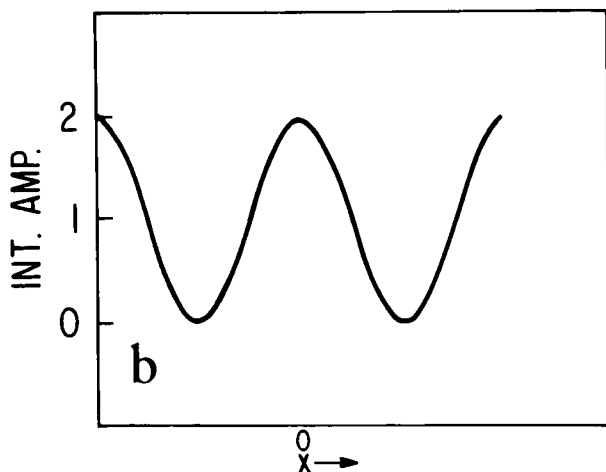the phased array under
discussion.



FIG. 1b.--Sketch of interfer-
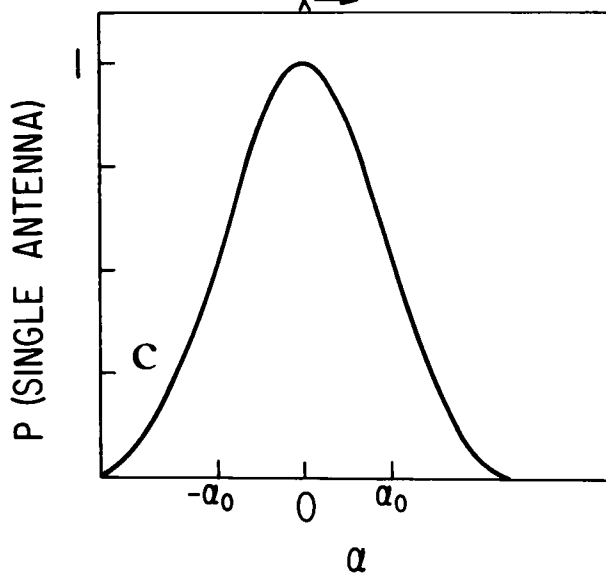ence pattern for two-element
array of point sources.



FIG. 1c. Sketch of beam
pattern for single paraboloid
antenna.

the interference pattern and beam pattern dependences upon x and y. Equation 3 can be written (using $f_1$, a Guassian weighting)

$$dP_0(r,x) = I\{1 + \cos[2\pi(d/\lambda)\sin(x/r)]\}^2 \exp[-\ln(2)(x^2+y^2)/(r^2\alpha_0^2)]\,dx\,dy \ .$$

(5)

This can be written in the integral form

$$P_0 = Ir^2 \int_0^{\sin(\alpha)} \{1 + \cos[2\pi(d/\lambda)\sin(u)]\}^2 \exp[-\ln(2)\,u^2/\alpha_2^2]$$

$$\int_0^\tau \exp[-\ln(2)\,v^2/\alpha_0^2]\,du\,dv \ , \tag{6}$$

where $x/r = u$ and $y/r = v$ and $\tau = (\sin^2(\alpha_0) - u^2)^{\frac{1}{2}}$ .

Results and Conclusions

    Integration of Eq. 6 can be done numerically with ease, for the second portion, $\mathrm{erf}(\tau)$ is well known and available from tabulations. The results of such an integration are shown in Figure 2. The integration was actually carried out to twice the halfwidth, for experience has shown the necessity for including contributions beyond the halfwidth (Thomson et al., 1978). Inasmuch as the value of $\alpha_0$ for the Argonne system is not yet precisely known, various likely values are assumed, yielding the different curves. Equivalently, the curves could correspond to using different frequencies, for beamwidth should be proportional to the wavelength, and thus higher frequencies should yield smaller beamwidths. Each integration is normalized by the value for $P_0$ with no second transmitter or interference pattern (that is, Equation 6 without the $(1 + \cos(ax))$ term). Thus, the maximum possible value is four and the minimum value something greater than one because $d/\lambda$ is assumed to be an integer for each case (an integer ensures the interference pattern to be a maximum in the center where the power per unit area is greatest). Figure 3, in which $f_2$ is used rather than $f_1$, shows similar values.

    All the curves illustrate the maximum gain in efficiency for small values of $d/\lambda$. It is at these values that the interference pattern has a wide principal
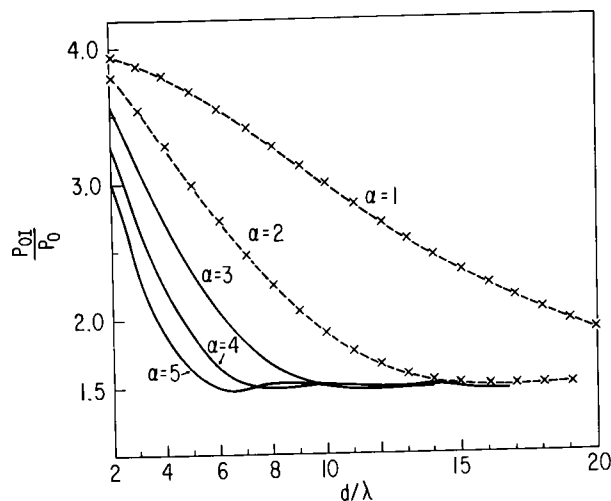
129

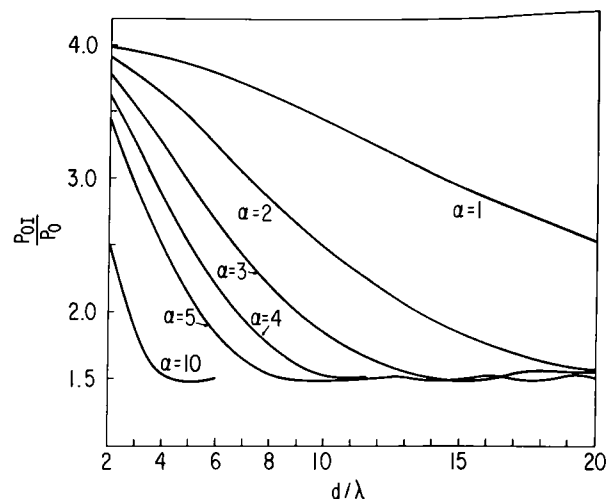FIG. 2.--Calculated values of the ratio $P_{0I}/P_0$ for Gaussian beam weighting.

FIG. 3.--Calculated values of the ratio $P_{0I}/P_0$ for beam weighting $\sin^2(x)/x$.

lobe, which eventually becomes wider than the principal lobe of the single transmitter. At larger values of $d/\lambda$ the solution approaches a limit of 1.5 about which it oscillates as changes in $d/\lambda$ change the number of maxima that "fit" within the limits of integration.

Apparently an improvement of 50% is easily achieved by using a two-element array. However, larger increases would be more difficult, for the antennae as they now exist cannot be placed much less than eight wavelengths apart. For this value of separation, one gets significant improvement over 1.5 only for $\alpha_0$ equal to 4° or less. Best estimates for this system are that $\alpha_0$ is approximately 5°, which precludes much gain over 50% unless the separation can be reduced significantly. Experimental efforts will be directed towards determination of $\alpha_0$ appropriate to the Aerovironment systems.

This approach has assumed that the phased array is used for transmitting only, i.e., a single antenna is then used for receiving the back-scattered signals. If it is possible to use both receivers simultaneously, the gain in signal level would then be about $(1.5)^2$ over the present single system. Whether or not this can, in fact, be achieved must be determined by experiment.

The type of approach outlined in this report can be used to consider a large phased array (e.g., 16−81 elements placed on the order of one to two

130

wavelengths apart), which yields considerably enhanced power output, but into a much smaller solid angle. While this achieves better horizontal resolution, the actual received power is dependent upon the area "illuminated" as well, and it is the integral of the product which is important.

The feasibility of a small phased array that can be quickly dismantled into two separate sodar systems will be tested in the coming year. If theory is correct, there should be a noticeable increase in received signal strength. Detection of planetary boundary-layer heights considerably beyond the present 800–900 meter capability will then be routinely possible.

References

Beran, D. W. and F. Hall, 1973: Remote sensing applications in air pollution meteorology. Preprints, 2nd Joint Conference on Sensing of Environmental Pollutants, Washington, D.C., Dec. 10–12, pp. 241–245.

Coulter, R. L., 1976: System geometry and interpretation of sodar data. Ph.D. thesis, Penn. State University, pp. 37–94.

_____, 1977: Mixing layer heights from the Rush Experiment, This report.

Kristenson, L., 1977: Risø National Laboratory, Denmark. Private communication.

Miller, E. L., 1975: Use of an acoustic sounder array to study urban atmospheric structure. Argonne National Laboratory Radiological and Environmental Research Division Annual Report, ANL-75-60, Part IV, pp. 87–88.

_____, 1976: Acoustic sounding investigation of the effects of boundary layer decoupling on long distance pollutant transport. Argonne National Laboratory Radiological and Environmental Research Division Annual Report, ANL-76-88, Part IV, pp. 24–29.

Shaw, N. A., 1974: Observations of atmospheric structure using an acoustic sounder, Argonne National Laboratory Radiological and Environmental Research Division Annual Report ANL/RER/75-2,

Thomson, D. W. and R. L. Coulter, 1974: Analysis and simulation of phase coherent acdar sounding measurements. J. Geophys. Res. 79, 5541–5549.

_____, R. L. Coulter, and Z. Warhaft, 1978: Simultaneous measurements of turbulence in the lower atmosphere using sodar and aircraft. J. Appl. Meteorol, in press.

Wycoff, R. J., D. W. Beran, and F. Hall, 1973: A comparison of the low level radiosonde and the acoustic echo sounder for monitoring atmospheric stability. J. Appl. Meteorol. 12, 1196–1204.

# AN EXPERIMENTAL DETERMINATION OF PROBE-LENGTH REQUIREMENTS FOR STUDY OF WAKES BEHIND CYLINDERS[*]

C. M. Sheih,[†] J. J. Finnegan,[‡] E. F. Bradley,[‡] and P. J. Mulhearn[‡]

## Introduction

Turbulent wakes behind circular cylinders have attracted much special attention in experimental studies of turbulent shear flows (e.g., Townsend, 1947, 1949a, and 1949b; Palmer and Keffer, 1972). In these studies, the hot-wire lengths used in the measurements are about the same size as the cylinder diameters. Since the magnitude of the turbulent energy near each cylinder probably peaks at a scale near the diameter of the cylinder, the use of such large wire lengths may have attenuated the turbulence signals.

Attenuation of turbulence signals by a hot-wire sensor in unobstructed uniform flow has been studied by many investigators. Uberoi and Kovasznay (1953), using formulations which they derived for the line-averaged, one-dimensional spectrum of the streamwise velocity component obtained from a single hot wire, calculated signal attenuations under conditions of isotropic turbulence with the wire length much larger than the scales of energy-containing eddies. Wyngaard (1968) extended this work by using numerical integrations and by substituting Pao's formula for the spectrum of total turbulent energy into one of the relations derived by Uberoi and Kovasznay. Roberts (1973) extended the work further by developing a method that does not require the assumption of a particular form for the three-dimensional energy spectrum. In the latter method, correction of the spatial attenuation of the measured spectrum (attenuation due to spatial averaging) can be calculated by a simple iterative scheme solving the integral equation relating the measured spectrum to the true spectrum of turbulence.

---

Unfortunately, the above schemes developed for uniform flow conditions cannot be applied to highly nonuniform turbulent wakes behind cylinders. Therefore, an experimental method which determines changes in measured turbulence intensity as a function of the ratio of hot-wire length to cylinder diameter will be used to investigate the error involved in the attenuation of measured turbulence signals by the spatial averaging of a hot wire.

## Description of the Experiment

The experiment was conducted in the Pye Laboratory of CSIRO Environmental Mechanics Division, Australia. A detailed description of the tunnel was given by Wooding (1968). The constant-temperature hot-wire anemometer used in the present study was designed and constructed by Sheih and Lipschutz (1974). The hot wires were 3 $\mu$m-diameter tungsten, and their lengths were chosen according to the length scale of the energy-containing eddies in a turbulent wake. Specifically, if we define the length scale of the wake as the lateral distance from the centerline of the wake to a point where the turbulent energy is reduced to 50% of its maximum value, the wake-length scale estimated from Townsend (1976) is

$$L = 0.6 \left[(x - x_0)d\right]^{\frac{1}{2}} \qquad \text{for } x > x_0 , \qquad (1)$$

where x is the downstream distance from the cylinder, $x_0$ is 25 d, and d is the diameter of the cylinder. Since measurements were made at 34 diameters from the cylinders, a length scale of L = 1.8 d was used in selecting the range of hot-wire lengths in the experiment. The wire lengths were $\ell$ = 0.1, 0.2, 2, and 4 cm and the cylinder diameters were d = 1 and 2 cm. The free-stream wind velocities used in the studies were $u_\infty$ = 5 and 10 m s$^{-1}$.

For each combination of wire length, cylinder diameter and mean wind velocity, measurements were taken behind a vertical cylinder by a single hot wire positioned at the center of the wake and successively oriented horizontally across the wake (along y), vertically (along z) and at a 45-degree angle in the x-z plane. These three arrangements were chosen because they are the most common orientations used in measuring turbulence in a wake.

133

## Results and Discussion

To illustrate the effect of wire length on measured turbulence intensities, nondimensionalized mean squares of measured turbulence as functions of the nondimensionalized hot-wire length are shown in Figure 1 for the horizontally oriented wires. The variable $u'_{y,\ell}$ represents velocity fluctuations measured with a wire length $\ell$ oriented along y, and $\ell_0$ is the smallest wire length used in the experiment. The data for various combinations of mean wind velocity and cylinder diameter converge fairly well to a single curve and indicate that the scaling parameters are well chosen. If the curve were extended to intersect with the vertical axis $(\ell = 0)$, the vertical coordinate at the point of intersection would correspond to the unattenuated value of the normalized turbulent signal. This extrapolation indicates that the turbulent energy measured by the smallest wire in the present study was only a few percent smaller than the unattenuated signal. Hence, the smallest wire can be used to estimate the unattenuated signal for scaling the measured signals, with only small errors resulting. Figure 1 also shows that when the wire length is equal to the scale of the wake, i.e., when the abscissa is equal to unity, the measured mean square turbulence is only 38% of the true turbulent energy. Since a single curve fits all data reasonably well, the results can be used to estimate the spatial attenuation of the hot wires used by other investigators. For one of the experiments by Townsend (1947), the parameters used were $\ell = 1$ mm, $d = 1.12$ mm, and $x = 19$ d. The corresponding value for $\ell/L$ is 0.18 and the measured turbulent energy estimated from Figure 1 is about 85% of the unattenuated value. Further, it appears that the conclusions obtained earlier for Figure 1 are equally applicable to the other wire orientations; the corresponding nondimensionalized curves, which are not illustrated here, are almost exactly the same as that shown in Figure 1.

Spatial attenuation of the mean wind velocity by the wire is not important for most types of experiments and has not attracted much attention in the past. However, neglection of the velocity defect might not be valid in wake studies because the mean velocity is not uniform across the wake, and one will not be able to obtain a local mean velocity if the wire length is too long.
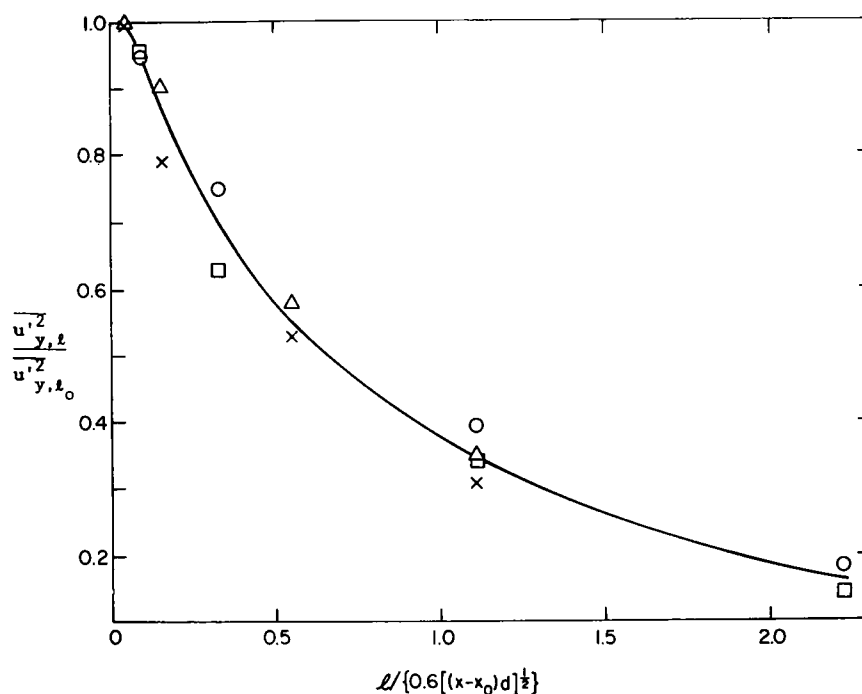
FIG. 1.--Normalized turbulent intensity as function of the hot-wire length normalized by the scale of the cylinder wake. The cylinder is vertical and the hot wire is mounted horizontally. The symbols are for various combinations of free-stream mean wind velocity ($u_\infty$ in m s$^{-1}$) and cylinder diameter (d in cm); $(u_\infty, d) = (5,1)$ (O), $(5,2)(\triangle)$, $(10,1)(\square)$, and $(10,2)(X)$. ANL Neg. 149-71-428)
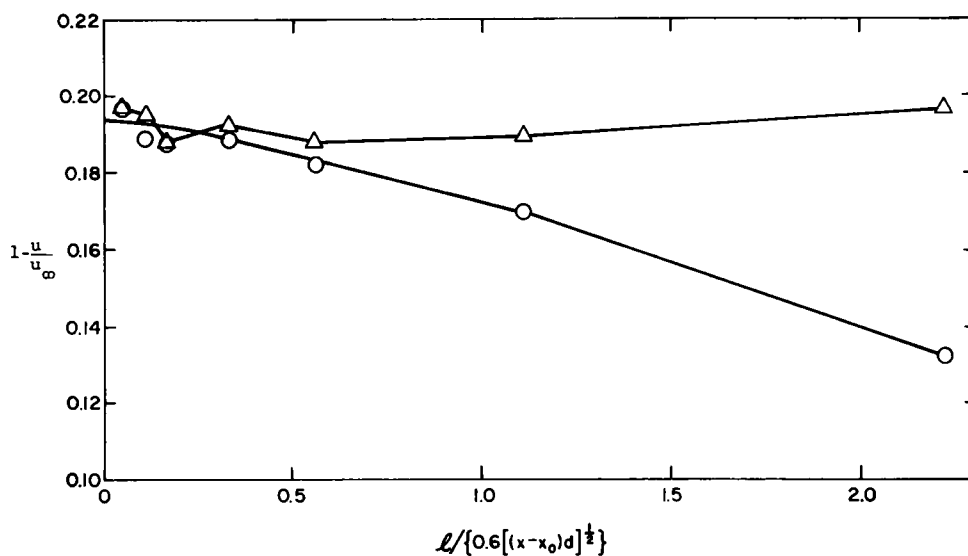


FIG. 2.--The measured mean wind velocity-deficit factor as functions of hot-wire length for wires mounted horizontally (O), and vertically ($\triangle$). (ANL Neg. 149-77-430)

135

To investigate the behavior of the measured local mean wind velocity (u) as a function of wire length, mean velocities were measured for various wire lengths for wires mounted horizontally and vertically. The results are plotted in Figure 2. The vertical coordinate of the figure is the normalized deviation of the local mean wind velocity from the free-stream velocity. This form of "velocity-deficit factor" is adopted because it is a conventional method for presenting profiles for mean wind velocities in a wake. For a horizontally mounted wire, the velocity-deficit factor is reduced from 0.19 to 0.14 as the ratio of the wire length to the wake length scale increases from 0.3 to 2.2. For the vertically mounted wire the mean velocity should be uniform and indeed the measured values for the velocity-deficit factor do not appear to depend upon the wire length. The slight deviation of the data from a constant value may be caused by experimental errors, such as inability to place the hot wire repeatedly at exactly the same location in the wake; this has a greater effect on the measurements with a vertically mounted wire than with a horizontally mounted wire.

It should be noted that the present analysis is not valid for measurements taken at distances in the neighborhood of, or smaller than, $x_0$ (25 cylinder diameters) because the scale for the similarity theory expressed by Eq. 1 will no longer be valid. Intuitively, one might expect that the characteristic length scale of turbulent fluctuations in the wake is dominated by the cylindrical diameter. It is likely that near $x = x_0$, the larger of d or $L = 0.6 [(x - x_0)d]^{\frac{1}{2}}$ is the dominating length scale. It can be shown by solving for d when $d = L$ that the length scale d dominates when $x < 28\, d$. In the absence of experimental data for this region, one can only state that the wire length has to be much smaller than the cylinder diameter in order to minimize the spatial attenuation of the measured turbulence signals.

## References

Palmer, M. D. and J. F. Keffer, 1972: An experimental investigation of an asymmetrical turbulent wake. J. Fluid Mech. 53, 593—610.
Roberts, J. B., 1973: On the correction of hot-wire turbulence measurements for spatial resolution errors. Aeronaut. J. 77, 405—412.

Sheih, C. M. and R. C. Lipschutz, 1974: Hot-wire anemometer equipment for short-fetch covariance applications. Argonne National Laboratory Radiological and Environmental Research Division Annual Report, ANL-8060, Part IV, pp. 151—159.

Townsend, A. A., 1947: Measurements in the turbulent wake of a cylinder. Proc. R. Soc. London, A190, 551—561.

_____, 1949a: Momentum and energy diffusion in the turbulent wake of a cylinder. Proc. R. Soc. London, A197, 124—140.

_____, 1949b: The fully developed turbulent wake of a circular cylinder, Aust. J. Sci. Res. 2, 451—468.

_____, 1976: The structure of turbulent shear flow. Cambridge University Press, New York.

Uberoi, M. S. and K. S. G. Kovasznay, 1953: On mapping and measurement of random fields. Q. J. Appl. Math. 10, 375—393.

Wooding, R. A., 1968: A low-speed wind tunnel for model studies in micrometeorology. CSIRO Div. Plant Industry Tech. Paper No. 25.

Wyngaard, J. C., 1968: Measurement of small-scale turbulence structure with hot wires. J. Sci. Instrum. Series 2, 1, 1105—1108.

# ADDITIONAL MEASUREMENTS OF THE KOLMOGOROV-VON KARMAN PRODUCT OBTAINED IN ITCE-76[*]

P. Frenzen and R. L. Hart

---

In an "add-on" experiment conducted during the International Turbulence Comparison Experiment held in Australia late in 1976 ("ITCE-76"; also see Hicks et al., 1976), additional measurements were obtained of mean and turbulent wind distributions in conditions sufficiently steady to evaluate the relation between the Kolmogorov and von Karman constants. Previous experimental results as well as the significance of the implicit relation between these two important boundary-layer scale factors are discussed elsewhere (Frenzen, 1973, 1977). It can be added that, since the so-called K-von K product which the Kolmogorov-von Karman relation defines can be evaluated with little more than ordinary micrometeorological measurements, the results obtained provide convincing independent checks on values of the individual constants determined by more complex experimental procedures.

In the present study, an analysis of data collected during ITCE-76 has been combined with a similar analysis of measurements made in Australia in 1968 to show that the K-von K product value determined from the results of the earlier experiment alone is evidently incorrect. The error was caused by a failure to take full account of the limitations upon the normalized spectral frequency range imposed by the high wind speeds of the first field experiment. A supplementary analysis designed to demonstrate the dynamic response of the low-inertia anemometers used in the experiments did suggest that this might have been the cause: an upward revision of the apparent K-von K product from a value of 0.140 to 0.157 was indicated by spectra recomputed to extend into higher frequencies (Frenzen, 1974). But in that note, this alternative conclusion was discounted on the grounds that the higher frequency variance density estimates involved came from spectral regions beyond one-half the Nyquist frequency, and were therefore statistically less reliable. Additional turbulence

---

spectra computed from the 1976 measurements are now found to show similar behavior; the $-5/3$ slopes required to evaluate a stable estimate of the product do not become fully established until normalized frequencies exceed 2 rather than 1, the latter being the value assumed in the first analysis. Figure 1 shows that the data sets from the two field experiments support one another in that they tend to converge upon a constant value of the K-von K product in spectral regions above $nz/\overline{u} \simeq 2$.

Turbulence spectra for this study have been computed from wind records sampled at intervals of $dt = 0.1$ s, thus defining a maximum natural spectral frequency of $n_m \equiv 1/(2\ dt) = 5$ Hz. Since wind speeds during the 1968 experiment approached $\overline{u} \simeq 12$ m s$^{-1}$, the maximum normalized spectral frequencies were limited to $n_m z/u \cong 0.4\ z$. It follows that well-established $-5/3$ slopes could not have been detected below $z \sim 5$ m. In contrast, the winds in 1976 averaged only 6 m s$^{-1}$, and therefore normalized spectral ranges were effectively doubled at all heights. For these one-dimensional spectral computations utilizing cup-anemometer wind measurements, all velocities were again corrected for contamination by transverse fluctuations, and the modified Taylor hypothesis taking account of the advective effects of larger scale velocity fluctuations was employed. These corrections are described in detail in the earlier reports previously cited.

To provide the data for the plot of $\alpha_1 k^{4/3}$ vs. n in Figure 1, individual estimates of the K-von K product were computed from each spectral density estimate using a modified form of the Kolmogorov-von Karman relation. Rewriting the equation for the one-dimensional spectrum in the inertial subrange, we define the function

$$\phi_*(n) = n^{5/3} \cdot E(n) = \alpha_1 (\epsilon \overline{u})^{2/3} , \tag{1}$$

which evidently becomes a constant when $E(n) \propto n^{-5/3}$. In the usual notation n here represents the natural frequency in Hz, $E(n)$ is the variance density of the longitudinal velocity per unit frequency, $\alpha_1$ is the Kolmogorov constant for the one-dimensional turbulence spectrum, $\epsilon$ is the rate of turbulence dissipation, and $\overline{u}$ is the mean wind speed. By combining the above with the wind
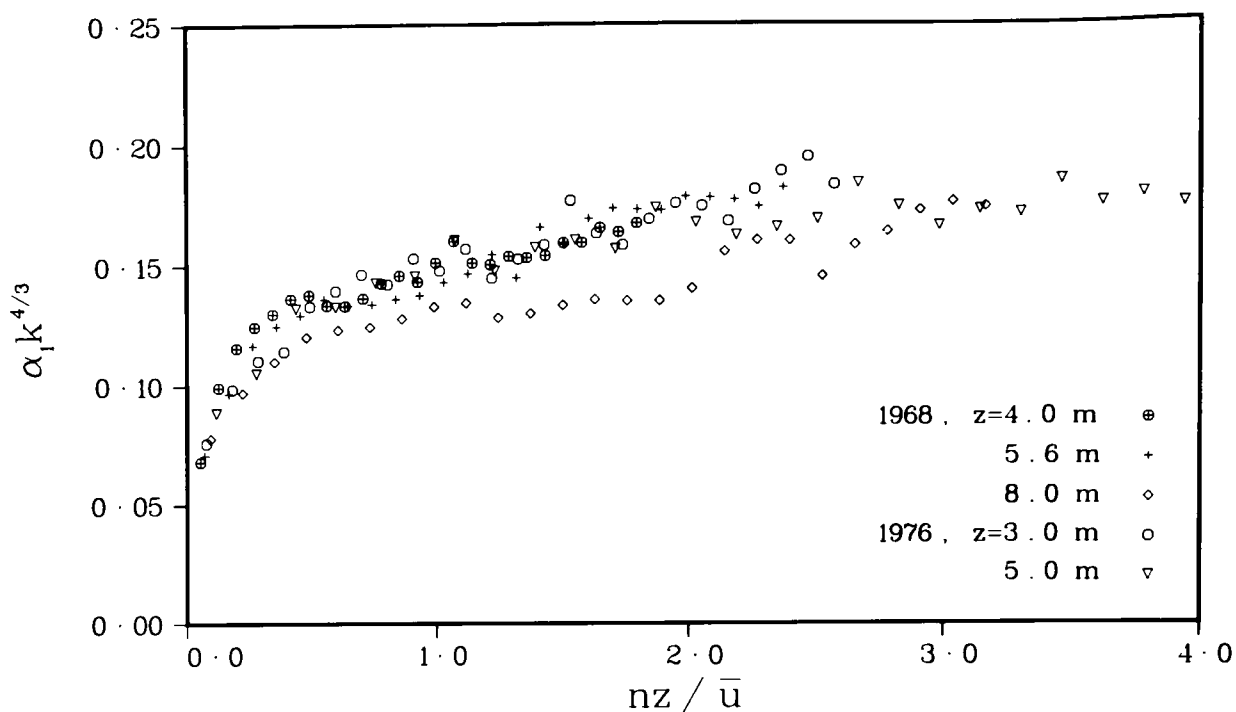
FIG. 1.--Spectral distribution of K-von K product estimates $(\alpha_1 k^{4/3})$ vs. the normalized frequency of the variance density estimate on which each was based.

profile and turbulent energy budget relations in the manner detailed in previous reports (Frenzen, 1973), a spectral distribution of estimates of the K-von K product itself is obtained:

$$\alpha_1 k^{4/3} = \phi_*(n) \cdot (2\pi z/\overline{u})^{2/3} \cdot (\ln z_2/z_1)^2/(\overline{u}_2 - \overline{u}_1)^2 . \qquad (2)$$

Here k represents the von Karman constant, and the numerical factor $(2\pi)^{2/3}$ has been included in order to retain the conceptual convenience of natural frequency (Hz) in a relation designed to develop the more familiar magnitude of $\alpha_1 \approx 0.5$ appropriate to spectra expressed in terms of angular frequency.

Distributions defined by Eq. 2 are plotted in Figure 1 using the data of both experiments. As expected, values of $\alpha_1 k^{4/3}$ increase with increasing n, quasi-asymptotically, up to a constant magnitude presumably uniquely defined by the correct values of the two scale factors. But as noted earlier (and counter to previous assumptions), that constant value is not attained until $n \geq 2\ \overline{u}/z$.

140

The average of all estimates of $\alpha_1 k^{4/3}$ obtained for $n > 2\ \bar{u}/z$ is 0.171. Taking $k = 0.41$ as the more certain of the individual scale factor values (e.g., see Hicks, 1976, or Garratt, 1977), this collective result implies $\alpha_1 = 0.56$. From another point of view, only one of the five $\alpha_1 k^{4/3}$ distributions shown provides enough data above $nz/\bar{u} \simeq 2.0$ for a meaningful selection to be made; this will be seen to be the set based on measurements made at $z = 5$ m in 1976. Since half the normalized Nyquist frequency for this case is 2.0, the inclusion of product estimates corresponding to somewhat higher spectral frequencies can not be avoided; but a fairly flat region seen to extend from $1.9 < nz/\bar{u} < 2.5$ can be taken to provide the most reliable subset of the data from the two experiments. Averaging the five estimates of $\alpha_1 k^{3/4}$ within this region gives

$$\langle \alpha_1 k^{4/3} \rangle = 1/5(0.173 + 0.167 + 0.162 + 0.165 + 0.168) = 0.167 \pm 0.005,$$

where the range of uncertainty is taken to be full range of the values averaged. Again, for $k = 0.41$, this implies $\alpha_1 = 0.55 \pm 0.02$.

For comparison, some recent values determined for these constants are listed in Table 1.

Table 1. Some recent values determined for the Kolmogorov ($\alpha_1$) and von Karman (k) constants; * indicates the value $k = 0.41$ used in the present analysis to determine $\alpha_1$.

| k | $\alpha_1$ | Reference |
|---|---|---|
| (0.41*) | $0.55 \pm 0.02$ | Present results |
| $0.41 \pm 0.02$ | | Hicks (1976) |
| $0.41 \pm 0.025$ | | Garratt (1977) |
| | $0.50 \pm 0.02$ | Champagne et al. (1977) |
| | $0.54 \pm 0.01$ | Williams and Paulson (1977) |

## Acknowledgements

## References

Champagne, F. J., C. A. Friehe, J. C. Larue, and J. C. Wyngaard, 1977: Flux measurements, flux estimation techniques, and fine scale turbulence measurements in the unstable surface layer over land. J. Atmos. Sci. $\underline{34}$, 515−530.

Frenzen, P., 1973: The observed relation between the Kolmogorov and von Karman constants in the surface boundary layer. Boundary-Layer Meteorol. $\underline{3}$, 348−358.

_____, 1974: On the response of low-inertia cup anemometers in real turbulence; a reply. Boundary-Layer Meteorol. $\underline{6}$, 523−526.

_____, 1977: A generalization of the Kolmogorov-von Karman relationship and some further implications on the values of the constants. Boundary-Layer Meteorol. $\underline{11}$, 375−380.

Garratt, J. R., 1977: Review of drag coefficients over oceans and continents. Mon. Weather Rev. $\underline{105}$, 915−929.

Hicks, B. B., P. Frenzen, and M. L. Wesely, 1976: Some preliminary results from the 1976 ITCE: Anemometory. Argonne National Laboratory Radiological and Environmental Research Division Annual Report ANL-76-88, Part IV, pp. 127−132.

_____, 1976: Reply to comments. Boundary-Layer Meteorol. $\underline{10}$, 237−240.

Williams, R. M. and C. A. Paulson, 1977: Microscale temperature and velocity spectra in the atmospheric boundary layer. J. Fluid Mech. $\underline{83}$, 547−567.

# A THREE-DIMENSIONAL NUMERICAL SIMULATION OF THE ATMOSPHERIC EFFECTS OF A COOLING POND

Tetsuji Yamada

---

Accurate evaluation of the inadvertent atmospheric effects of the release of large amounts of heat and moisture from cooling ponds is a matter of great concern among meteorologists, environmentalists, and engineers. Numerical simulations provide a supplement or alternative to field data collection which can be laborious and difficult during winter, and form a basis for the prediction of effects.

The main objectives of these numerical simulations are 1) to compute perturbations in wind, temperature, water vapor, and turbulence produced by surface inhomogeneities associated with a cooling pond and 2) to identify the critical factors in production of fog and clouds over a cooling pond. In order to accomplish these goals, five numerical simulations, two cases in autumn and three cases in winter, are conducted. The numerical simulations are compared with data from autumn field studies of heat exchange processes over a cooling pond at the Commonwealth Edison Dresden Station in northern Illinois (Hicks et al., 1977) and with visual observations of the effects of that cooling pond during a cold winter (Shannon and Everett, 1978).

The mathematical formulations of the model and the numerical procedures involved are considered in detail in Yamada (1978a) and will not be discussed here. The model, which is based on second-moment turbulence equations and ensemble cloud relations (used to compute the mass of cloud water), has many desirable features in comparison with models employing eddy viscosity coefficients. The most significant improvement is the parameterization of turbulence. For example, buoyancy effects associated with thermal and water vapor stratification are properly considered. Furthermore, turbulence is allowed to have memory by retaining the tendency and advection terms in the turbulence-energy equation.

## Boundary Conditions

Table 1 summarizes the boundary conditions for the five case studies. Boundary conditions for Case 1 and Case 2 are constructed from the surface measurements given by Hicks et al. (1977) for 12 and 22 September, 1975. The relative humidity of the ambient air is estimated from observations at Midway Airport on those days. The boundary conditions for Case 3 are determined from typical values observed during the period December 1976 to February 1977, when most of the easily visible plumes and clouds were noted. Water temperature recorded at the tower near the pond center and wind speeds roughly estimated near the pond by a hand-held anemometer are used, but relative humidities are estimated from observations at Argonne, since relative humidities measured at the cooling pond are considered unreliable because of calibration drift and icing on the instrument shelters. Finally, Cases 4 and 5 are added in order to illustrate the sensitivity of the results to the boundary conditions. For Case 4 the relative humidity is reduced to 50% from 90% in Case 3, and for Case 5 the geostrophic wind speed is reduced by a factor of 4 from the value in Case 3.

Table 1. Summary of the boundary conditions used in the simulations. The geostrophic wind components $U_g$ and $V_g$ are in x and y directions, respectively. The surface temperatures $T_1$ and $T_2$ are for the land and the cooling pond, respectively. The relative humidity RH is for the air at the inflow boundary.

| | Case | | | | |
|---|---|---|---|---|---|
| | 1 | 2 | 3 | 4 | 5 |
| $U_g = V_g$ (m s$^{-1}$) | 5.6 | 2.2 | 4.0 | 4.0 | 1.0 |
| $T_1$, °C | 15 | 15 | -10 | -10 | -10 |
| $T_2$, °C | 28 | 28 | 20 | 20 | 20 |
| RH, % | 60 | 60 | 90 | 50 | 90 |

## Results and Discussions

### Cases 1 and 2

A comparison of model computations with observations of sensible and latent heat fluxes is given in Table 2. The observed values are the arithmetic means of all observations between 1200 and 1600 CST. The computed values are for the center of the model pond.

Table 2. Computed and observed surface sensible and latent heat fluxes for Case 1 (12 September 1975) and Case 2 (22 September 1975).

| | Computed | | Observed | |
|---|---|---|---|---|
| Case | H, W m$^{-2}$ | LE, W m$^{-2}$ | H, W m$^{-2}$ | LE, W m$^{-2}$ |
| 1 | 173 | 692 | 260 | 597 |
| 2 | 106 | 436 | 119 | 415 |

The computed differences between Case 1 and Case 2 are due to the fact that the geostrophic wind in Case 1 is approximately 2.5 times greater than that in Case 2. The corresponding ratios of the computed sensible and latent heat fluxes in Case 1 to those in Case 2 are both approximately 1.6. The ratios of the observed surface wind speed, sensible heat flux, and latent heat flux in Case 1 to those in Case 2 are 2.6, 2.2, and 1.4, respectively.

### Case 3

Figure 1 shows the computed horizontal wind field at 0.2 m above the surface (Yamada, 1978b). Wind speed increases from 1.4 m s$^{-1}$ at the inflow boundary to 3.8 m s$^{-1}$ over the cooling pond. This acceleration of wind speed is caused by the decrease of the roughness length from that over the land $(3 \times 10^{-2}$ m, assumed) to that over the water $(5 \times 10^{-5}$ m, typically) and by the temperature difference between the land and the pond. Horizontal convergence and divergence produce the vertical wind distribution shown in Figure 2. A maximum upward motion of 3.5 cm s$^{-1}$ is produced over the downstream edge of the cooling pond.
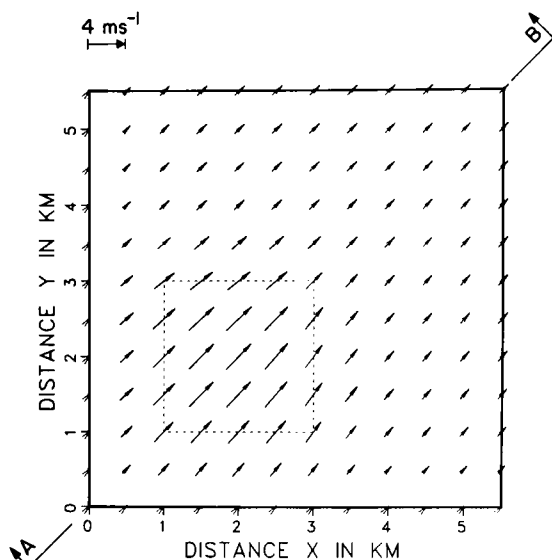
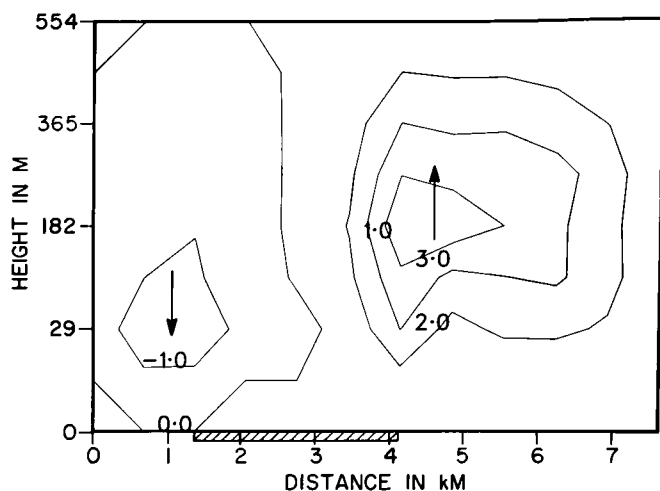FIG. 1.--Horizontal wind vectors at 0.2 m above the surface. The cooling pond is outlined by dashed lines.

FIG. 2.--Distribution of the vertical wind component in a vertical plane through the diagonal A-B shown in Figure 1. Units are in cm s$^{-1}$. The cooling pond is indicated by hatching.

Thermal plumes produced by the cooling pond may be reconstructed from temperature distributions in horizontal planes, such as shown for 0.2 m, 9 m, and 139 m above the surface (Figure 3). As shown in Figure 3a, air temperature drops to -5°C only 20 cm above the warm water (20°C). A rapid decrease of air temperature over the cooling pond is verified by observations of heavy accumulations of ice on an instrument tower located near the center of the pond (Shannon and Everett, 1978). The maximum temperature is displaced downwind with height. Water-vapor plumes (not shown here) display features similar to those of the temperature plumes. Additional features are that maximum condensation occurs at the first grid level (0.2 m) above the cooling pond and the cloud penetrates to 180 m above the surface.

Cases 4 and 5

Sensitivity of the results is examined by varying the boundary conditions that were assumed in Case 3. In the first run, Case 4, the relative humidity at the inflow boundary is assumed to be 50%. As a result, no condensation occurs, except a small amount over the cooling pond at the first grid level (0.2 m). Turbulence energy is slightly reduced from that in Case 3.
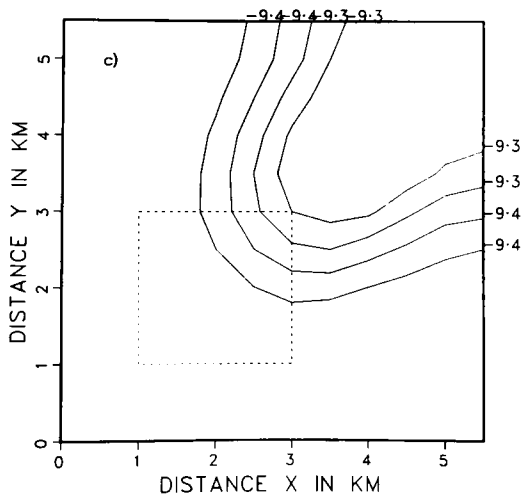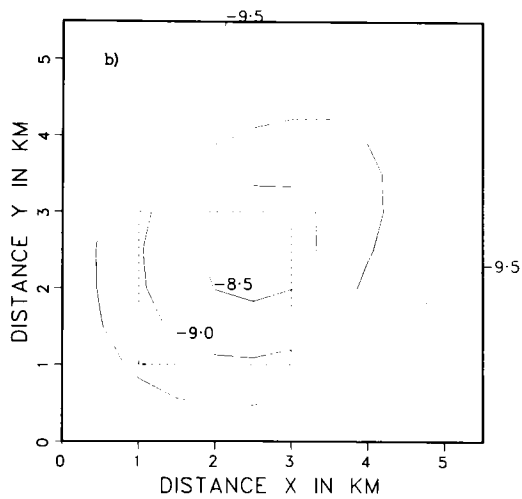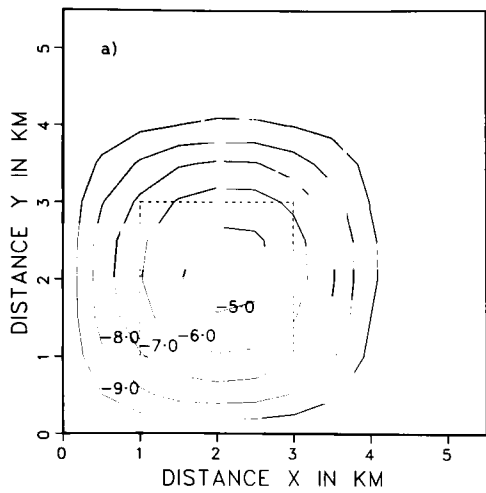
146

FIG. 3.--Horizontal distributions of
liquid water potential temperature at
a) 0.2 m, b) 9 m, and c) 138 m above
the surface. Units are degrees Celsius.
The cooling pond is outlined by dashed
lines.

On the other hand, very little change is found in the distribution of the mean wind, temperature, and water vapor. In the second run, Case 5, the geostrophic wind speed is assumed to be smaller by a factor of four than that of Case 3. The most significant difference resulting from the geostrophic wind reduction is found in the vertical wind speed distribution, as might be expected. The maximum upward motion is 9.3 cm s$^{-1}$, compared to 3.5 cm s$^{-1}$ in Case 3.

References

Hicks, B. B., M. L. Wesely, and C. M. Sheih, 1977: A study of heat transfer processes above a cooling pond. Water Resources Res. 13, 901—908.
Shannon, J. D. and R. G. Everett, 1978: The effect of the severe winter upon a cooling pond fog study. Bull. Am. Meteorol. Soc. 59, 60—61.
Yamada, T., 1978a: A three-dimensional, second-order closure numerical model of mesoscale circulations in the lower atmosphere. Argonne National Laboratory Radiological and Environmental Research Division Report ANL/RER-78-1, 67 pp.
_____, 1978b: A preliminary result of a three-dimensional numerical simulation of cloud formation over a cooling pond. In proceedings of AIAA/ASME Thermophysics and Heat Transfer Conference, Palo Alto, California, May 24—26, 1978, 79—87.

# OPTIMIZATION VIA NONLINEAR PROGRAMMING OF A DISCRIMINANT FUNCTION FOR COOLING-POND FOG CONDITIONS

J. D. Shannon

During the winter of 1976—1977 a study of cooling-pond fog was conducted at Dresden (Everett and Zerbe, 1976). The immediate purpose of the study was to characterize fog frequency and intensity; the long-term goal is to develop improved methods for the prediction of cooling-pond fog. The original experimental plan included three instrument shelters, containing hygrothermographs, placed on the dike around the warmest pond, and a commercial instrument package (Climatronics Corp., model EWS) on a tower platform in the middle of the pond. However, rime icing on the shelters and the tower led to many of the data being of doubtful quality at best. Measurements of water temperature below the tower were of acceptable accuracy, although there were periods of no data when extended sieges of bad weather prevented servicing. A local resident made observations of the fog conditions twice daily. There were five categories of fog conditions (no fog, slight fog, fog, fog becoming stratus, and stratus). Some misunderstandings about the categories, however, led to the fog conditions being reclassified in this study as no fog (no fog or slight fog) and fog (fog, fog becoming stratus, and stratus). Atmospheric variables measured at Argonne, along with the water temperature, were used in various combinations as predictors of the fog-no fog condition in a discriminant function optimized via nonlinear programming.

A technique described by Meisel (1972) was chosen. The method involves adjusting a surface of separation between categories in order to minimize the amount by which misclassifications are incorrect, instead of simply to minimize misclassifications. The separation surface can be given a non-zero width and thus become a zone of separation. Briefly, the mathematical technique can be expressed as follows.

For sample sets $Y_1$ and $Y_2$ of n-dimensional data, such as simultaneous observations of air temperature and humidity and water temperature, associated with two mutually exclusive and exhaustive categories, such as fog and no fog,

149

we wish to find a discriminant function or hyperplane $w \cdot x = 0$ in n-dimensional sample space such that

$$w \cdot y > d \qquad \text{for } y \in Y_1 \, , \tag{1a}$$

and

$$w \cdot y < d \qquad \text{for } y \in Y_2 \, , \tag{1b}$$

where y is an augmented sample $(x_1, x_2, \ldots x_n, 1)$, $w = (w_1, w_2, \ldots w_n, w_{n+1})$, and d is a constant (the half-width of the "dead" zone). We will minimize the cost function C, defined as

$$C = \frac{1}{M} \sum_{j=1}^{M} f_i \left( \frac{d - w \cdot y_j}{\| \omega \|} \right) \quad . \tag{2}$$

Set Y of samples in $Y_1$ and negatives of samples in $Y_2$ contains M members, $\omega' = (w_1, w_2, \ldots w_n)$ is an unaugmented n-dimensional weight vector, and

$$f_i(Z) = \begin{cases} 0 & Z \le 0 \\ Z & Z > 0 \end{cases} \quad , \tag{3a} \tag{3b}$$

where subscript i indicates that other functions would be acceptable.

Generally, a gradient technique is the most efficient way to minimize C.

$$w^{i+1} = \begin{cases} w^i + \dfrac{\epsilon_i}{M} D(w^i, y_j) & \text{if } w^i \cdot y_j < d \\ w^i & \text{if } w^i \cdot y_j \ge d \end{cases} \tag{4a} \tag{4b}$$

where

$$D(w, y) = \frac{y}{\| \omega \|} - \frac{(w \cdot y - d) \omega *}{\| \omega \|} \, , \tag{5}$$

$\omega *$ is the (n + 1)-dimensional vector: $\omega * = (w_1, w_2, \ldots w_n, 0)$, and $\epsilon_i$ is a constant (usually near zero).

When the technique is applied to the cooling-pond fog problem, the elements making up the observation vectors must be determined. It seems evident that water surface temperature ($T_s$), ambient air temperature ($T_a$), and ambient relative humidity (RH) are important, but the particular form of the data might vary. For instance, $(x_1, x_2, x_3)$ might be $(T_s, T_a, RH)$, or

$(T_s, T_s - T_a, es_s - RH * es_a)$, where $e_s$ is the saturation vapor pressure for $T_s$ or $T_a$ and thus $x_3$ is a vapor pressure deficit (VPD). Physical arguments indicate that fog should be more frequent with high $T_s$, low $T_a$, and high RH, but correlations between the variables may mask the individual effects. For instance, fog is much more common in winter, when $T_s$ is relatively low, than in summer, when $T_s$ is high, because of corresponding changes in $T_a$ and RH. The form of the observation vectors used in the resuls shown here is $(x_1, x_2, x_3) = (T_s - T_a, T_a, VPD)$. Admittedly, $T_s$, the water temperature measured by the submerged probe, is somewhat warmer than the temperature of the surface skin; a more rigorous treatment of the problem would require some systematic correction.

When sorting the data vectors into two groups, such that a discriminant function developed from half of the total data set can be tested with the other half, it is important to avoid the introduction of a temporal bias. Selecting every other point would put morning observations in one group and afternoon observations in the other. Therefore, the data vectors are sorted by every other pair (in effect every other day).

Table 1 shows the discriminant functions developed from data group A, data group B, and the entire data group (A + B), and their effectiveness in category classification. A positive value of the discriminant function indicates a category prediction of no fog, while a negative value indicates a prediction of fog. Misclassifications are totaled for both the dependent data group and the entire data group. The dead zone has a width of 0.01 for the dependent data groups (with which the functions were optimized), but has a zero width for the entire data group, since the functions are being tested and not optimized.

Table 1. Discriminant Functions for Fog Prediction

| Data group | Discriminant function | Dependent data | | Total data | |
|---|---|---|---|---|---|
| | | No. obs. | No. errors | No. obs. | No. errors |
| A | $-0.0102x_1 + 0.0128x_2 + 0.0174x_3 + 0.1470$ | 86 | 4 | 172 | 14 |
| B | $-0.0093x_1 + 0.0090x_2 + 0.0292x_3 + 0.0695$ | 86 | 12 | 172 | 12 |
| A + B | $-0.0080x_1 + 0.0073x_2 + 0.0285x_3 + 0.0625$ | 172 | 16 | 172 | 13 |

Additional data will be collected in a more reliable manner during 1978. The results will be used to compare purely statistical methods of fog prediction (such as shown above) to a method involving physical concepts (Hicks, 1977). The goal is to eventually develop a model to predict cooling-pond fog frequency and intensity, before construction, based upon area climatology and pond design.

References

Everett, R. G. and G. A. Zerbe, 1976: Winter field program at the Dresden cooling ponds. Argonne National Laboratory Radiological and Environmental Research Division Annual Report 76-88, Part IV, pp. 108—113.

Hicks, B. B., 1977: The prediction of fog over cooling ponds. J. Air Pollut. Control Assoc. 27, 140—142.

Meisel, W. S., 1972: Computer-Oriented Approaches to Pattern Recognition, Academic Press, New York, pp. 55—65.

# THE USE OF THE TOTAL TOTALS INDEX AS AN AID TO FORECASTING SEVERE WEATHER IN NORTHERN ILLINOIS

Douglas L. Sisterson

## Introduction

On 13 June 1976, a tornado killed two residents and extensively damaged the town of Lemont, 10 km southwest of ANL. The same tornadic system passed through the Laboratory site later that afternoon and damaged several buildings, as well as surrounding wooded areas (Fujita, 1976). The dynamics of tornados and thunderstorms are fairly well understood, but specific locations and intensities of storms are virtually unpredictable; although storm intensity and movement can be monitored by weather radar, echoes characteristic of severe weather can be seen only after a storm has developed. A means of anticipating meteorological conditions conducive for the development of severe weather is necessary for early warning purposes. This note summarizes the results of a pilot study that tested a simple, objective stability index for predicting the occurrence of severe weather.

## Data Acquisition

The operational value of the Total Totals Index (TTI) (Miller et al., 1965) as a predictor of severe weather within a 100 km radius of ANL was tested during the spring of 1977. The TTI was chosen because, of several such indices now in use, it is by far the simplest (Miller, 1975). It is defined as:

$$TTI = (T_{850} - T_{500}) + (Td_{850} - T_{500}) ,$$

where $T_{850}$ represents the 850 mb temperature, $Td_{850}$ is the 850 mb dew-point temperature, and $T_{500}$ is the 500 mb temperature. The first term $(T_{850} - T_{500})$ represents the static instability of the atmosphere, essentially the measure of the potential for vertical displacement of dry air due to buoyancy. The second term $(Td_{850} - T_{500})$ represents an approximate measure of the convective instability of the atmosphere. The latter can be described as a form of potential

atmospheric instability that can be triggered when a parcel of air is lifted above its level of condensation; instability results when the ambient lapse rate is greater than moist adiabatic. The two terms, therefore, constitute an approximate measure of the overall potential instability of the atmosphere. A significant advantage of the index is the ease with which it can be computed from information readily available from the National Weather Service.

Generally, TTI values < 40 indicate that the atmosphere is sufficiently stable to make strong convective activity (i.e., thunderstorms) unlikely. For TTI values between 40 and 50, the atmosphere is sufficiently unstable to support strong convection. For TTI values greater than 50, the atmosphere is highly unstable, and the chance for the development of severe weather (i.e., intense thunderstorms or tornados) is correspondingly high. These critical values of the TTI are both geographically and seasonally dependent. In this short study conducted at ANL during the spring of 1977, the tentative critical value for thunderstorm development was found to be near 43; data were insufficient for a critical value for severe weather development to be determined. Severe weather events, therefore, were counted as thunderstorm events for statistical analysis of the TTI as a predictor of thunderstorm activity.

The upper-air data used to compute TTI values were obtained from the 1200Z (0600 CST) Peoria, Illinois, sounding. Peoria, the rawinsonde station nearest ANL (150 km distant), lies to the southwest and thus provides the best measure of the characteristics of those air masses (moving from SW to NE) typically associated with severe weather in northern Illinois. The TTI is computed by 1030 local time.

During the 108 days of this study, rawinsonde data were available on 102 days. Southwesterly winds at 500 mb occurred on 45 of the 102 study days. An "event," defined for the purpose of this study as either a thunderstorm or a severe weather occurrence within 100 km of ANL, was verified by one or more of the following methods: television, radio, National Weather Service weather radio, or direct observation at ANL. A storm was considered severe if wind gusts over 25 m s$^{-1}$, half-inch hail, or a tornado or funnel cloud occurred.

## Data Analysis

A comparison of the TTI forecasts versus observations is shown in Table 1. A chi-square test shows that the table is significant at the 0.1% level; e.g., there is less than a 0.1% probability that the distribution in Table 1 could have occurred by chance. The skill score (S) is +0.57 as defined by

$$S = \frac{R - E}{T - E} \; ,$$

where R is the number of correct forecasts (the sum of the diagonal elements in Table 1), T is the total number of forecasts, and E is the corresponding number of correct forecasts that could have occurred by chance.

Table 2 shows the frequency of events observed in southwesterly winds compared to the frequency of events observed in all other wind directions. The flow was southwesterly on only 44% of the study days, but 74% of the days with thunderstorms and 90% of the days with severe weather had southwesterly flow. Events occurred on 58% of the days with southwesterly winds but on only 12% of other days.

A favorable combination of both convective instability and static instability must exist for thunderstorm development. Figure 1 contains a plot of convective instability versus static instability. The 45 degree line through the origin represents saturation at 850 mb, while the short lines parallel to it represent 850 mb dew-point depressions. Curves of constant TTI are orthogonal to the dew-point depression lines. Seventy-seven percent of the cases contained in empirically-derived boundaries formed by the saturation and TTI = 43 lines represent occurrences of days with thunderstorm activity, sometimes severe. In a few cases, events occurred with low values of TTI, and in a few others no events occurred for values of TTI within the aforementioned area. Although individual points may be explained by various meteorological arguments, no general method can be used to dismiss these points.

## Conclusions

The use of the Total Totals Index provides an early means of assessing the potential for thunderstorm activity within a 100 km radius of ANL.

Table 1.  Contingency table for the Total Totals Index for southwesterly flow.

|  |  | Observations | |
|---|---|---|---|
|  |  | No event | Thunderstorm |
| Forecasts | < 43 | 12 | 2 |
|  | > 43 | 7 | 24 |

Table 2.  Comparison of the convective intensity on days with southwesterly 500 mb flow with the convective intensity on days with flow from the other quadrants.

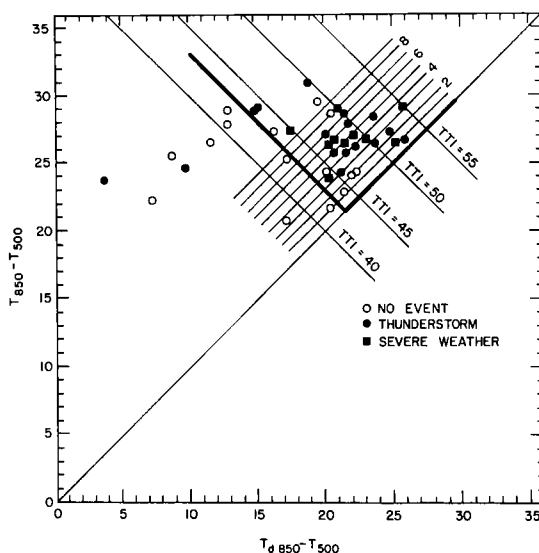|  | No event | Thunderstorm | Severe | Total days |
|---|---|---|---|---|
| Southwesterly winds | 19 | 17 | 9 | 45 |
| Winds other than south through west | 50 | 6 | 1 | 57 |
| Total | 69 | 23 | 10 | 102 |



FIG. 1.--Verification of the Total Totals Index, plotted as convective instability versus static instability. Four no-event points with negative abscissas are not plotted. (ANL Neg. 149-78-10-R1)

156

Thunderstorm activity occurred 77% of the time it was forecast in this study, with severe weather on one thunderstorm day in three. Perhaps of equal importance is the forecast of no thunderstorms; on 75% of the days with south-westerly winds (when severe weather might otherwise have been considered possible), a forecase of no thunderstorm activity was correct. For winds from the other three quadrants, no thunderstorm activity occurred on 88% of the days, regardless of the Total Totals Index. Further, storms did not occur for an index of less than 27. Thus, when especially critical laboratory operations requiring favorable weather are considered, the Total Totals Index provides a simple, objective assessment of the conditions to be expected later in the day.

## Acknowledgements

## References

Fujita, T. T., 1976: The Lemont-Argonne Tornado of June 13, 1976. Satellite and Meso-Meteorological Research Paper No. 144, University of Chicago.

Miller, R. C., A. Waters, and L. Bartlett, 1965: The use of 500 mb − 850 mb totals in severe weather forecasting. National Weather Service Library, Kansas City, Missousi.

Miller, R. C., 1975: Notes on analysis in severe storm forecasting procedures of the Air Force Global Weather Central. Revised, Air Weather Service Technical Report #200, Hq. Air Weather Service, Scott AFB, Illinois.

# THE ANL 403 MHZ RADIOSONDE SYSTEM[*]

R. L. Hart, F. R. George,[†] L. S. VanLoon,[‡] B. B. Hicks, and F. Kulhanek

Recent emphasis on problems concerning atmospheric pollutant transport has resulted in increased interest in the fine structure of the lower atmosphere, particularly in the diurnal cycle of the planetary boundary layer (PBL). In an effort to provide an inexpensive alternative to commercially available instrumentation for sampling of the PBL, new radiosonde instrumentation has been developed for obtaining temperature profiles with an accuracy of better than 0.4°C and a resolution of better than 0.05°C. When the new radiosondes are used in conjunction with the WHAT system (an automatic, double-theodolite, balloon-tracking system), balloon position and air temperature data are obtained at one-second intervals. For a balloon rise rate of $3 \text{ m s}^{-1}$, these measurements are obtained at three-meter vertical intervals.

The current version of the ANL minisonde is a simple and inexpensive device that uses a monolithic timer of the 555 type, a polycarbonate capacitor, and a bead thermistor in a rapid-response, temperature-sensing, audio-frequency oscillator. The pulse output of this audio-frequency generator modulates a single-transistor, radio-frequency (RF) oscillator/transmitter, which has an RF tank consisting of a one-turn coil printed on the circuit board and an adjustable ceramic capacitor.

To improve the ability of a commercial receiver to recover weak signals, a signal conditioner, which utilizes a "phase-lock-loop" to track the audio-frequency output from the receiver's FM (frequency modulation) detector, has been added. This circuit locks onto the frequency of the input and rejects any high-frequency noise. When the FM detector output becomes too weak for the loop to maintain lock, the circuit first tries to reestablish lock. If lock is not

attained within a short period of time, the circuit then disconnects the output.

In routine operations in the PBL, the radiosondes are used in a "structure-sonde" mode, i.e., they are released automatically from a rising balloon at a predetermined altitude by a simple barometric release mechanism to obtain two consecutive profiles through the lower atmosphere. The release mechanism consists of a small polyethylene bottle, a plastic tube, and a special water-soluble paper. As the balloon ascends, the decreasing atmospheric pressure allows the air in the bottle to expand. Water forced up the tubing wets and dissolves the paper and thus releases a parachute with the radiosonde.

The radiosonde-WHAT system has been used at ranges up to 20 km in several experiments in recent years. The data recorded on computer-compatible magnetic tape in the field have been processed with the aid of a computer to produce high-resolution vertical profiles of wind and temperature. The temperature profiles are considerably more detailed than those obtained with conventional radiosondes, which typically transmit a temperature signal intermittently at 100 to 150 m intervals below 2 km. While the standard radiosondes have similar accuracy and resolution to the type discussed here, the ANL type are smaller, considerably less expensive, and transmit the temperature information continuously.

# AN EDDY-CORRELATION MEASUREMENT OF PARTICULATE DEPOSITION FROM THE ATMOSPHERE [*]

M. L. Wesely, B. B. Hicks, W. P. Dannevik, [†] S. Friselle, [†] and R. B. Husar[‡]

Eddy-correlation techniques have been applied to measure directly the vertical flux of small particles in the size range 0.05—0.1 μm. A site 2—5 km downwind of several sources associated with refineries was chosen to ensure detectably high concentrations of small particles in a large open field. At 5 m above a moderately rough surface of grass, the eddy fluxes of momentum, heat, and particles were obtained with use of fast-response devices, including a particle sensor operating on the principle of diffusion charging. The particle deposition velocities during a brief series of measurements in light winds varied from 1.0 to 0.1 cm s$^{-1}$ as conditions changed from unstable to stable. The results support the contention that, for particles smaller than 1 μm, the deposition velocity of particles in light to moderate winds may be about 1 cm s$^{-1}$, rather than the 0.1 cm s$^{-1}$ that has been popular with some numerical modelers.

# RELATIONSHIPS BETWEEN DRY DEPOSITION RATES AND CONCENTRATIONS AT HEIGHTS OF 50-200 M[*]

M. L. Wesely

For application of regional-scale numerical models of the behavior of sulfur compounds in the atmosphere and interpretation of aircraft measurements of $SO_2$ and particulate concentrations, it is necessary sometimes to understand the relationships of concentrations at heights of 50 to 200 m to dry deposition rates at the surface. With the assumption of no local sources of pollutants, simple relationships can be obtained by empirically extrapolating modified surface-layer expressions of eddy diffusivity to such heights, which are about one-tenth the height of the planetary boundary height. The simple formulations that result indicate that the effects of atmospheric stabilities can have an overwhelming effect. For example, with typical daytime conditions, the vertical fluxes are large and the deposition velocities are nearly the same near the surface as they are at greater heights. At night, the vertical fluxes are often nearly zero, even though a strong variation of deposition velocity with height exists.

# ON THE BOWEN RATIO AND SURFACE TEMPERATURE AT SEA[*]

B. B. Hicks and G. D. Hess

---

Gradients of temperature and humidity above water surfaces are analyzed in order to determine the dependence of the long-term average Bowen ratio $\beta$ (the ratio of sensible to latent heat flux) on surface temperature. The least-squares fit that results from investigations of six such bodies of data, and which is supported by recent direct measurements of the fluxes by eddy correlation techniques, can be expressed as $\beta = 0.63 \, \gamma / s - 0.15$, where $\gamma$ is the ratio of the specific heat of air at constant pressure to the latent heat of vaporization of water, and $s$ is the slope of the saturated specific humidity curve at the surface temperature. This expression forms the basis of a model which can be used to determine the average surface temperature from routine observations of air temperature and humidity at sea.

---

# ON THE RELATIVE IMPORTANCE OF SINGLE-PARTICLE AND RELATIVE DIFFUSION FOR PLUME DISPERSION*

C. M. Sheih

---

An observed horizontal wind velocity spectrum is used to compute the plume horizontal dispersion coefficients due to single-particle and relative diffusion. The results show that the instantaneous plume width (or dispersion coefficient) is primarily determined by relative diffusion. If the averaging time increases, meandering of the center line of the instantaneous plume will also contribute to the apparent plume width in terms of the mechanisms of single-particle diffusion. As the averaging time increases further, single-particle diffusion will become at least as important as relative diffusion. Calculations for horizontal dispersion in the atmosphere up to $10^5$ downstream from release show that plume dispersion is dominated by relative diffusion for averaging times up to one-tenth of the time from release (the plume age) and that dispersion is dominated by single-particle diffusion for averaging times larger than 10 times the plume age. For averaging times between 0.1 to 10 times the plume age, both types of diffusion are important.

---

163

# A TURBULENCE MODEL APPLIED TO GEOPHYSICAL FLUID PROBLEMS[*]

G. L. Mellor[†] and T. Yamada

A turbulence-closure model developed at Princeton University is reviewed and examples of simulations by this model are given. Empirical constants in the hypotheses by Rotta and Kolmogorov have been established for the model from laboratory experiments of geophysical interest, and a variety of cases in atmospheric and oceanic fluid dynamics have been simulated, including both the near-surface and the entire, diurnally varying atmospheric boundary layers, dispersion of pollution from a point source in the atmospheric boundary layer, development of oceanic surface mixed layers and bottom layers, and global atmospheric circulations. The model and the fixed set of constants perform well in predicting diverse neutral flows. The same model, with no alteration, predicts density-stratified flows in a manner that far exceeds prior expectations.

# A NUMERICAL EXPERIMENT ON POLLUTANT DISPERSION IN A HORIZONTALLY-HOMOGENEOUS ATMOSPHERIC BOUNDARY LAYER*

T. Yamada

A simplified turbulence-closure model is proposed and utilized for simulation of three-dimensional pollution dispersion. Since the complexity of the present model lies between the complexities of the Level 2 and 3 models discussed in Mellor and Yamada (1974, J. Atmos. Sci., 31, 1791–1806), it may be tentatively referred to as a "Level 2.5 model." The Level 2.5 model is much simpler than the Level 3 model because only one transport equation for the turbulent energy must be solved, while seven transport equations must be solved in the Level 3 model when fields of wind, temperature, water vapor, and pollutant concentration are simulated. It is for this simplicity that the Level 2.5 model is proposed, despite certain deficiencies in comparison with higher-level models. In simulation of the diurnally varying planetary boundary layer of the "Wangara" experiment, the Level 2.5 model reproduces well the Level 3 model results except in the layer near the ground. When a three-dimensional mass-conservation equation for a chemically inert pollutant is integrated numerically, with use of mean and turbulence fields from the numerical simulation of Wangara data, large diurnal differences are produced in the computed profiles of pollutant concentration, due to changes in stability. Surface pollutant concentrations are significantly reduced during the night when the simulated source is high enough (200 m) to be effectively decoupled from the surface.

PUBLICATIONS BY THE STAFF OF THE ATMOSPHERIC PHYSICS SECTION FOR
THE PERIOD JANUARY–DECEMBER 1977

Journal Articles, Book Chapters, etc.

J. A. Eastman and D. H. Stedman
A FAST RESPONSE SENSOR FOR OZONE EDDY-CORRELATION FLUX MEASURE-
MENT
Atmos. Environ. 11, 1209–1211 (December 1977)

P. Frenzen
A GENERALIZATION OF THE KOLMOGOROV-VON KARMAN RELATIONSHIP AND
SOME FURTHER IMPLICATIONS ON THE VALUES OF THE CONSTANTS
Boundary-Layer Meteorol. 11, 375–380 (May 1977)

B. B. Hicks
THE PREDICTION OF FOG OVER COOLING PONDS
APCA J. 27, 140–142 (February 1977)

B. B. Hicks and G. D. Hess
ON THE BOWEN RATIO AND SURFACE TEMPERATURE AT SEA
J. Phys. Oceanogr. 7, 141–145 (January 1977)

B. B. Hicks and H. S. Goodman
SEASONAL AND LATITUDINAL VARIATIONS OF ATMOSPHERIC RADIOACTIVITY
ALONG AUSTRALIA'S EAST COAST (150°E LONGITUDE)
Tellus 29, 182–188 (March-April 1977) (Work done while at CSIRO)

B. B. Hicks and C. M. Sheih
SOME OBSERVATIONS OF EDDY MOMENTUM FLUXES WITHIN A MAIZE
CANOPY
Boundary-Layer Meteorol. 11, 515–519 (July 1977)

B. B. Hicks, M. L. Wesely, and C. M. Sheih
A STUDY OF HEAT TRANSFER PROCESSES ABOVE A COOLING POND
Water Resources Res. 13, 901–908 (December 1977)

G. Mellor (Princeton U.) and T. Yamada
A TURBULENCE MODEL APPLIED TO GEOPHYSICAL FLUID PROBLEMS
Symposium on Turbulent Shear Flows 1, 6.1–6.14 (1977)

C. M. Sheih
APPLICATION OF A STATISTICAL TRAJECTORY MODEL TO THE SIMULATION
OF SULFUR POLLUTION OVER NORTHEASTERN UNITED STATES
Atmos. Environ. 11, 173–178 (February 1977)

C. M. Sheih
A PUFF-GRID MODEL FOR PREDICTING POLLUTANT TRANSPORT OVER AN
URBAN AREA
APCA J. <u>27</u>, 784–785 (August 1977)

C. M. Sheih
MATHEMATICAL MODELING OF PARTICULATE THERMAL COAGULATION AND
TRANSPORT DOWNSTREAM OF AN URBAN AREA SOURCE
Atmos. Environ. <u>11</u>, 1185–1190 (November 1977)

M. L. Wesely and B. B. Hicks
SOME FACTORS THAT AFFECT THE DEPOSITION RATES OF SULFUR DIOXIDE
AND SIMILAR GASES ON VEGETATION
APCA J. <u>27</u>, 1110–1116 (November 1977)

M. L. Wesely, B. B. Hicks, W. P. Dannevik, S. Frisella, and R. B. Husar
AN EDDY-CORRELATION MEASUREMENT OF PARTICULATE DEPOSITION FROM
THE ATMOSPHERE
Atmos. Environ. <u>11</u>, 561–563 (July 1977)

T. Yamada
A NUMERICAL EXPERIMENT ON POLLUTANT DISPERSION IN A HORIZONTALLY
HOMOGENEOUS ATMOSPHERIC BOUNDARY LAYER
Atmos. Environ. <u>11</u>, 1015–1024 (November 1977)


Conference Papers and Abstracts

J. D. Shannon and M. L. Wesely
OBJECTIVE PLACEMENT OF SENSORS FOR A REGIONAL TURBIDITY NETWORK
Preprint Volume, Fifth Conference on Probability and Statistics in
Atmospheric Sciences  Nov. 15–18, 1977, Las Vegas, Nevada, 260-264.
Published by Am. Meteorol. Soc., Boston, Mass.

C. M. Sheih
ON THE RELATIVE IMPORTANCE OF SINGLE-PARTICLE AND RELATIVE DIFFUSION
FOR PLUME DISPERSION
Preprint Volume, Fifth Conference on Probability and Statistics in
Atmospheric Sciences, Nov. 15–18, 1977, Las Vegas, Nevada, 260-264.
Published by Am. Meteorol. Soc., Boston, Mass.

C. M. Sheih, G. D. Hess, and B. B. Hicks
DESIGN OF NETWORK EXPERIMENTS FOR REGIONAL-SCALE ATMOSPHERIC
POLLUTANT TRANSPORT AND TRANSFORMATION
Preprint Volume, Joint Conference on Applications of Air Pollution
Meteorology, Nov. 29–Dec. 2, 1977, Salt Lake City, Utah, 364–371.
Published by Am. Meteorol. Soc., Boston, Mass.

M. L. Wesely
RELATIONSHIPS BETWEEN DRY DEPOSITION RATES AND CONCENTRATIONS
AT HEIGHTS OF 50—200 M
     AIChE 70th Annual Meeting, Nov. 13—17, 1977  New York.  Microfiche.
     Published in Meeting Program, p. 84.

D. H. Stedman, R. B. Harvey, J. A. Eastman, D. J. Fingleton  and J. Wallace
OZONE FORMATION OVER LAKE MICHIGAN
     4th Joint Conference on Sensing of Environmental Pollution, AMS, ACS,
     AIAA, AICE, IEEE, ISA, DOT, EPA, ERDA, HUD, NASA, NOAA, DOS,
     USGS, New Orleans, Louisiana, 6—11 November 1977.

M. L. Wesely and R. G. Everett
CHANGE IN ALBEDO DUE TO AEROSOLS AS INFERRED FROM MEASUREMENTS
OF SOLAR RADIATION AT THE SURFACE OF THE EARTH
     Transactions, Am. Geophysical Union <u>58</u>, 789 (August 1977) (Abstract)

Internal:

| | | |
|---|---|---|
| E. G. Pewitt | R. L. Martin | R. L. Hart |
| M. V. Nevitt | R. G. Matlock | P. E. Hess |
| R. O. Ivins | S. A. Miller | B. B. Hicks |
| R. E. Rowland | D. Grahn | M. Inokuti |
| R. M. Adams | D. P. O'Neil | R. A. Kucera |
| J. E. Baird | F. G. Prohammer | F. C. Kulhanek |
| K. Brubaker | L. L. Prucha | J. S. Marshall |
| J. E. Carson | J. J. Roberts | J. E. Miller |
| C. L. Cheever | W. R. Robinson | J. D. Shannon |
| E. J. Croke | D. M. Rote | C. M. Sheih |
| P. T. Cunningham | S. J. Rudnick | D. L. Sisterson |
| P. Failla | J. Sedlet | S. A. Spigarelli |
| K. R. Ferguson | W. K. Sinclair | A. F. Stehney |
| F. R. George | C. M. Stevens | F. E. Throw |
| J. Gray | F. W. Thalgott | G. T. Tisue |
| P. F. Gustafson (4) | R. Winston | M. A. Wahlgren |
| W. Harrison | B. Yamartino | M. L. Wesely |
| J. R. Haumann | RER Division (100) | C. A. Yack (10) |
| B. Holt | S. Berman | T. Yamada |
| S. Johnson | F. R. Clark (10) | G. A. Zerbe |
| L. C. Just | D. Cook | A. B. Krisciunas |
| A. S. Kennedy | J. A. Eastman | M. Fieldhouse |
| M. R. Kraimer | D. N. Edgington | ANL Contract File |
| R. Kumar | R. G. Everett | ANL Libraries (5) |
| J-L. Lee | P. Frenzen | TIS Files (5) |

External:

DOE-TIC for distribution per UC-11 (237)
Manager, Chicago Operations Office
Chief, Office of Patent Counsel, C4
J. L. Liverman, USDOE
President, Argonne Universities Association
Radiological and Environmental Research Division Review Committee:
    F. I. Badgley, U. Washington
    W. J. Bair, Pacific Northwest Labs.
    R. S. Caldecott, U. Minnesota
    A. W. Castleman, Jr., U. Colorado
    H. L. Friedell, Case Western Reserve U. Hospitals
    E. D. Goldberg, Scripps Inst. of Oceanography
    D. Kleppner, Massachusetts Inst. Technology
    G. H. Lauff, Michigan State U.
    W. H. Smith, Yale U.
AUA Biology Representatives:
    W. C. Ashby, Southern Illinois U.
    R. M. Bock, U. Wisconsin
    R. C. Bockrath, Jr., Indiana U.
    R. S. Caldecott, U. Minnesota, St. Paul
    W. Chavin, Wayne State U.
    J. Courtright, Marquette U.

W. F. Danforth, Illinois Inst. Technology
H. S. Ducoff, U. Illinois, Urbana
A. Eisenstark, U. Missouri, Columbia
D. Feir, Saint Louis U.
R. W. Greene, U. Notre Dame
D. L. Hartl, Purdue U.
J. O. Hutchens, U. Chicago
B. H. Judd, U. Texas, Austin
G. M. Maggiora, U. Kansas
H. J. McDonald, Loyola U. Medical Center, Maywood, Ill.
M. C. Miller, U. Cincinnati
W. C. Myser, Ohio State U.
R. R. Novales, Northwestern U.
J. W. Osborne, U. Iowa
R. J. Robel, Kansas State U.
R. C. Rustad, Case Western Reserve U.
S. Silver, Washington U.
E. A. Stull, U. Arizona
A. S. Sussman, U. Michigan
P. W. Todd, Pennsylvania State U.
M. J. Ulmer, Iowa State U.
I. Ungar, Ohio U.
J. J. Wolken, Carnegie-Mellon U.
L. Wolterink, Michigan State U.
Ackerman, B., Illinois State Water Survey, Springfield
Ackermann, W. C., Illinois State Water Survey, Springfield
Ahlen, J. W., Illinois Legislative Council, Springfield
Allen, L. H., Jr., U. Florida
Air Pollution Control Association, Library, Pittsburgh
Anthes, R. A., Pennsylvania State U.
Arya, S. P. S., North Carolina State U.
Atlas, D., National Center for Atmospheric Research, Boulder
Atmospheric Sciences Lab., White Sands Missile Range
Aubert, E. J., NOAA, Ann Arbor
Auerbach, S. I., Oak Ridge National Lab.
Axtel, C. E., Big Rock Plant, Consumers Power Co.
Ayres, J., U. Michigan
Bahr, T. G., Michigan State U.
Ball, R., Michigan State U.
Ballantine, D., DBER, USDOE
Ballert, A. G., Great Lakes Commission, Ann Arbor
Barad, M. L., Hanscom AFB, Mass.
Barr, S., Los Alamos Scientific Lab.
Battan, L. J., U. Arizona
Bayer, K., U. Wisconsin, Milwaukee
Beadle, R. W., DBER, USDOE
Beeton, A. M., U. Wisconsin
Belter, W. G., Office of Environmental Affairs, USDOE
Berk, S. D., Naval Environmental Prediction Research Facility,
    Monterey
Berman, S., State U. College at Oneonta, NY
Bhardwaja, P. S., IIT Research Institute
Bierly, E., National Science Foundation
Bingham, G., Lawrence Livermore Lab.

Birchfield, G. E., Northwestern U.
Blackadar, A. K., Pennsylvania State U.
Bolen, J. J., DRL, USNRC
Booras, S., Illinois Inst. for Environmental Quality, Chicago
Bornstein, R. D., San Jose State U.
Botts, L., Lake Michigan Federation, Chicago
Brady, P., U. North Dakota
Braham, R. R., Jr., U. Chicago
Brown U., Chairman, Dept. of Engineering
Burstein, S., Wisconsin Electric Power Station, Milwaukee
Businger, J. A., U. Washington
California, U. of, Los Angeles, Chairman, Dept. of Meteorology
Campbell, G. S., Washington State U.
Casey, P., International Assoc. for Great Lakes Research,
    Fairport, New York
Cermak, J. E., Colorado State U.
Changnon, S. A., Illinois State Water Survey, Springfield
Charlson, R. J., U. Washington
Chen, N., ATDL/NOAA, Oak Ridge
Ching, J., National Center for Air Poll. Control, USEPA,
    Research Triangle Park
Chock, D. P., General Motors Corp., Warren, Mich.
Coblenz, J., Illinois Environmental Protection Agency, Springfield
Cocanougher, J., Miami U., Oxford, O.
Collette, T., Commonwealth Edison Co., Chicago
Colorado State U., Library, Dept. of Atmospheric Sciences
Comey, D. D., Business Men for the Public Interest, Chicago
Commonwealth Edison Co., Dept. of Environmental Planning, Chicago
Connecticut, U. of, Chairman, Dept. of Meteorology
Cornell U., Agricultural Experiment Station, Geneva
Cornell U., Librarian, Microclimatology Research Unit
Cornett, J. S., Air Resources Laboratory, Las Vegas
Corotis, R., Northwestern U.
Corrsin, S., Johns Hopkins U.
Coutant, C. C., Oak Ridge National Lab.
Craig, R. A., Florida State U.
Crawford, T. V., Savannah River Lab.
Crook, L. T., Ann Arbor
Csanady, C. T., Woods Hole Oceanographic Inst.
Cushing, C. E., Pacific Northwest Lab.
Dahlman, R., DBER, USDOE
Davidson, K. L., U. S. Naval Postgraduate School
Davies, T. T., Grosse Ile Lab., USEPA
Deardorff, J. W., Oregon State U.
Delumyea, R., Washington U.
Dempsey, T., Chico, Calif.
DePena, R., Pennsylvania State U.
Dickerson, M., Lawrence Livermore Lab.
Dickson, C. R., NOAA, Idaho Falls
DiNunno, J., NUS Corp., Rockville
Dittmar, R. A., Wallops Flight Center
Drake, R., Battelle Pacific Northwest Lab.
Drescher, W. J., U. S. Geological Survey, Madison
Droppo, J., Battelle Pacific Northwest Lab.

Duke U., Chairman, Dept. of Environmental Science
Durham, J. L., USEPA, Research Triangle Park
Durso, M. P., Health and Safety Lab., USDOE, New York
Eddy, A., U. Oklahoma
Eidson, W. W., Drexel U.
Eissenberg, D., Oak Ridge National Lab.
Elderkin, C., Battelle Pacific Northwest Lab.
Elliott, W. P., NOAA, Silver Spring
Engelmann, R. J., ERL, NOAA, Boulder
Epstein, E. S., U. Michigan
Eschenroeder, A. Q., General Research Corp., Santa Barbara
Evanoff, J., Dept. of Environmental Control, City of Chicago
Evans, R. D., Scottsdale, Ariz.
Fay, C. W., Wisconsin Electric Power Co., Milwaukee
Fichtl, G. H., NASA Marshall Space Flight Center
Fleagle, R. G., U. Washington
Florida, U. of, Chairman, Dept. of Meteorology
Forster, W., DBER, USDOE
Friedlander, S., California Inst. of Technology
Friehe, C. A., U. California, San Diego
Friend, J., Drexel U.
Gates, D. M., U. Michigan
Gatz, D., Illinois State Water Survey, Springfield
Gifford, F. A., Jr., NOAA, Oak Ridge
Gillani, N., Washington U.
Golden, J. C., Jr., Commonwealth Edison Co., Chicago
Gray, W., Colorado State U.
Great Lakes Basin Commission, Librarian
Groppi, M., Commonwealth Edison Co., Chicago
Gross, T., DBER, USDOE
Hadlock, R., Battelle Pacific Northwest Lab.
Hales, J. M., Battelle Pacific Northwest Lab.
Halitsky, J., Croton-on-Hudson, New York
Hall, F. F., NOAA, Boulder
Hanna, S. R., ATDL/NOAA, Oak Ridge
Harley, J. H., Health and Safety Lab., USDOE, New York
Harper, D., Metropolitan Sanitary District of Chicago
Harris, W. F., Oak Ridge National Lab.
Harvard U., Chairman, Dept. of Meteorology
Haugen, D. A., Wave Propagation Lab., NOAA, Boulder
Hawaii, U. of, Chairman, Dept. of Meteorology
Heffter, J. L., NOAA, Silver Spring
Hewson, E. W., Oregon State U.
Hidy, G. M., Environmental Research and Technology, Inc.
Hilst, G., The Research Corp. of New England
Hitchcock, D. R., Farmington, Conn.
Hoffman, H., Oak Ridge National Lab.
Hosker, R. P., Jr., ATDL/NOAA, Oak Ridge
Huber, A. H., USEPA, Research Triangle Park
Humphrey, P. A., USEPA, Research Triangle Park
Husar, R. B., Washington U.
IIT Research Institute, Document Library
Illinois Environmental Protection Agency, Manager,
    Div. of Air Pollution Control
Illinois State Water Survey, Librarian

Illinois, U. of, Circle Campus, Library
Iowa State U., Chairman, Dept. of Meteorology
Jacko, R., Purdue U.
Jarecki, E. A., Great Lakes Basin Commission, Ann Arbor
Jaworski, N. A., Grosse Ile Lab., USEPA
Joseph, A. B., USNRC
Kaimal, J. C., Wave Propagation Lab., NOAA, Boulder
Kao, S. K., U. Utah
Kern, C. D., Savannah River Lab.
Kern, C. W., Northern Indiana Public Service Co., Hammond
Klappenbach, E., USEPA, Chicago
Knox, J. B., Lawrence Livermore Lab.
Kreitzburg, C. W., Drexel U.
Lee, B., Jr., Commonwealth Edison Co., Chicago
Lettau, H. H., U. Wisconsin
Lilly, D. K., National Center for Atmospheric Research, Boulder
Linsky, B., U. West Virginia
Lipschutz, R., Pennsylvania State U.
Lohr, L. L., Jr., U. Michigan
London, J., U. Colorado
Long, P., NOAA/NWS, Silver Spring, Md.
Lordi, D. T., Metropolitan Sanitary District of Greater Chicago
Ludwig, G. R., Cornell Aeronautical Lab.
Lyons, W. A., U. Wisconsin, Milwaukee
MacCracken, M. C., Lawrence Livermore Lab.
Machta, L., NOAA, Silver Spring
Mahlman, J., Princeton U.
Mantis, H., U. Minnesota
Marht, L., Oregon State U.
Markee, E., DRL, USNRC
Martell, E. A., National Center for Atmospheric Research, Boulder
Martin, D., St. Louis U.
Martin, J. H., Sheaffer & Roland, Inc., Chicago
Maryland, U. of, Chairman, Dept. of Engineering
Mellor, G., Princeton U.
Meroney, R., Colorado State U.
Miami, U. of, Inst. of Atmospheric Science, Coral Gables
Michael, P., Brookhaven National Lab. (3)
Michigan, U. of, Great Lakes Research Div.
Miksad, U. Texas, Austin
Miller, A., San Jose State U.
Miller, E., Corvallis, Ore.
Miller, J. M., Air Resources Lab., NOAA, Silver Spring
Miskimen, T. A., American Electric Power Service Corp., New York
Missouri, U. of, Chairman, Dept. of Atmospheric Science, Columbia
Missouri, U. of, Chairman, Dept. of Meteorology, Rolla
Miyakado, K., Princeton U.
Mohnen, V. A., SUNY at Albany
Molle-Christensen, E. L., Massachusetts Inst. Technology
Mortimer, C. H., U. Wisconsin, Milwaukee
Moses, H., DBER, USDOE
Mueller, H. F., NOAA, Las Vegas
Murphy, T. J., DePaul U.
Murray, J. R., Murray & Trettle, Inc.

Nappo, C. J., Jr., Oak Ridge Operations Office, USDOE
NASA Goddard Space Flight Center, Librarian
NASA Langley Research Center, Technical Library
NASA Lewis Research Center, Librarian
National Center for Atmospheric Research, Library, Boulder
National Oceanic and Atmospheric Admin., Library, Silver Spring
National Weather Service, Headquarters, Silver Spring
Nevada, U. of, Desert Research Inst.
Newell, R. E., Massachusetts Inst. Technology
New Jersey Agricultural Experiment Station, Cook College-Rutgers U.
Newman, L., Brookhaven National Lab.
New York, City U. of, Chairman, Dept. of Meteorology
Nichols, G., Jr., M. D., Manchester, Mass.
Nickerson, E. C., National Oceanic and Atmospheric Admin., Boulder
Niemeyer, L. E., USEPA, Research Triangle Park
Northeastern U., Library, The Technical Institute
Noshkin, V. E., Lawrence Livermore Lab.
Notre Dame, U. of, Library, Dept. of Meteorology
Odum, H. T., U. Florida
Ogura, Y., U. Illinois
Oklahoma, U. of, Chairman, Dept. of Meteorology
Orville, R. E., SUNY at Albany
Osburn, W. S., DBER, USDOE
Ostlund, H. G., U. Miami, Fla.
Ott, W., USEPA, Rockville
Panofsky, H. A., Pennsylvania State U.
Papetti, R., USEPA, Washington
Pashayan, D., USEPA, Washington
Patrinos, A., Oak Ridge National Lab.
Paulson, C. A., Oregon State U.
Phillips, J. H., USEPA, Chicago
Pielke, R. A., U. Virginia
Platzman, G. W., U. Chicago
Pocalujka, L., Sargent & Lundy, Chicago
Pogany, D., Illinois Div. of Energy, Springfield
Porter, R., Illinois Inst. of Technology
Poston, H. W., Dept. of Environmental Control, City of Chicago
Powers, C. F., Pacific Northwest Water Lab., Corvallis
Prospero, J. M., Rosenstiel School of Marine and Atmospheric Science,
    Miami
Pruitt, W. O., U. California, Davis
Quon, J., Northwestern U.
Ragotzkie, R. A., U. Wisconsin
Raman, S. S., Brookhaven National Lab.
Randerson, D., Air Resources Lab., NOAA, Las Vegas
Rao, S., ATDL/NOAA, Oak Ridge
Raynor, G. S., Brookhaven National Lab.
Record, F. A., GCA Corp., Bedford, Mass.
Reed, G. A., Wisconsin Michigan Power Co., Two Rivers, Wis.
Reed, J. W., Sandia Labs.
Reichle, D. E., Oak Ridge National Lab.
Reifsnyder, W. E., Yale School of Forestry & Environmental Studies
Reiter, E. R., Colorado State U.
Reynolds, J. Z., Consumers Power Co., Jackson, Mich.

Rhode Island, U. of, Chairman, Dept. of Environmental Science
Robbins, J., U. Michigan
Robinson, E., Washington State U.
Robinson, G. D., Center for the Environment and Man, Hartford, Conn.
Rosenberg, N. J., U. Nebraska
Rossin, A. D., Commonwealth Edison Co., Chicago
Rouse, F. O., Great Lakes Basin Commission, Ann Arbor
Rudloff, W. K., U. Petroleum and Minerals, Portage, Ind.
Rutgers University, College of Agriculture & Environmental Science,
    Chairman
Ryan, P. J., Bechtel Corp.
Ryznar, E., U. Michigan
Salmon, E., McLean, Va.
Sargent, S. L., Div. Solar Energy, USDOE
Saucier, W., North Carolina State U.
Saunders, G. W., DBER, USDOE
Saylor, J. H., NOAA, Great Lakes ERL, Ann Arbor
Scandanavian Documentation Center, Washington
Schelske, C. L., U. Michigan
Schubert, J. F., Savannah River Lab.
Schwartz, S., Brookhaven National Lab.
Schwerdtfeger, W., U. Wisconsin
Semonin, R., Illinois State Water Survey
Serafin, R. J., National Center for Atmospheric Research, Boulder
Shaffer, W., NOAA/NWS, Silver Spring
Shiermeier, F., EPA, Creve Coeur, Mo.
Shinn, J., Lawrence Livermore Lab.
Sievering, H., Governors State U.
Simpson, C. L., Battelle Pacific Northwest Lab.
Sinderman, R. W., Consumers Power Co., Jackson, Mich.
Slade, D. H., DBER, USDOE
Smith, D., Environmental Analysts, Inc., Garden City, New York
Smith, M., Smith-Singer Meteorologists, Inc., Massapequa, New York
Snyder, W. H., USEPA, Research Triangle Park
Spengler, K. C., American Meteorological Society, Boston
Sprugel, G., Jr., Illinois Natural History Survey
Start, G. E., NOAA, Idaho Falls
Stearns, C. R., U. Wisconsin
Stegen, D. G., Science Applications, Inc., La Jolla
Stempora, T., Commonwealth Edison Co., Chicago
Stirm, W., Purdue U.
Stoermer, E. F., U. Michigan
Strange, R. H., II, National Science Foundation
Strong, A., National Weather Service, Chicago
Swinebroad, J., DBER, USDOE
Swope, P., National Weather Service, Chicago
Tanner, C. B., U. Wisconsin
Tedeschi, P., Illinois Dept. of Public Health, Springfield
Templeton, W. L., Battelle Pacific Northwest Lab.
Tennessee, U. of, Chairman, Dept. of Meteorology
Tepper, M., NASA Headquarters, Washington
Texas A&M U., Librarian, Dept. of Oceanography and Meteorology
Texas, U. of, Atmospheric Science Group, Austin
Thiess, P. E., Catholic U. of America

Underwood, R. L., U. S. Dept. of Transportation, Washington
U. S. Air Force, Hdq., Air Weather Service, Scott AFB, Ill.
U. S. Army Ballistic Research Labs., Director, Aberdeen Proving
    Ground
U. S. Dept. of Agriculture, Library, Washington
U. S. Dept. of the Interior, Bu. of Reclamation, Denver
U. S. Dept. of the Interior, Library, Washington
U. S. Dept. of Transportation, Librarian, Transportation Systems
    Ctr., Cambridge, Md.
U. S. Dept. of Transportation, Library, Washington
U. S. Environmental Protection Agency, Nat. Envtl. Res. Ctr.,
    Cincinnati
U. S. Naval Postgraduate School, Chairman, Dept. of Meteorology
Van der Hoven, I., NOAA, Silver Spring
Vesselinovitch, S. D., Billings Hospital, Chicago
Volchok, H. L., Health and Safety Lab., USDOE, New York
Wagner, N. K., U. Texas, Austin
Waldman, R. R., National Weather Service, Chicago
Warren, R. W., Great Lakes Commission, Ann Arbor
Weinman, J. A., U. Wisconsin
Weins, M. J., U. Illinois, Chicago
Wendell, L. L., Battelle Pacific Northwest Lab.
Whitby, K. T., U. Minnesota
White, C., Environmental Measurements, Inc., Annapolis
Wildung, R. E., Battelle Pacific Northwest Lab.
Wilson, W. E., National Center for Air Pollution Control,
    USEPA, Research Triangle Park
Winchester, J. W., Florida State U.
Woods Hole Oceanographic Institution, Document Library
Wyngaard, J. C., Wave Propagation Lab., NOAA, Boulder
Wyoming, U. of, Dept. of Atmospheric Resources
Yale U., Chairman, Dept. of Geology and Geophysics
Young, J., U. Wisconsin
Yu, T., National Oceanic and Atmospheric Adm., Washington
Zar, H., USEPA, Chicago
Zar, K., U. Chicago

Foreign:

Comision Nacional de Energia Atomica, Library, Buenos Aires,
    Argentina
Bradley, E. F., CSIRO, Canberra City, Australia
C.S.I.R.O., Div. of Atmospheric Physics, Librarian,
    Mordialloc, Australia
C.S.I.R.O., Div. of Environmental Mechanics, Librarian,
    Canberra, Australia
C.S.I.R.O., Div. of Land Research, Librarian, Deniliquin, Australia
Commonwealth Meteorology Research Centre, Librarian,
    Melbourne, Australia
Dyer, Dr. A. J., Div. of Atmospheric Physics, C.S.I.R.O.,
    Mordialloc, Australia
Linacre, Prof. E. T., Macquarie U., North Ryde, Australia
Melbourne, U. of, Librarian, RAAF Academy/Physics Dept., Australia
Philip, Dr. John R., C.S.I.R.O., Canberra, Australia

Priestley, Dr. C. H. B., C.S.I.R.O., Mordialloc, Australia
Radok, Dr. U., U. Melbourne, Australia
Schwerdtfeger, Prof. P., Flinders U. of South Australia,
    Bedford Park, Australia
Shaw, Dr. Neal A., Hawthorne, Australia
Turner, Prof. S., Australian National University, Sutherland,
    Australia
Weapons Research Establishment, Adelaide, Australia
British Columbia, U. of, Librarian, Vancouver, Canada
Canada Centre for Inland Waters, Librarian, Burlington, Canada
Davenport, A. G., U. Western Ontario, London, Canada
Elder, Dr. Floyd, Canada Centre for Inland Waters, Burlington,
    Canada
Fry, Dr. F. E. J., U. Toronto, Canada
Hage, Prof. K. D., U. Alberta, Edmonton, Canada
Kramer, Prof. J. R., McMaster U., Hamilton, Canada
Martin, Dr. Hans C., Atmospheric Environment Service, Downsview,
    Canada
McCulloch, Mr. James A. W., Atmospheric Environment Service,
    Downsview, Canada
McGill U., Chairman, Dept. of Meteorology, Montreal, Canada
Meyerhof, Ms. Dorothy P., Radiation Protection Bureau, Ottawa,
    Canada
Misener, Dr. A. D., U. Toronto, Canada
Moroz, W. J., J. F. Naclaren Environmental Consultants, Willowdale,
    Canada
Munn, Dr. R. E., U. Toronto, Canada
Oke, Prof. T. R., U. British Columbia, Vancouver, Canada
Rodgers, Prof. G. K., U. Toronto, Canada
Skinner, Ms. M. M., Atmospheric Environment Service, Downsview,
    Canada
Summers, Prof. Peter, Atmospheric Environment Service, Downsview,
    Canada
Thurtell, Prof. G. W., Guelph, Canada
Toronto, U. of, Library, Serials Dept., Canada
Tuller, Dr. Stanton E., U. Victoria, Canada
Vollenweider, Dr. R. A., Canada Centre for Inland Waters,
    Burlington, Canada
Whelpdale, Dr. D. M., Atmospheric Environment Service, Downsview,
    Canada
Tseng, Dr. Chung-Yi, Inst. of Physics, Nankang, China
Busch, Dr. Niels E., Danish AEC, Risø, Denmark
Kristenson, L., Risø National Lab., Roskilde, Denmark
Chamberlain, Dr. A. C., UKAEA, Harwell, England
Chester, Dr. Roy, U. Liverpool, England
Inst. of Oceanographic Sciences, Librarian, Wormley, England
Liss, Dr. Peter, U. East Anglia, Norwich, England
Meteorological Office Library, Bracknell, England
Pierson, Dr. D. H., UKAEA, Harwell, England
Smith, Dr. F. B., Meteorological Office, Bracknell, England
Taylor, P. A., U. Southampton, England
Hartwig, Battelle-Institut e.V., Frankfurt, Germany
Hasse, Prof. L., U. Hamburg, Germany

Munnich, Dr. K. O., Physikalische Inst. der Universitat
    Heidelberg, Germany
Meteorologisches Inst. der Universitat Hamburg, Librarian,
    Germany
Roth, Dr. R., Technischen Universitat Hannover, Germany
Lal, Dr. Devendra, Physical Research Lab., Ahmedabad, India
Manes, Dr. Alexander, Israel Meteorological Service, Bet-Dagan,
    Israel
Neumann, Prof. Yehuda, U. Jerusalem, Israel
Vittori, Dr. O., Laboratorio Microfisica dell' Atmosfera,
    Bologna, Italy
Inoue, E., National Inst. of Agricultural Sciences, Tokyo, Japan
Kitabayashi, K., National Res. Inst. for Pollution and Resources,
    Tokyo, Japan
Ogawa, Y., National Inst. for Environmental Sciences, Tokyo, Japan
Sahashi, Prof. Ken, Okayama U., Japan
Osterberg, C. L., Intern. Atomic Energy Agency, Monaco-Ville,
    Monaco
Gjessing, Dr. D. T., Norwegian Defense Research Establishment,
    Kjeller, Norway
Tennekes, H., Royal Netherlands Meteorological Inst., Debilt,
    The Netherlands
Papua New Guinea, U. of, Physics Dept.
Granat, Dr. L., U. Stockholm, Sweden
Academy of Sciences of the USSR, Librarian, Inst. of Atmospheric
    Physics, U.S.S.R.

178